

The Pennsylvania State University

The Graduate School

College of Engineering

# 3D Printing of a Thermoset, Citrate Base Polymer

A Thesis in

Bioengineering

by

Gerald Kirk

Copyright 2017 Gerald Kirk

Submitted in Partial Fulfillment  
of the Requirements  
for the Degree of

Master of Science

December 2017

The thesis of Gerald Kirk was reviewed by and approved\* by the following:

Jian Yang  
Professor of Biomedical Engineering  
Thesis Advisor

Nanyin Zhang  
Professor of Biomedical Engineering  
Electrical Engineering

Yong Wang  
Professor of Biomedical Engineering

William Hancock  
Professor of Biomedical Engineering  
Graduate Program Chair

\*Signatures are on file in the Graduate School

## Abstract

Significant effort in the field of Bioengineering has been devoted to the fabrication and application of scaffold materials as one third of the tissue engineering trifecta: cells, materials, and growth factors. While traditional fabrication techniques, notably porogen leaching and gas foaming, have resulted in widely applied and functional scaffolds, such constructs exhibit a large degree of variability and are difficult to replicate more complex, physiological geometries. These limitations have increased interest in additive manufacturing as an alternative, generating significant research and development focus on both scaffold materials and scaffold fabrication techniques.

Currently, additive manufacturing is split into two major categories: bio (cell) printing, and scaffold printing. While the former relies on gel-based materials, including alginate, collagen, gelatin, Polyethylene Glycol PEG, and mixtures of the above (due to their water solubility, relatively mild printing conditions, and ability to facilitate nutrient transfer to encapsulated cells from the surrounding tissue), the latter has traditionally used thermoplastic, biocompatible polymers such as Poly Caprolactone (PCL), Polylactic Acid (PLA), Poly Lactic-co-glycolic Acid (PLGA), as well as ceramics, and metals. The latter are capable of post-print cell seeding or of direct cell recruitment *in vivo*. The material choice for use in additive manufacturing is determined primarily by the ability to form solid constructs rapidly upon printing through temperature- or pH-regulated gelation, free radical crosslinking, shear thickening, or solidification from a melted state, among other methods.

In this study, we explore the use of citrate based, thermoset polymers as a new class of materials for additive manufacturing. This study includes the modification of an off-the-shelf 3D printer commonly used for filament extrusion of PLA thermoplastics, with a micro extrusion system consisting of a pressurized pneumatic system, syringe reservoir, and needle extruder. Further, we formulate novel composite bio-inks to facilitate the printing of thermoset, citrate based pre-polymers prior to irreversible crosslinking. This was done to increase the manufacturability of citrate based polymers, allowing these class of materials to expand its suitable tissue scaffold applications. 3D printed constructs were explored as a skin substitute, using additive manufacture allowed thin scaffolds to be manufacture and tested for this application.

Three materials are studied to evaluate printability using the modified printer: PCL, a known printable thermoplastic, Poly-(Octamethylene Citrate) (POC), a well-studied thermoset, and POC-Ca, a thermoset modified with the addition of calcium ions. Composite inks are formed with hydroxyapatite and salt with vary concentrations to determine the optimal concentration for composite inks. The printability study is conducted via evaluations of a printed scaffold by three methods: visual observation of extrudability and filament formation, quantifying the circularity of a single printed layer (demonstrating shape fidelity), and comparison between the theoretical areas of printed holes and their experimentally determined values. Scaffolds were designed for the printability evaluations were 12 mm x 12 mm with 9, 2mm holes, with a scaffold thickness of 0.4 mm.

Overall, results demonstrate that citrate based composites can be designed as functional bio-inks printable to 2 mm resolution into consistent, thin films. Thus, this work

demonstrates the ability to adapt additive manufacturing to generate thermoset tissue engineering scaffolds that could not previously be created with traditional manufacturing techniques.

# Table of Contents

List of Figures .....	ix
List of Tables .....	xiv
<b>Chapter 1: Introduction .....</b>	<b>1</b>
<b>Background .....</b>	<b>1</b>
<b>Design of Skin Substitutes .....</b>	<b>3</b>
Wound Healing Process .....	3
Parameters for viable skin substitutes .....	5
<b>Use of Citrate Base Polymers in Regenerative Medicine .....</b>	<b>8</b>
<b>Traditional Manufacturing Techniques for Creating Scaffold Scaffolds.....</b>	<b>10</b>
Gas Foaming .....	11
Phase Separation .....	11
Electro Spinning.....	12
Salt leaching and solvent casting .....	12
<b>Additive Manufacturing Techniques .....</b>	<b>12</b>
Inkjetting: .....	13
Laser Assisted: .....	15
Microextrusion: .....	17
Materials.....	18
<b>Conclusion .....</b>	<b>20</b>
<b>Project Goals .....</b>	<b>21</b>
<b>Project Aims .....</b>	<b>23</b>
<b>Chapter 2: Methods.....</b>	<b>24</b>
<b>Polymer Synthesis .....</b>	<b>24</b>

POC .....	24
POC-Ca .....	25
Polycaprolactone (PCL) .....	25
<b>Printer Modification: .....</b>	<b>26</b>
Ultimaker’s Original Assembly .....	26
Modification .....	32
Test Procedure, Testing Matrix .....	34
Scaffold Printing and Preparation: Printability Assessment .....	34
<b>Printability Evaluation .....</b>	<b>36</b>
Ink Compositions .....	37
Rheology: .....	37
Filament Morphology: .....	37
Circularity and Area Evaluation: .....	38
SEM Morphologies: .....	39
<b>Printed Skin Scaffold Evaluation: .....</b>	<b>40</b>
Ink Preparation .....	40
Scaffold Fabrication: Application assessment .....	40
Mechanical .....	42
Water Vapor Permeability .....	43
WVT Procedure .....	45
Data Processing .....	45
<b>Oxygen Permeability .....</b>	<b>47</b>
<b>Chapter 3: Results .....</b>	<b>47</b>
<b>Filament Morphology .....</b>	<b>47</b>

<b>Rheology .....</b>	<b>48</b>
<b>Circularity and Area.....</b>	<b>50</b>
<b>SEM morphologies .....</b>	<b>54</b>
<b>Mechanical Testing .....</b>	<b>67</b>
POC-Ca Mechanics:.....	72
<b>Water Vapor Permeability.....</b>	<b>74</b>
Oxygen Permeability.....	75
<b>Chapter 4: Discussion .....</b>	<b>76</b>
1. Rheological analysis .....	79
2. Filament morphology .....	80
3. Percentages of Successfully Printed Pores .....	81
6. Mechanical .....	84
7. water vapor permeability and oxygen permeability. ....	84
Conclusion .....	85
<b>Chapter 5: Future Direction .....</b>	<b>86</b>
<b>Printing of Citrate Based Polymers .....</b>	<b>86</b>
<b>Printed Scaffold for use as a Skin Substitute .....</b>	<b>87</b>
<b>References: .....</b>	<b>88</b>

## List of Figures

Figure 1, Ultimaker 2 general layout, ( <a href="https://ultimaker.com/en/products/ultimaker-2-plus/specifications">https://ultimaker.com/en/products/ultimaker-2-plus/specifications</a> ) .....	27
Figure 2, A cross-sectional view of the Ultimaker 2, showing the stepper motors and pulley system used to move and locate the print head ( <a href="https://grabcad.com/library/ultimaker-2-2">https://grabcad.com/library/ultimaker-2-2</a> ) .....	28
Figure 3 (files released by Ultimaker found on github), model assembly poster on Grabcad, by lilian monomax. ( <a href="https://grabcad.com/library/ultimaker-2-2">https://grabcad.com/library/ultimaker-2-2</a> ) .....	29
Figure 4 Blown out veiw of ultimaker 2 printer head files found at <a href="https://github.com/Ultimaker/Ultimaker2">https://github.com/Ultimaker/Ultimaker2</a> .....	31
Figure 5: Schematic of syringe holding bracket (mm) .....	32
Figure 6: Shows the completely modified Ultimaker 2, a: Norson Efd proformus III, pneumatic dispense and air regulator: Norson 5ml syringe, c: Pressure regulator and air filter, d: pneumatic actuator pedal, e. adapter plate.....	33
Figure 7 Printability Scaffold Design, created using SolidWorks® .....	36
Figure 8 Example of threshold boundaries, boundaries set so the pore morphology was distinct .....	39
Figure 9 Highly porous printed scaffold constructs for wound dressings .....	41

Figure 10 design of printed mechanical meshes .....	42
Figure 11, graphical representations of steady state water transmission .....	46
Figure 12 evaluations of extruded filament morphology, if the samples runs thick or thin morphologies of the printed part will be loss .....	48
Figure 13, MCR 302 rheometer amplitude sweep .....	49
Figure 14, MCR 302 rheometer Viscosity cure .....	50
Figure 15: 1. PLA, 2. POC, 3. POC 25% Salt, 4. POC 50% Salt, 5. POC 75% Salt, 6. POC 25% HA, 7. POC 50% HA, 8. POCCa, 9. POCCa 25% Salt, 10. POCCa 50% Salt, 11. POCCa 75% Salt, 12. POCCa 25% HA, 13. POCCa 50% HA, 14. PCL, 15. PCL 25% Salt, 16. PCL 50% salt, 17. PCL 75% Salt, 18. PCL 25% HA, 19. PCL 50% HA, 20. PCL 75% HA.....	51
Figure 16 Precantage of succesfully printed holes, the horizontal line indicates the success rate (85%) for further evaluation.....	51
Figure 17 Distribution of Cicularity for printed holes, values closer to 1, indicate greter circularity.....	52
Figure 18 distribution of the areas of each pore from printed constructs, theoretical areaa of 3.14 mm <sup>2</sup> is shown by the horizontal line .....	53
Figure 19: SEM Image of 3D printed PLA film; top view.....	55
Figure 20: SEM Image of 3D printed PCL scaffold with 25% Salt incorporated and leached; top view .....	56

Figure 21: SEM Image of 3D printed PCL scaffolds with 50% Salt incorporated and leached; top view .....56

Figure 22: SEM Image of 3D printed PCL scaffolds with 75% Salt incorporated and leached; top view .....57

Figure 23: SEM Image of 3D printed POC film; top, cross section and side views .....58

Figure 24: SEM Image of 3D printed POC scaffolds with 25% Salt incorporated and leached; top view .....58

Figure 25: SEM Image of 3D printed POC scaffolds with 25% Salt incorporated and leached, cross section and side views.....59

Figure 26: SEM Image of 3D printed POC scaffolds with 50% Salt incorporated and leached; top view .....59

Figure 27: SEM Image of 3D printed POC scaffolds with 50% Salt incorporated and leached, cross section and side views.....60

Figure 28: SEM Image of 3D printed POC scaffolds with 75% Salt incorporated and leached; top view .....60

Figure 29: SEM Image of 3D printed POC scaffolds with 75% Salt incorporated and leached, cross section and side views.....61

Figure 30: SEM Image of POC 25% HA top view.....62

Figure 31: SEM Image of 3D printed POC scaffolds with 25% HA incorporated and leached, cross section and side views..... 62

Figure 32: SEM Image of 3D printed POC scaffolds with 50% HA incorporated and leached; top view ..... 63

Figure 33: SEM Image of 3D printed POC scaffolds with 50% HA incorporated and leached; top, cross section and side views..... 63

Figure 34: SEM Image of 3D printed POCCa scaffolds with 25% Salt incorporated and leached; top view..... 64

Figure 35: SEM Image of 3D printed POCCa with 25% Salt incorporated and leached, cross section and side views..... 65

Figure 36: SEM Image of 3D printed POCCa scaffolds with 50% Salt incorporated and leached. 65

Figure 37: SEM Image of 3D printed POCCa scaffolds with 50% Salt incorporated and leached, cross section and side views..... 66

Figure 38: SEM Image of 3D printed POCCa scaffolds with 75% Salt incorporated and leached. 66

Figure 39: SEM Image of 3D printed POCCa scaffolds with 75% salt incorporated and leached; top, cross section and side views ..... 67

Figure 40: Peak Stress [MPa] of PCL films, all films not otherwise labelled are printed, error bars represent 1  $\sigma$  STD..... 68

Figure 41: Initial Modulus [MPa] of PCL films, all films not otherwise labelled are printed, error bars represent 1  $\sigma$  STD. .... 69

Figure 42: Strain at break [%] of PCL films, all films not otherwise labelled are printed, error bars represent 1  $\sigma$  STD. .... 69

Figure 43: Peak Stress [MPa] of POC films, all films not otherwise labelled are printed, error bars represent 1  $\sigma$  STD. .... 70

Figure 44: Initial [MPa] of POC films, all films not otherwise labelled are printed, error bars represent 1  $\sigma$  STD. .... 71

Figure 45: Strain at Break [%] of POC films, all films not otherwise labelled are printed, error bars represent 1  $\sigma$  STD. .... 71

Figure 46: Peak Stress [MPa] of POC-Ca films, all films not otherwise labelled are printed, error bars represent 1  $\sigma$  STD. .... 72

Figure 47: Initial Modulus [MPa] of POC-Ca films, all films not otherwise labelled are printed, error bars represent 1  $\sigma$  STD. .... 73

Figure 48: Strain at Break [%] of POC-Ca films, all films not otherwise labelled are printed, error bars represent 1  $\sigma$  STD. .... 73

Figure 50 Permeability Graph, Showing the linearity of the permeation trend, suggesting the permeation is in steady state ..... 74

## List of Tables

Table 1 Current Skin Substitutes on the Market [52] .....	6
Table 2 Test Matrix.....	34
Table 3, evaluation of area of the printed holes and circularity of the printed holes.....	54
Table 4, PCL Mechanical Properties Overview, All Samples that do not otherwise specify are printed.....	68
Table 5 POC Mechanical Properties Overview, All Samples that do not otherwise specify are printed.....	70
Table 6 POC Mechanical Properties Overview, All Samples that do not otherwise specify are printed.....	72
Table 7: Water vapor transmission rates .....	75
Table 8: Oxygen Permeability.....	75
Table 9, Filled in Test Matrix .....	78

# Chapter 1: Introduction

## Background

Bio-fabrication uses traditional and novel manufacturing techniques to produce constructs consisting of biological materials and mechanisms [1]. Bio-fabrication was defined by Payne and associates as *“the marriage between biology and microfabrication”*[2]. As a process supporting many active research fields such as regenerative medicine, tissue engineering, and complex drug delivery systems, the use of a simple definition clarifies the role of bio-fabrication in its support of these other fields of study. Tissue Engineering (TE) was first defined in 1993 as *“an interdisciplinary field that applies the principles of engineering and life sciences towards development of biological substitutes that restore, maintain, or improve biological tissue function or a whole organ.”* Further, Regenerative Medicine (RM) has been defined as *“the application of tissue science, tissue engineering, and related biological and engineering principles that restore the structure and function of damaged tissue and organs”* [3].

Many considerations need to be considered to create viable tissue scaffolds. Some of the considerations include: the vast variance in data resulting from the complexity attendant to living systems, constrictions on fabrication techniques produced by the living systems bio-engineering aims to serve (tissue structure), restrictions on materials selection necessitated by the need for bio-compatibility, limited biomass availability, and the significant challenges associated with scale-up from a laboratory environment to full-scale production [4,5].

Traditional manufacturing techniques aimed to develop the closest condition to the native tissue as possible by varying pore sizes and architectures and by utilizing the most bio-compatible materials. Additive manufacturing (or 3D printing) has increased the ability to create defined microstructures and has even been utilized to print living cells directly, creating final viable tissue constructs with limited post processing. Additive manufacturing solves many problems associated with traditional scaffold creation techniques by mimicking more closely the native architectures of tissues. 3D printing allows researchers to create new structures that were either not previously possible or efficiently produced using traditional techniques. Research is currently working towards on-demand fabrication of tissue scaffolds and medical devices [6]. Currently for Citrate based polymers there is a limitation in the manufacturability, limited to basic molding, casting, and salt leaching techniques. This study aims to increase the manufacturability of citrate based polymers with the use of additive manufacturing. Exploration of the resulting scaffolds produced by this process are explored for suitability as a skin substitute.

In the following sections a review of current methods of wound healing and skin substitutes are presented, followed by a review of Citric Acid based polymers as it relates to uses in tissue engineering. Next, an overview of traditional manufacturing techniques for scaffold fabrication in tissue engineering is presented. Finally, current additive manufacturing techniques used in biomedical engineering are discussed. This review presents the parameters needed for creation of a suitable skin substitute as well as current manufacturing techniques that have been used in tissue engineering and suggests the utilization of citrate based polymers

for a skin substitute in a novel additive manufacturing process that was created from an off-the-shelf 3D printer.

## Design of Skin Substitutes

### Wound Healing Process

Wound healing is a normal biological process, consisting of four phases: hemostasis, inflammation, proliferation, and remodeling. For complete healing, all four phases must occur in the proper sequence and timeframe [7]. Any interruption in these phases will create delay healing, often leading to chronic wounds. The first step to wound healing is hemostasis, which is the process that causes bleeding to stop by vascular constriction, followed by platelet aggregation, degranulation, and fibrin formation (thrombus). Second, inflammation occurs, where neutrophils, monocytes, and lymphocytes infiltrate the wound site. The monocytes then differentiate into macrophages to aid debris removal. Third, proliferation starts as re-epithelialization, angiogenesis, collagen synthesis, and extracellular matrix formation occur. Fourth, collagen remodeling and alignment, vascular maturation, and reconstruction occurs [8].

Once the skin is injured either by surgery or trauma an acute wound is formed and will move through the healing process following a predictable timeframe and process as described above. Chronic wounds develop from acute wounds when the healing process is interrupted and frequently enter a state of pathologic inflammatory response which halts the healing process. Most chronic wounds are associated with ischemia, diabetes, venous stasis disease, or pressure. Chronic wounds affect about 3 to 6 million people in the United States, and 85% of

the people affected by these wounds are 65 years or older [9,10]. Chronic wounds require intervention to complete healing, if healing can be accomplished.

Another way to classify wounds are by the amount of damage done to the epidermis and dermis of the skin. Wounds can be divided into epidermal, superficial partial thickness, deep partial thickness, and full-thickness wounds. Epidermal injuries typically consist of light scalds, scratches or grazing, or sunburns, and are experienced with slight pain. Superficial partial thickness affects the epidermis structures and partial thicknesses of the dermis structure. This injury type is accompanied by severe pain and blistering, especially in cases of thermal trauma. These wounds heal by epithelialization from margins of the wound, spreading from hair follicles and basal keratinocytes[11]. Deep thickness wounds affect a greater portion of the dermis, and take longer to heal. Scarring will occur and be pronounced in this wound type as fibroplasia is more intensive in the repairing process. Finally, full-thickness injuries involve complete and full destruction of the epithelial-regenerative elements. This wound type heals by contraction from the epithelial components from the edge of the wound [12]. Full-thickness wounds more than 1 cm in diameter require skin grafting or a skin substitute and can lead to extensive scarring. Currently the gold standard for treatment of full-thickness wounds is treatment with a split thickness auto-graft [13].

The wound healing process summarized here allows for regeneration of skin to close wounds. Sometimes this process can be impaired and result in very long healing times or even chronic wounds. Chronic wound sites are usually in a state of chronic inflammation and contain bacteria and bacterial products such as endotoxins and metalloproteinases which negatively affect the healing process [14].

Factors that can retard the wound healing process include protein deficiency, obesity, smoking, vitamin deficiencies, and the pH of the wound site [8].

The surface pH value of the wound site directly influences the biochemical reactions taking place in the wound healing process. It has been demonstrated that the pH of a wound can cause antimicrobial effects, oxygen release, angiogenesis, and bacterial toxicity [15]. It has been observed that wounds with higher alkalinity have lower healing rates in both acute and chronic wounds as compared to wounds with a neutral pH [16].

The use of various acids such as acetic acid, boric acids, and hyaluronic acid has been reported in wound treatments of soft tissue infection and burn infections [17]. Washing wounds with these acids in concentrations of 1-5% has been shown to negatively affect bacterial formation and proven to be an effective treatment for infected wounds. Some authors have proposed the use of citric acid as an effective treatment for pseudomonas wound infection [18,19]. It has also been shown as an effective treatment for a variety of other bacteria such as *Staphylococcus aureus*, *Escherichia coli*, *Klebsiella* spp., *Proteus* spp., *Citrobacterspp.*, *S. epidermidis*, *streptococci*, and *enterococci* [17].

#### Parameters for viable skin substitutes

While autografts are the gold standard for full-thickness skin grafts, there are a few complications that produce a need for skin substitutes. When a patient's injury covers the majority of the patient's body (e.g., major burns) there are not enough donor sites from which to obtain autografts [20]. To solve this issue multiple skin grafts can be taken from the same site, allowing for re-epithelialization of the graft site [21]. Skin substitutes include cultured

autologous keratinocytes as well as the use of engineered skin substitute. Shakespear et al, 2005 outlines four major components needed in skin replacement products [22]:

1. Protection: providing a mechanical barrier from micro-organisms and a vapor barrier
2. Procrastination: early wound debridement (some wound cover is needed until permanent wound closure can be achieved by skin graft, important in extensive burns)
3. Promotion: delivery to the wound site of growth factors, cytokines, dermal matrix components to promote natural host wound-healing
4. Provision: application of new structures, such as dermal collagen or cultured cells.

Multiple companies have started creating skin substitutes, many based around the use of decellularized allograft to create a feasible product. While fewer use synthetic materials to mimic the dermal structure, some companies will seed fibroblasts or keratinocytes to increase the effectiveness of the skin substitute. **Error! Reference source not found.** summarizes companies who currently produce synthetic skin substitutes.

Table 1 Current Skin Substitutes on the Market [52]

Skin Substitute	Material Used	Details	Seeded Cells	Duration Of Cover	Treatment Site
Dermograft (Advance BioHealing, Inc., New York, NY and La Jolla Ca, Usa)	Polyglycolic acid (Dexon) or polyglactin-910 (Vicryl), PLA, ECM	Aim to mimic histological structure of native skin where both the dermal and epidermal layers are present	neonatal allogeneic fibroblasts	Temporary	Dermal
Integra (Integra NeuroScience, Plainsboro, NJ, USA)	Silicone 1st layer, Collagen and glycosaminoglycan 2nd layer	Most Widely accepted skin Substitute, with a bilaminar Scture pore size: 20-200 um	none	Silastic layer removed, collagen layer perminant	Dermal
Allo derm, (LifeCell Corporation, Branchburg, NJ, USA)	Acellular deepithized cadaver dermis	Preserved basement membrane 0.4-0.8 mm thick	none	Perminant	Dermal
Biobrane, (UDL laboratories, Inc., Rockford, IL, USA)	Silicon, nylon mesh, and collagen	bilaminate membrane, nylon mesh fabric bonded to a thin layer of silicone	none	Temporary	Dermal
My Skin, (CellTran Ltd, Sheffield, UK)	Silicone layer	Semi-confluent Keratinocytes seeded onto a silicone support layer with a specaillized surface treatment	Keratinocytes	Perminant	Epidermal
PolyActive, (HC implants BV, Leiden, The Netherlands)	PEO/PBT	bilaminar, with a seeded matrix of polyethylene Oxide and a hard polybutlyne component	keratinocytes, fibroblast	Temporary	Dermal, Epidermal

If there is any non-biodegradable component to the synthetic skin substitute it is required that the substitute be labeled as temporary and must be removed once sufficient healing has occurred. This results in most synthetic skin substitutes being temporary and used in conjunction with autograft as a covering for full-thickness wounds. They are also used as covering for partial-thickness wounds that still require protection and thereby assist in the wound healing process.

When considering design of an engineered skin substitute it is important for the material scaffold to closely match the properties for the native skin. Skin has complex physiological and physiochemical composition properties make it such an effective outer-most layer against most exogenous factors [23]. Important biophysical properties of skin include its mechanical properties, pH, and epidermal hydration[23,24].

It is also critical to consider mimicking the mechanical properties of the skin, which has an ultimate tensile strength from 1 to 40 MPa, initial modulus of 0.5- 2 MPa, and a percent strain of 12-126% [24–26]. This variation in the mechanical properties is caused by many influences including age, gender, location on the body, and hydration level [27]. For intact skin the surface pH is acidic, varying between 4.0 and 6.0, with the higher pH regions associated with the most hydrated portions, which occur around skin folds [28]. The hydration level of skin also plays an important role in maintaining hemostasis. The normal hydration levels of skin vary depending on its location. As examples, in the corneal layer between 15-20 % of its mass is considered water, in living areas of the epidermis, water constitutes as much as 70% of the mass [29].

With these properties in mind, along with the four major components needed in skin replacement products expressed [22], engineered skin scaffolds should form a protective layer from the exterior environment and should mimic the native properties of skin (mechanics, pH values, and water absorption properties). Citrate based materials can account for most of these parameters, and the chemical makeup of the scaffold material will affect the pH, to create an acidic environment during scaffold degradations.

## Use of Citrate Base Polymers in Regenerative Medicine

Many established thermoplastic polymers have been utilized in tissue engineered scaffolds and regenerative medicine, such as poly(lactic acid) (PLA), poly(glycolic acid), and their copolymers because of their extensive use in products approved by the US Food and Drug Administration [30,31]. Thermoplastics are limited by the fact that the intrinsic properties of the material do not proactively interact with cell behavior because the chemical composition of these thermoplastics do not provide beneficial chemicals upon degradation or directly stimulate the surround tissues, thereby failing to trigger beneficial cell responses.

Exploration into the use of biodegradable thermosets with elastomeric properties was proposed as a replacement of the thermoplastic materials due to the disadvantages of the latter. One polymer that has favorable chemical compositions upon its decomposition uses citric acid as the main cross-linking monomer. This thermoset formulation was described as a new class of polyester, referred to as poly (Octamethylene Citrate) (POC). These materials have found widespread use by modification of the processing condition during manufacturing, as well as the chemical modification, such as adjustment of diol and poly-acid incorporated [32].

Citric acid was used as the cornerstone monomer for the design of a biodegradable elastomer because of its multifunctional behavior, minimal toxicity, and its relative low cost. Citric acid has three carboxyl groups and one hydroxyl group. This provides its key advantage: allowing it to be used in pre-polymer formation with polyols, in a simple poly-condensation reaction. During pre-polymer formation, the carboxyl and hydroxyl side groups can be partially preserved, allowing for conjugation of bio-active molecules. It was also shown that varying the crosslinking condition of the pre-polymer permits tuning of the mechanical properties. As an example, raising the temperature and the crosslinking time increases the crosslinking density in the material, thereby increasing the mechanical strength while decreasing elasticity and slowing the degradation rates [33]. By introducing azide and alkyne during pre-polymer formation, citric acid based polymers can take advantage of click chemistry, where a thermal click reaction occurs between alkyne and azide groups, greatly increasing the mechanical strength of the bio-material.

Citrate based polymers also exhibit antimicrobial properties. Despite advances made in the cleanliness of surgical practices, microbial infection remains a challenge for many surgical procedures and for *in vivo* application of synthetic biomaterials. Bacterial growth assessment of citrate based polymers was done via optical density through culturing of *Escherichia coli* and *Staphylococcus aureus* for 28 hours. Results showed that POC is the most effective anti-microbial agent of the poly (diol citrate) materials, showing similar anti-bacterial properties to a simple citric acid wash. An explanation for this behavior is that the released citric acid transverses the cell membrane, lowering the intracellular pH and causing cell death [34].

Citric acid based polymers can be tuned to specific tissue needs while maintaining appropriate degradation time for applications in main tissue engineering fields. Composite citrate polymers with the addition of hydroxyapatite have been presented as a viable bone scaffold. Modified citrate based polymers have been used for drug delivery systems, imaging techniques, soft tissue, and cardiovascular applications.

Unfortunately, while they show high feasibility as a novel bio-material, the manufacturability of citrate-based polymers is lacking. Only traditional manufacturing methods apply to these materials because the majority of them are thermosets and there go through an irreversible crosslink process, limiting workability. Consequently, most scaffold materials are manufactured using either salt/leaching methods, if pores are desired or, for solid scaffolds, compositions are evaporated down into workable putties and pressed into a mold, or rolled into composite sheets.

### Traditional Manufacturing Techniques for Creating Scaffold Scaffolds

Tissue scaffolds can be defined as three dimensional and highly porous structures with the majority of the pores connected to each other, allowing them to serve as templates to facilitate cell ingrowth during degradation of the scaffold[35]. The scaffolds provide structural support for the native tissue as it repairs itself. Scaffolds define a 3D space in the wound repair site but all provide the first biochemical cues for the native tissue [36]. The fabrication method must be carefully chosen to provide the best mimicry for the native tissue at the wound site, while also accounting for biocompatibility, biodegradability, appropriate porosity, appropriate mechanical integrity for the given tissue, and finally the chemical markers and growth factors

needed in the make-up of the scaffold [36]. Keeping all these factors in mind, tissue scaffolds are created from a vast assortment of materials and utilize many methods. In this section, an overview will be presented of manufacturing techniques that will be classified as traditional manufacturing, such as gas foaming, phase separation, electrospinning and solvent/salt leaching.

### Gas Foaming

Mooney et al 1996 introduced gas foaming into tissue engineering [37]. Gas foaming creates a porous scaffold without the use of organic solvents, which is advantageous since residues from the organic solvent inhibits cell adhesion to the scaffold [37]. Gas foaming is a process where gaseous decomposition occurs, during drying or curing of the prepared material[38]. This gaseous decomposition occurs at elevated temperatures when gas is forced at high pressure to saturate the material in its liquid state. The polymer is then returned to atmospheric pressure, causing the gas solubility to decrease and the gas to be released from the polymer, thereby creating pores. The polymer is then thermally quenched to set the physical state of the material [39].

### Phase Separation

Phase separation uses a technique where polymer is dissolved in a suitable solvent, then loaded into a mold. The mold is then lowered in temperature until a liquid-liquid phase separation interaction occurs, and the two phases are bi-continuous [37,40]. The liquid-liquid mixture is then quenched at the appropriate time and temperature, forcing the polymer to quickly solidify. This causes a solid-liquid phase to occur, where the solvent is still in the liquid phase and could be sublimed to produce the highly porous foam. Additives such as

hydroxyapatite can be suspended in the polymer phase depending upon the needs of the specific application [40].

### Electro Spinning

Electrospinning is a technique that produces non-woven meshes with very high surface area; it has gathered considerable attention in the biomedical field due to its great potential in tissue engineering and drug delivery [41]. Electro-spun fibers usually have diameters in the tens of microns, and synthetic and natural materials can be utilized in the process [42].

Electrospinning is a very simple process where the polymer, either in solution or from a melt, is drawn by high voltage to a grounded plate [41].

### Salt leaching and solvent casting

Salt leaching and solvent casting both involve mixing of insoluble impurities, such as sodium chloride particles, into solvent polymer solutions. The polymer solution is cast into membranes and left to fully cure, or crosslinked. After the polymer solution has solidified, the salt particles are leached out leaving behind a porous structure. Pore size is controlled by the relative size of the salt crystal and the porosity is controlled by the relative salt weight fraction to polymer [38].

## Additive Manufacturing Techniques

The goal of Bioprinting is to assemble cells in a high throughput manner to eventually lead to the assembly of full tissue constructs for both therapeutic and research needs [43]. Many hurdles directly impede the ability to print living tissue, including the ability for functional vasculature, control of stem cell differentiation paths, limiting the foreign body response, and

finally matching the mechanical properties of the native tissue. Bioprinting allows for the patterning of biological materials, cells, and growth factors suspended in bio-materials to mimic tissues. The most common techniques for the patterning of cells and construction of scaffolds for tissue engineering applications are microextrusion, inkjetting, and laser-assisted methods [44]. Important parameters to consider when designing a Bioprinting process include mechanical properties, crosslinking conditions and their effects on cell viability, stresses occurring during printing (thermal, physical, chemical) and finally post processing of the printed constructs. It is common for cells to be either seeded after the printing process or directly printed. In the latter case consideration of cell survivability during printing is crucial. In general, all 3D-printers use a model created in a computer-aided design software package (such as SolidWorks®). This model is then converted to a STL (STereoLithography) file, which breaks the model up into its basic component, describing them as unrestricted triangulated surfaces. Finally, the STL file is converted to a g-code (or machining code) that allows the printer to know the location of printing deposition, or laser pathing depending on the printing method, the g-code tells the motors where to move, how fast, and what path to follow.

#### Inkjetting:

Inkjet printer or drop-on-demand printers are the most common printers for both biological and non-biological uses. Inkjet printers are found in most every household, and work on the basis of deposition of controlled volumes of a liquid at a defined location. The first inkjet based bio-printers were modified from commercially available household 2D printers [45,46]. To do this the ink cartage was replaced with biological material and the paper was replaced by a controllable z-axis stage [46]. Later, specifically designed inkjet printers replaced cartridges

with a sophisticated thermal or acoustic print head to finely control the deposition of bio-inks [45,47,48]. The thermal or acoustic print heads provide forces to the liquid to extrude single droplets onto a substrate to form the final construct. Thermal inkjet printers function by heating the print head nozzle by electrical currents, anywhere from 200 ° - 300 °C. A concern of researchers was that this high temperature would negatively impact the cell, protein, or DNA viability in the bio-inks. While there is a slight impact on biological components in the bio-ink, the thermal duration is so short (less than 2  $\mu$ s) that the viability of the ink is maintained [47,49]. Adjusting the temperature of the printed head and the duration the heat is applied controls the droplet size formation.

The other common way of extruding droplets for ink-jet printing is utilization of acoustic forces to create uniform droplets, which is achieved using a piezoelectric crystal that creates an acoustic wave inside the print head to break the liquid into droplets [50]. In this method, the frequency of acoustic waves and pulse duration are used to control the droplet size. The advantages of using acoustic properties for inkjet printing are that it avoids harmful heat formation during the printing process, thereby reducing the potential loss of cell viability or the denaturing of DNA present in the bio-inks [49,51]. Some disadvantages to the printing method have arisen due to the use of high frequencies such as 15-25 kHz; these could damage the cell membrane or cause cell lysis. Additionally, the materials utilized in this printing method have a very low viscosity (below 10 centipoise) limiting the available materials for this printing method [48,52,53]. The main drawback to using inkjetting methods for bio-materials is the requirement that the bio-ink be liquid when printing. This means the liquid must then form a solid after printing, either by ultra-violent light, chemical crosslinking, pH induced solidification,

or thermal gelation (cooling) [54,55]. However, most crosslinking conditions are toxic to cell, causing membrane damage or death [56].

In other printing methods, crosslinking remains a prominent problem. However, other printing methods can be printed at much higher viscosities, such as laser-assisted printing and micro extrusion, broadening the available materials for printing. These are discussed in the following sections.

#### Laser Assisted:

Laser-assisted printing has been used in multiple fields, and falls into two categories in the field of bio-printing: laser sintering scaffold printing, and laser-induced forward transfer printing.

Laser sintering employs a carbon dioxide laser beam to sinter thin layers of powdered polymeric materials to form solid three dimensional structures[57]. During the printing process the laser tracks over a powdered print bed, selectively sintering the cross-sectional area of the printed part. The interaction between the laser and the powder bed raises the temperature of the powder to the ceramic sintering point, or if a polymer powder is used to the glass transition temperature of the polymer; this fuses the particles together. The use of this method to construct scaffold materials remains limited due to the high temperatures during printing because sufficient temperature is needed for sintering of the material particles. The high temperatures allow for the use of materials with higher strengths, and selective laser sintering can be used to make highly porous constructs with high percentages of hydroxyapatite (HA) [58], making this printing method favorable for formation of bone scaffolds. However, if drug

delivery along with cell seeding is needed both need to be done after the printing process because of the high temperature induced during printing.

The other laser assisted printing method is laser induced forward transfer printing, and has been shown to deposit cells in a very precise structure. This method has been successfully applied to biological material, such as peptides, DNA, and cells [59,60]. This printing method employs a pulsed laser beam, a focusing system, a ribbon that has the a layered structure that includes donor transport support (glass), a laser absorbing layer (gold/titanium), a layer of biological material (hydrogels and or cells), and a receiving substrate facing the biological material [44]. The laser is focused onto the ribbon to generate a high-pressure bubble that propels cell-containing material from the ribbon to the receiving substrate. This method produces very high resolutions; factors that affect the resolution include the laser influence (energy delivered per unit), surface tension of the ribbon, wettability of the substrate and the air gap between the ribbon and the substrate, and the thickness and viscosity of the biological material [61]. This laser assisted process results in very high cell viability, with cell deaths caused by the printing process reportedly being negligible. Such viability is mainly due to this being a nozzle-free printing method, so no unnecessary shear forces are applied to the cells during printing. A wider range of viscosities can be used in this printing method (anywhere from 1-300 mPa/s), and cells can be printed using seeding densities as high as  $10^8$  cl/ml with micro-scale resolutions of a single cell per drop [62]. Some disadvantages of this method are cost and time of production. While printing rates are high during printing, preparation of the ribbons is time consuming and will become more complicated if multi-cell compositions are to

be employed. Since this method uses cells during printing, the candidate printing materials are limited to hydrogels.

In other printing methods such as microextrusion, many more materials beyond hydrogels can be utilized for scaffold fabrication. However, this comes at a cost to cell viability and integration due to the extrusion and shearing forces experienced during printing.

#### Microextrusion:

Microextrusion deposits a solid bead of material on the printing surface [44]. The extrusion head is mounted on a robotic stage that controls its (x, y, z) orientation [43]. Most commercially available printers operate on this same principle: the z stage being controlled by a surface on an elevating stage and the (x, y) coordinates controlled by some sort of actuation arm [63]. Material is extruded through a micro-nozzle by a variety of systems, either pneumatic air pressure, a mechanical piston, or a screw. This deposits a 2D layer that is then solidified physically or chemically, which provides the stability and the platform for the next 2D layer to be deposited, thereby forming a 3D construct [64]. Of the three bioprinting methods, microextrusion has the lowest feature resolution (i.e., bead resolutions of around 5  $\mu\text{m}$  - 200  $\mu\text{m}$ , print speeds from 10-50  $\mu\text{m}/\text{s}$  and printable material viscosities from 30-6 $\times 10^7$  mPa/s) [43]. A range of fluid properties that can be printed, providing microextrusion with a wider pool of candidate materials.

Pneumatically controlled microextrusion printers benefit from a simple driving mechanism, with the force being limited to the air pressure capabilities of the system; they are

capable of extruding high viscosity solutions [62]. While mechanically controlled systems that utilize a screw or piston tend to be more complicated, they provide more control over extrusion flow because there is no delay-effect caused by gas volumes.

Microextrusion-printers do however have limitations. Printed cells can experience decreased cell viability due to extrusion forces exerted on the cells during printing; cell viabilities ranging from 40-86% have been reported. Greater viability can be achieved with decrease in pressure and increase in nozzle diameter because it generates lower shear forces [65,66].

With all the printing methods discussed, one of two options can be adopted to construct tissue engineered products: printed scaffolds with cells, or printed scaffolds without cells. When printing with cells, the usable biomaterials are greatly diminished. In order to support life, some, if not all, of the bio-ink composition needs to be composed of a hydrogel, either from natural or synthetic sources. When looking for an ideal material for Bioprinting, some main features need to be considered.

## Materials

When considering materials for Bioprinting it is important to consider the following key features:

1. **Printability:** Properties that directly affect the printability, handling and deposition of the materials. These can include viscosity, gelation methods, crosslink-factor and rheological properties.

2. Biocompatibility of the material: The material should minimize immunogenic response, and should actively contribute to the biological functions which the material is looking to replace.
3. Degradation properties and byproducts: Degradation of the material should match the ability of the native cells to infiltrate the space and deposit Extra-cellular matrix (ECM) in replacement of the scaffold.
4. Structural and mechanical properties: Should be chosen based on the mechanical properties of the targeted construct.
5. Material biomimicry: Engineering of functional and dynamic material properties should be based on the characteristics of the tissue repaired [44].

Common materials chosen for bio-printing consist of soft hydrogels. These utilize the addition of living cells to aid in the specific healing process. This allows for addition of growth factors and novel drug delivery systems, along with allowing cells encapsulation with the hydrogel solution can provide sufficient nutrients to the cell to keep them viable through the printing process. Common hydrogels used in printing include alginate, collagen, gelatin, and Pluronic. These materials are preferred because of their ability to form solids prior to printing, either by temperature control, chemical crosslinking, pH control, or gelation. Many other thermoplastic, biocompatible materials can be utilized in printing, however post processing steps are needed to allow for cell seeding, or additions of growth factor and/ or drugs. This negatively affects manufacturing times, but allows for the use of stronger materials that can more accurately match the native conditions. Common thermoplastics used for printing include PLA, PLGA, PEO, and PCL. Combinations of these materials and the previously mentioned

hydrogels have also been printed to produce constructs with better mechanical properties while still maintaining cell viability.

Common issues with these printing materials are low mechanical properties because hydrogels are generally weak materials. Also, problems tend to occur with degradation rate mismatch with tissue ingrowth. Hydrogels degrade too fast *in vivo*, while some of the thermoplastics degrade too slowly, taking years.

In tissue engineered scaffolds there is a distinct lack of printable materials that utilize thermoset polymers. Thermoset polymers have highly tunable mechanical properties and degradation profiles, because simple adjustments to crosslinking modulate these properties. Currently, the only thermosets used in additive manufacturing work on the principle of stereolithography printing (SLA), which utilizes a laser to crosslink the thermosets in a resin bath [29].

## Conclusion

Citric acid based polymers have shown great promise in many areas of tissue engineering; the use of citric acid as the cornerstone for polymer diversification has cemented it as a bio-active material. Being a thermoset makes the mechanical properties and degradation rates of citric acid based polymers easily controllable. However, being a thermoset also limits the available manufacturing techniques for this polymer group to only molding and casting processes.

Many 3D printed biomaterials show good viability as constructs with the use of cells and creation of complex geometries. In the microextrusion methods high viscosity solutions can be printed successfully for a wide range of materials. Bio-printed scaffolds are either printed with cells for increased regenerative process, and forced to be limited to hydrogel combination of materials or use bio-combatable thermoplastics that don't have favorable bio-activity *in vivo*. 3D printing has opened the door to the use of thermoplastic and hydrogel based polymers in the construction to print complex geometries for tissue engineering. Hydrogels while supporting good cell viability rarely show mechanical properties that show good mimicry of native tissue. Thermoplastic materials show bio-compatibility as inert materials and have favorable mechanical properties for tissue mimicry, but do tend to have non-beneficial degradation characteristics for use *in vivo*. 3D printing of thermosets has been limited to Laser printing methods that utilize vats of resin to be crosslinked by a laser in the additive manufacturing process.

## Project Goals

This work aimed to develop a successful method for the printing of citrate based polymers in composite ink solutions. Most citrate based pre-polymers are dissolved in an organic solvent for storage, the solvent is then needing to be removed as part of the manufacturing processes. In this project, the organic solvent was removed almost entirely to create a very viscous pre-polymer solution that could exhibit sufficient mechanical integrity to be printed, especially with the addition with composites components (e.g., hydroxyl appetite, and salt) that act as a supporting material.

While many bio-materials are printable, many bio-materials do not have bio-active qualities. The hydrogels used in bio-printing, while being able to support cells, do not have compatible mechanical properties for tissue applications. The citrate-based polymers investigated herein show mechanical properties that can be tuned via either chemical modification or modification to the crosslinking times and/or temperature. This tune-ability permits design of the bio-material to readily match a tissue application. Citrate based polymers also have good bio compatibility and release bio-active components during degradation.

In this project, we modified a commercially available 3D printer to permit it to print materials from solutions. Specifically, we converted the 3D printer into a microextrusion system that we used to screen materials, including the materials common to bio-printing, such as alginate and pluronic. The printer was then used to explore the printing of a citrate based polymer Poly(Octamethylene Citrate) (POC), a Calcium ion doped Poly(Octamethylene Citrate) (POCCa), and a Polycaprolactone (PCL), which served as the control material. A variety of printing inks were made to optimize the polymer to composite ratio, thereby enhancing the quality of the printed scaffolds. Pure polymers scaffolds of POC, POCCa, and PCL were printed as a baseline. This baseline was compared to the combination of two different composites mixtures, Hydroxyapatite (HA) and salt (NaCl), at concentrations relative to the polymer of 25%, 50%, and 75% by weight were added to the pure polymer formations to add necessary support during printing. As described herein, the composite component was shown to provide enough supporting structure to convert POC and POCCa from a non-viable printing material to a viable one.

## Project Aims

1. Modification of a commercially available FDM printer to perform as a micro-extrusion printer
  - i. Understanding of the dimensions and parameters of the 3D printer
  - ii. Design of the modification, and appropriate selection of proper conversion materials
2. Evaluation of the modified printers ability to print ink created from PCL, POC, and POCCa
  - i. Polymer Synthesis and Ink fabrication
  - ii. Initial assessments of inks
    - i. Extruded filament morphologies
    - ii. Rheological evaluation of inks
  - iii. Design of a 3D scaffold for evaluation of printability
  - iv. Printability Evaluation
    - i. Circularity measurements
    - ii. Area measurements
    - iii. Scanning Electron Microscope (SEM) layer analysis
3. Evaluation of printed scaffolds as a potential skin regeneration scaffold
  - i. Mechanical analysis of printed constructs
  - ii. Water vapor permeability of printed Constructs
  - iii. Water absorption
  - iv. Oxygen permeability of printed constructs

- v. SEM morphologies of printed constructs

## Chapter 2: Methods

### Polymer Synthesis

The goal of this work was to utilize a citrate-based biomaterial in an additive manufacturing process. To do this, poly (octamethylene citrate) (POC) was initially used in screening of the composite solution to aid in printability as POC is the basis for the majority of the Transformative Biomaterials and Biotechnology Lab (TBBL) thermoset biomaterials. Calcium ion doped poly (octamethylene citrate) (POC-Ca) was also investigated due to some unique properties that will be explored later in Chapter 3, Rheology section. Finally, polycaprolactone (PCL) was selected as a useful screen polymer due to its use in many tissue engineering fields, and its good printability.

#### POC

POC pre-polymer was synthesized from citric acid (CA) and octanediol (1,8)(OD) in a 1:1 ratio (Sigma Aldrich, St Louis, M). 0.1 moles of CA (19.212g) and 0.1 moles of OD (14.921g) were melted in a 100 mL round-bottom flask at 160 °C under stirring at 500 RPM for 10 minutes. The reaction flask was then removed from the oil bath and the temperature of the bath was reduced to 140 °C while ensuring that the melted solution was still being stirred following its removal, during which time it was held just over the bath. The flask of pre-polymer was returned to the oil bath once 140 °C was reached, stirring at 300 RPM. The stirring speed reduces as the viscosity of the pre-polymer melt increases and new chains form. Twitching of

the stir bar occurs once the viscosity is too high to stir, signifying that the speed needs to be reduced, first to 200 RPM, then to 100 RPM, and then finally to 80 RPM. Once the 80 RPM stir bar twitches the reaction is complete; 40 ml of 1,4-Dioxane is quickly added to dissolve the pre-polymer and the flask removed from the heat. After 24 hours stirring at room temperature the pre-polymer was purified by a precipitation procedure. Unreacted monomers were removed by precipitation in deionized (DI) water. The purified pre-polymer was then freeze-dried for 32 hours to remove any remaining solvent. Finally, the pre-polymer was dissolved at 50 wt% in ethanol.

#### POC-Ca

POC-Ca pre-polymer was synthesized from citric acid (CA) and octanediol (1,8)(OD) in a 1:1 ratio (Sigma Aldrich, St Louis, MO). 0.1 moles of CA (19.212g) and 0.1 moles of OD (14.921g) were melted in a 100 mL round bottom flask at 160 °C at 500 RPM for 10 min. The reaction flask was then removed from the oil bath and the temperature of the bath was reduced to 140 °C. Taking care that the melted solution is still stirring while removed, just over the bath. The flask of pre-polymer was returned to the oil bath once 140 °C was reached, stirring at 300 rpm. At this point, 0.02 moles Calcium Chloride Dihydrate (2.94 g) (Sigma Aldrich, St Louis, MO) was added in 10 ml DI water solution. The water is boiled off as the condensation reaction occurs. The subsequent reaction and pre-polymer processing is carried out identical to POC.

#### Polycaprolactone (PCL)

PCL was prepared from Polycaprolactone, Mn 70,000-90,000 (Sigma Aldrich, St Louis, MO). PCL was dissolved at the highest concentration possible in chloroform (Sigma Aldrich, St Louis, MO). Polymer concentration of 15 wt% was achieved for scaffold preparations.

## Printer Modification:

An Ultimaker 2 (DYNAMISM), was purchased for modification into a microextrusion based bio-printer. Printer modification was carried out in five steps, which are described in the following sections

1. Understanding Ultimaker's original design and assembly.
2. Testing of multiple extrusion methods.
3. Selection of extrusion method.
4. Design of pneumatic extrusion holder and set up.
5. Testing of pneumatic extrusion feasibility.

### Ultimaker's Original Assembly

The Ultimaker 2 in its native state is a fused deposition model (FDM) printer. Utilizing bipolar stepper motors capable of 200 steps/revolution, one for each axis (x,y,z), these motors allow for travel speeds from 30-300 mm/s. These motors permit accurate control of the nozzle placement at 12.5, 12.5, and 5 micron accuracies in the x,y, and z directions, respectively. One stepper motor controls the filament extrusion, which pushes a 3 mm filament through a pre-assembled nozzle head, of 0.4 mm diameter. The combination of this nozzle diameter and the motor controls allows for control of layer thicknesses between 20-200 microns. Other features available on this printer model include nozzle temperature control (80 °C - 260 °C) and build plate temperature control (50 °C – 100 °C). The print area allows for build volumes of 223 x 223 x 205 mm, and with overall dimensions of 342 x 493 x 588 mm. Figure 1 provides a general layout of the Ultimaker 2.

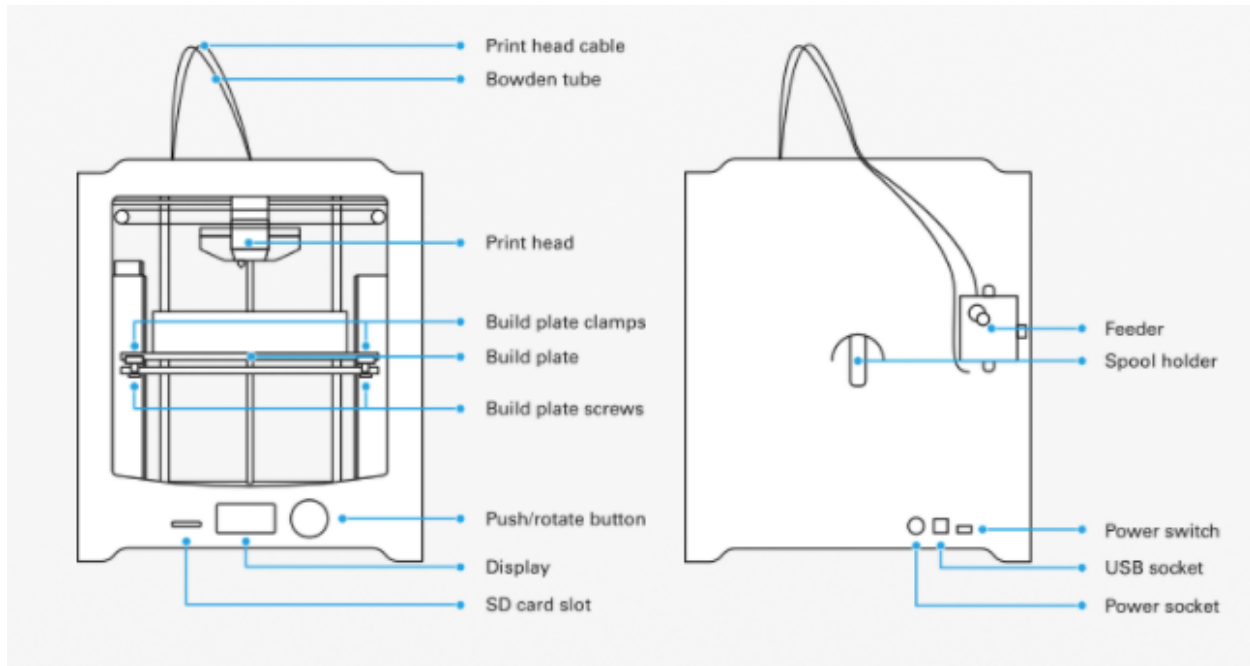


Figure 1, Ultimaker 2 general layout, (<https://ultimaker.com/en/products/ultimaker-2-plus/specifications>)

The build plate is suspended by a large screw controlled by a stepper motor. The build plate is a three-plate assembly, with two metal plates separated by screws to permit adjustment and leveling. The top metal plate is where a heating filament and temperature probe is laid to heat the third and top-most glass plate, which is the printing surface. Figure 2, provides a cross-sectional view from the side of the Ultimaker. Labeled are some key features of the Ultimaker assembly:

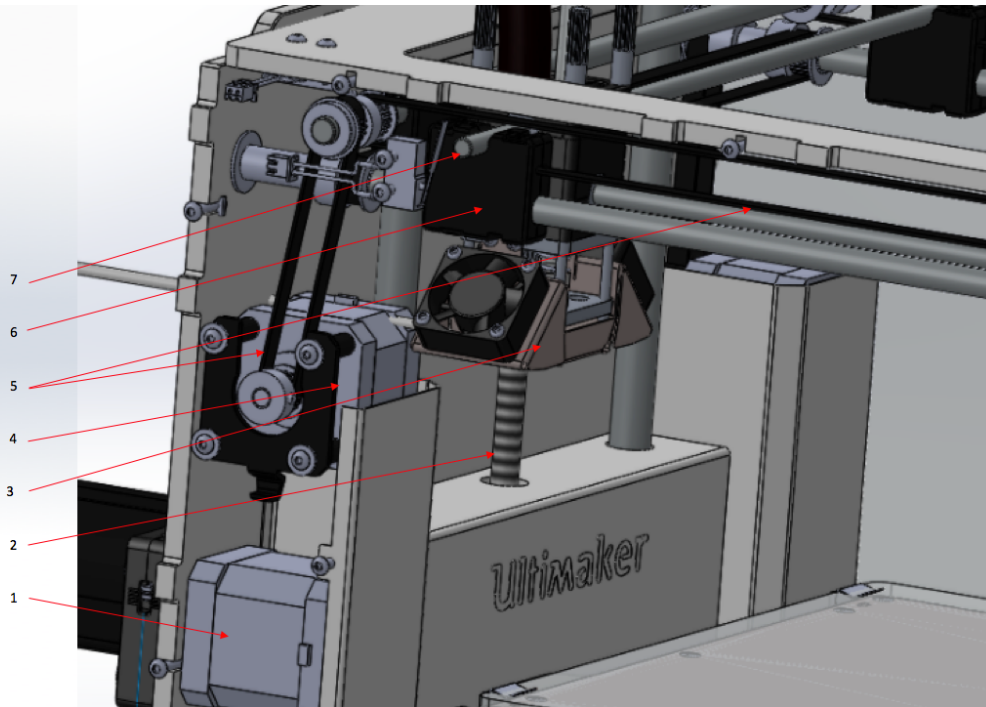


Figure 2, A cross-sectional view of the Ultimaker 2, showing the stepper motors and pulley system used to move and locate the print head (<https://grabcad.com/library/ultimaker-2-2>)

1. Stepping motor controlling the filament extrusion rate.
2. Z-axis screw: allows the build plate to be raised and lowered, controlled by a stepper motor at the bottom of the assembly.
3. Print head assembly: explained in more detail in Figure 3 and Figure 4.
4. Stepper motor that controls the y-axis printer head location using pulleys.
5. Pulleys to translate the motors rotational movement into traversing movement.
6. Pulley clamp adapter: attaches the pulleys to accompanying guiding rods to stabilize the movement.
7. X-axis guide rod that connects the printer head to the pulley assembly.

To allow a setup for microextrusion of solutions, the most modified part was the printer head assembly. In this application, a chamber with a dispensing method that applies some force on the solution needed to be attached or integrated onto the printer head assembly. So, the most attention should be paid to the Ultimaker extrusion head set up. Figure 3 shows a zoomed in model of the Ultimaker printer head assembly. The filament extrusion nozzle sits to the left of the printer head assembly and transverses through the printer head set up.

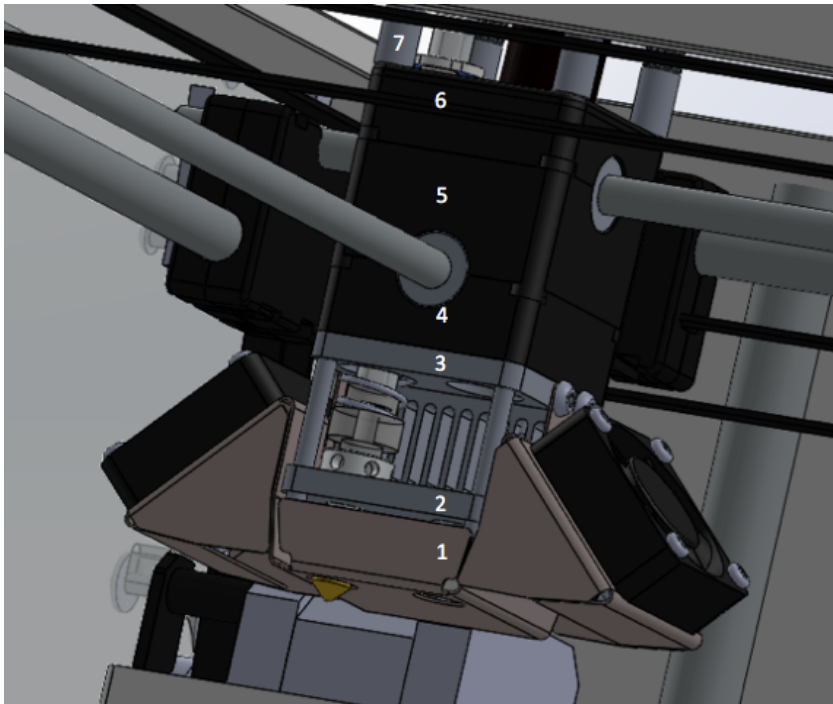


Figure 3 (files released by Ultimaker found on github), model assembly poster on Grabcad, by lilian monomax. (<https://grabcad.com/library/ultimaker-2-2>)

The printer head assembly, excluding the more detailed nozzle assembly, is composed of the following seven parts:

1. Fan holder and shroud: allows for filament cooling and keeps the printer head from giving off too much heat, which would cause the material to reach its glass transition temperature before extrusion, causing failure.
2. Nozzle head holder plate: Provides support to the nozzle head, cooling fan and radiator (not shown).
3. Top compression plate: Forces the assembly into a snug fit as a spring is placed between this plate and the nozzle holder plate to ensure tight assembly and seals the nozzle head assembly.
4. Print Head Bottom: holds the upper portion of the bearing for the y-axis control arm.
5. Print Head Middle: holds the lower portion of the bearing for the y-axis control arm and the upper portion of the x-axis control arm.
6. Print Head Top: holds the lower portion of the bearing for the x-axis control arm.
7. Finally, four long screws that travel from the top of part 6 all the way down to the threaded sections of part 1, clamping the springs, nozzle assembly, and bearing all together, forming the printer head.

While disassembling the printer it was decided that the approach to adapt the FDM printer to a microextrusion printer would be to create a bracket that allows a syringe to be mounted to the exterior of the printer head assembly. The bracket was designed by first assessing the dimension of the printer head assembly, shown in Figure 4, so that the bracket would have similar dimensions and fit seamlessly into the layout of the printer. This allows the printer the gain functionalities of a microextrusion printer, while also leaving in

place the native functionalities of the FDM printer. A FDM printer provides for rapid prototyping using PVA and other thermoplastic materials.

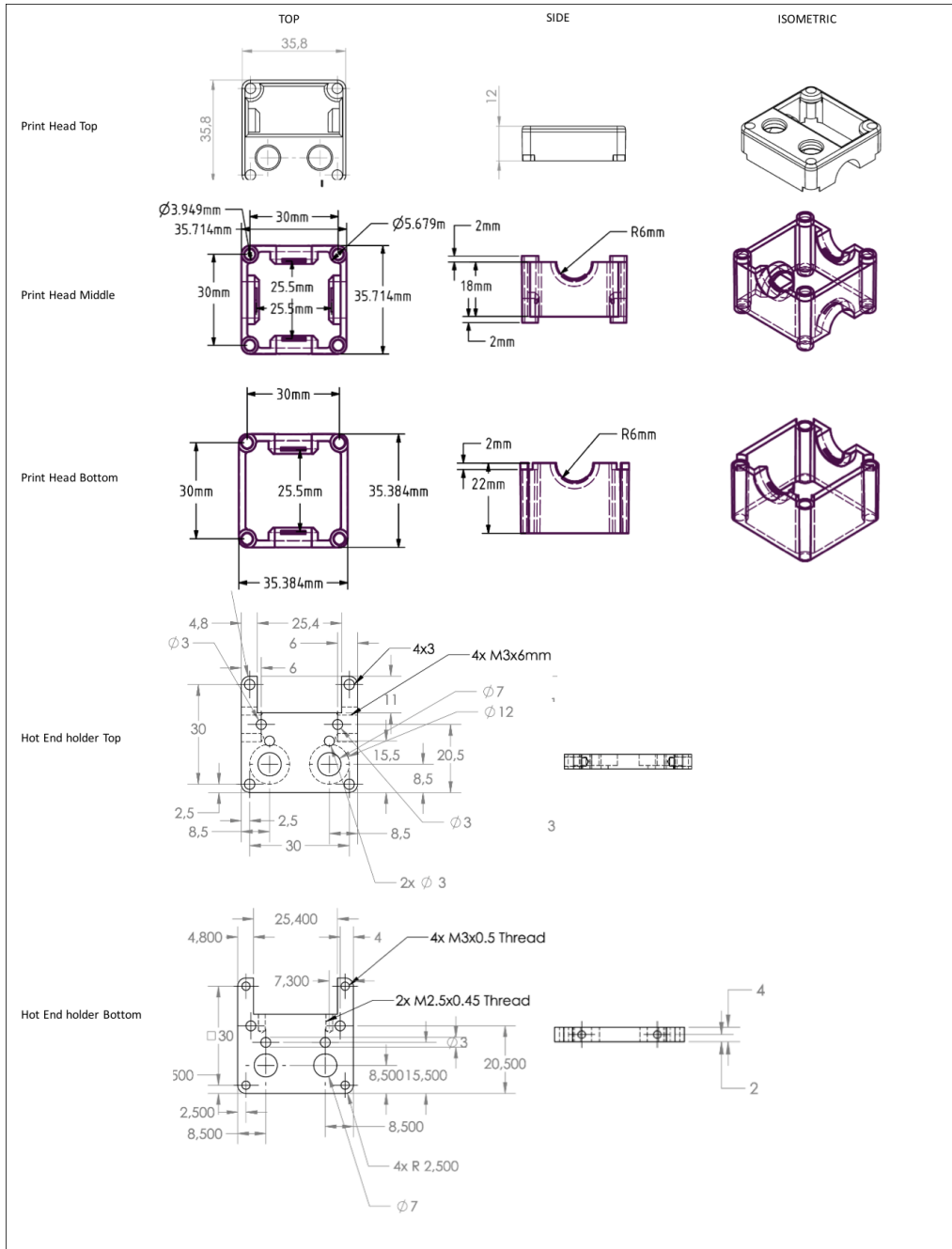


Figure 4 Blown out view of ultimaker 2 printer head files found at <https://github.com/Ultimaker/Ultimaker2>

## Modification

Modification of the final printer design was carried out as follows. The first step was to create a bracket for the printer head. The dimensions shown in Figure 4 were taken into consideration and a 5 mL syringe mounting bracket was designed to fit in between the print head bottom part and the hot end top part. The design is shown in Figure 5, and a final assembly is shown in Figure 6.

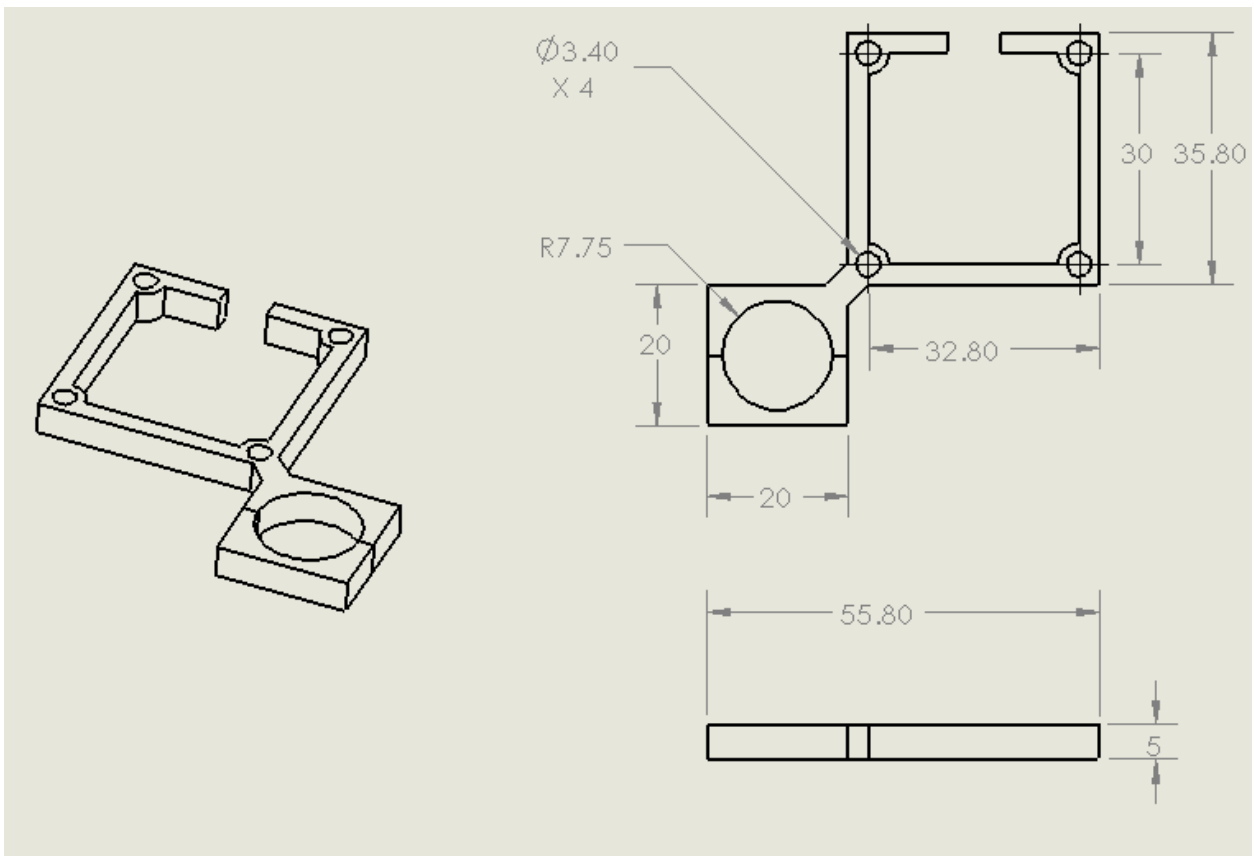


Figure 5: Schematic of syringe holding bracket (mm)

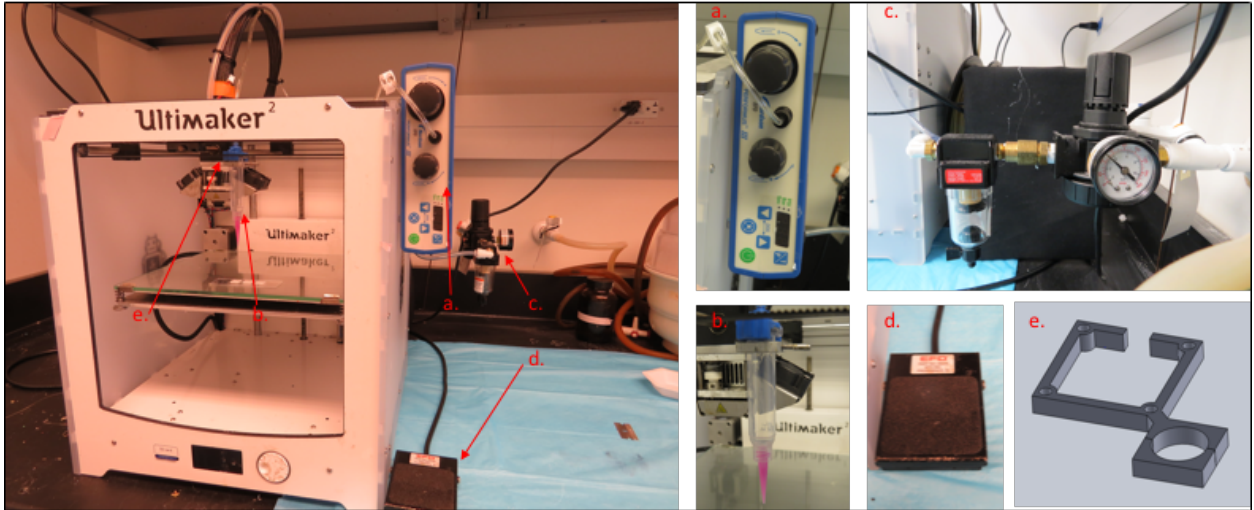


Figure 6: Shows the completely modified Ultimaker 2, a: Norson Efd proformus III, pneumatic dispense and air regulator; Norson 5ml syringe, c: Pressure regulator and air filter, d: pneumatic actuator pedal, e. adapter plate.

The full final assembly of the modified Ultimaker 2 consists of a 5ml syringe bracket mounted to the existing printer head with tubing and gaskets connecting the syringe to the EFD Norson Proformus III, a pneumatic actuator that controls air pressure into the syringe. This design keeps a consistent extruding force on any inks loaded into the syringe. The Proformus was connected to an air filtration system to keep any debris from damaging the actuator, and to another manual air pressure regulator, which receives and down-regulates the native air pressure lines in the building.

With printer modification complete, the evaluation of the new modification along with testing of the feasibility of printing a mixture was carried out. First, a viable scaffold design to test the printability was constructed, as described in the next section.

## Test Procedure, Testing Matrix

In Table 2 Test Matrix, is a testing matrix's that outlines all the ink composite formulations, along with all the tests that were performed on each ink composition.

Table 2 Test Matrix

Tests Performed	PLA	PLC						POC						POCCa								
		Pure	Salt			HA			Pure	Salt			HA			Pure	Salt			HA		
			25	50	75	25	50	75		25	50	75	25	50	75		25	50	75	25	50	75
Filament Morphology	Tested	Tested	Tested	Tested	Tested	Tested	Tested	Tested	Tested	Tested	Tested	Tested	Tested	Tested	Tested							
Percent Holes Printed	Tested	Tested	Tested	Tested	Tested	Tested	Tested	Not Tested	Tested	Tested	Tested	Tested	Tested	Tested	Not Tested							
Area	Tested	Tested	Tested	Tested	Tested	Tested	Tested	Not Tested	Tested	Tested	Tested	Tested	Tested	Tested	Not Tested							
Circularity	Tested	Tested	Tested	Tested	Tested	Tested	Tested	Not Tested	Tested	Tested	Tested	Tested	Tested	Tested	Not Tested							
SEM imaging	Tested	Tested	Tested	Tested	Tested	Tested	Tested	Not Tested	Tested	Tested	Tested	Tested	Tested	Tested	Not Tested							
Rheology, Viscosity	Not Tested	Tested	Not Tested	Tested	Not Tested	Not Tested	Not Tested	Not Tested	Tested	Not Tested	Tested	Not Tested	Not Tested	Not Tested	Not Tested							
Rheology, Amplitude Sweep	Not Tested	Tested	Not Tested	Tested	Not Tested	Not Tested	Not Tested	Not Tested	Tested	Not Tested	Tested	Not Tested	Not Tested	Not Tested	Not Tested							
Tensile Strength	Not Tested	Tested	Not Tested	Tested	Not Tested	Not Tested	Not Tested	Not Tested	Tested	Not Tested	Tested	Not Tested	Not Tested	Not Tested	Not Tested	Tested	Not Tested	Tested	Not Tested	Not Tested	Not Tested	Not Tested
Initial Modulus	Not Tested	Tested	Not Tested	Tested	Not Tested	Not Tested	Not Tested	Not Tested	Tested	Not Tested	Tested	Not Tested	Not Tested	Not Tested	Not Tested	Tested	Not Tested	Tested	Not Tested	Not Tested	Not Tested	Not Tested
% Strain	Not Tested	Tested	Not Tested	Tested	Not Tested	Not Tested	Not Tested	Not Tested	Tested	Not Tested	Tested	Not Tested	Not Tested	Not Tested	Not Tested	Tested	Not Tested	Tested	Not Tested	Not Tested	Not Tested	Not Tested
WVT	Not Tested	Tested	Not Tested	Tested	Not Tested	Not Tested	Not Tested	Not Tested	Tested	Not Tested	Tested	Not Tested	Not Tested	Not Tested	Not Tested	Tested	Not Tested	Tested	Not Tested	Not Tested	Not Tested	Not Tested
Water Absorption @ Day 10	Not Tested	Tested	Not Tested	Tested	Not Tested	Not Tested	Not Tested	Not Tested	Tested	Not Tested	Tested	Not Tested	Not Tested	Not Tested	Not Tested	Tested	Not Tested	Tested	Not Tested	Not Tested	Not Tested	Not Tested
Oxygen Permeability	Not Tested	Tested	Not Tested	Tested	Not Tested	Not Tested	Not Tested	Not Tested	Tested	Not Tested	Tested	Not Tested	Not Tested	Not Tested	Not Tested	Tested	Not Tested	Tested	Not Tested	Not Tested	Not Tested	Not Tested

## Scaffold Printing and Preparation: Printability Assessment

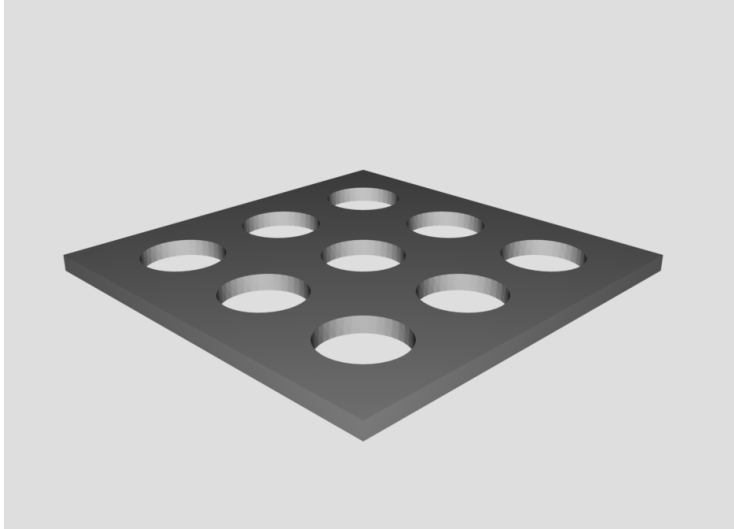
Ink compositions were tested by printing scaffolds with a known shape and size. The selected scaffold design was a 12mm x 12mm sample, with a thickness of 0.4 mm, as shown in

fig 7. The scaffold was designed to have 9, 2mm diameter holes through the scaffold. First the scaffold design was created in SolidWorks®, a computer aid design (CAD) modeling software. The designed scaffold was then exported as an STL (StereoLithography) file, also known as the standard triangle language. This file type was read by Ultimaker native processing software to create a g-code, a machining programming language that instructs the different motors when they should turn, how long to spin, how fast to spin, and what path to follow. Once the g-code was prepared, the composite mixtures were loaded into the syringe and printed.

The following constraints on the printer that were held consistent to eliminate variation between samples:

- nozzle diameter and shape (0.6mm, conical plastic nozzles),
- initial print bed height of 0.2 mm,
- step size of 0.2 mm, print speed of 10 mm/sec,
- room temperature heat bed and nozzle.

Three scaffolds were printed for each composite onto a glass slide. These three separate scaffolds had, in total, 27, 2 mm diameter holes. Two layers were printed resulting in an ideal scaffold height of 0.4 mm. After printing the POC/POC-Ca scaffolds were set in an oven to be crosslinked at 80 °C for 48 hours. This thermal treatment locks in the geometries for the POC/POC-Ca thermoset. PCL is a thermoplastic, so after printing the chloroform was left to evaporate in a fume hood, thereby returning the thermoplastic to a solid.



*Figure 7 Printability Scaffold Design, created using SolidWorks®.*

## Printability Evaluation

Printability was evaluated using a variety of tests. When evaluating new bio-inks for printability, it is important to have a good understanding of the ink properties before and after printing. To get a better understanding of the ink properties before printing, the bio-ink concentrations were evaluated, and rheological experiments were conducted. The inks were then manually extruded through the selected nozzle size to demonstrate that a solid filament can be formed. Scaffolds were then designed and used to assess the printability of each ink composition. Once the scaffolds were completed and crosslinked, samples were imaged using optical microscopy and SEM. The morphologies were evaluated, and circularity and area calculations were performed on each of the 27 holes.

## Ink Compositions

Ink compositions were composed of three materials: PCL, POC, and POC-Ca. Three additives were evaluated for printability: Pearl Powder, Hydroxyapatite, and Sodium Chloride. All additives were sifted through a 53  $\mu\text{m}$  sieve to ensure no aggregates would clog the printer nozzle. Multiple composite compositions were created to test their printability. Each pure polymer was tested along with each composite at concentrations of 25, 50, and 75 wt% to polymers. The concentrations of the polymers were held constant to limit variation. PCL was held at a 15 wt% concentration in chloroform, and POC/POC-Ca was concentrated from the initial 50 wt% concentration to 80 wt% concentration by evaporation in a still air environment for 12 hours. The polymer was then added slowly to the respective composite component and stirred to ensure even mixing and loaded into a 5ml syringe to be extruded by the printer.

## Rheology:

Rheological measurements were performed using a MCR 302 rheometer (Anton Paar, Ashland, VA, USA) with a 25 mm diameter cone-plate geometry and an angle of  $1^\circ$ . A constant temperature of  $25^\circ\text{C}$  was used. Amplitude sweep was conducted at a constant frequency of 1 Hz at a strain range from 0.01% to 100%. A rotational test (flow and viscosity curve) was carried out at a shear rate range from 0.01/s to 1000/s. The duration between each data point was decreased logarithmically from 100 s to 2 s.

## Filament Morphology:

Filament morphology was evaluated by visual observation of manually extruded inks. The inks should demonstrate clear filament formation, with good circular cross-section and no beading or falling back on itself. Filament morphology was observed qualitatively and given a

rating of 1-4, where one represents a bad morphological filament and a 4 represents a printable filament. Here “printable” is defined as a filament an even filament that doesn’t run or clump up, and maintains a similar diameter to that of the nozzle diameter.

#### Circularity and Area Evaluation:

Circularity was evaluated after crosslinking and curing was completed. Scans were taken using an Ethos Microscope at 1x magnification. ImageJ was used to evaluate the circularity and area of the printed pores. Circularity ( $f_{circ}$ ) is a common shape factor analysis method, which is a function of the perimeter (P) of a shape and the area (A), shown in eqn 1.

$$f_{circ} = \frac{4\pi A}{P^2} \quad (1)$$

A true circle has the highest circularity ( $f_{circ} = 1$ ) while more rectangular shapes will have  $f_{circ}$  values closer to zero. More favorably composed inks will exhibit higher circularity.

To further evaluate the printability of the ink compositions the area of the pore geometries was also quantified, using Image J. The theoretical area of each pore was calculated using eqn. 2 (below).

$$A = \pi r^2 \quad (2)$$

where A is the area of each pore and r is the pore radius. For the perfect printed scaffold the area of the pore will be  $3.14 \text{ mm}^2$ , as the radius of the designed pore was 1 mm. Area was evaluated in addition to circularity because if the ink composition was too thin or contracted during crosslinking the measured areas will tend to be greater than  $3.14 \text{ mm}^2$ . Conversely, if

the ink composition experiences any expansion or running together the area will tend to be less than  $3.14 \text{ mm}^2$ .

In ImageJ, analysis tools permits the user to set thresholds so that the program focusses on analysis of the pore shapes shown in . ImageJ evaluates the threshold areas based on the number of pixels present in an image. A scale is used to relate a distance to the number of pixels present. The software then calculates threshold areas, perimeters, and circularity, while also counting the number of separate areas corresponding to each pore printed. From this information evaluations can be made of the number of successfully printed pores as well as the distribution of actual areas and circularity exhibited by these pores.

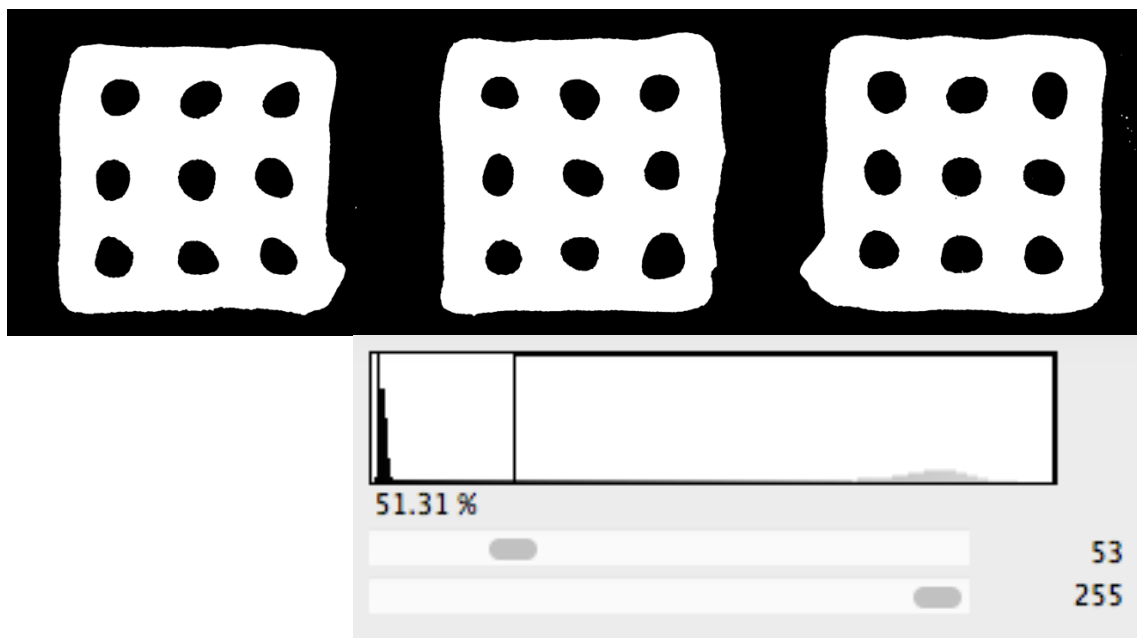


Figure 8 Example of threshold boundaries, boundaries set so the pore morphology was distinct

SEM Morphologies:

Scanning electron microscopy (SEM) (FESEM: Zeiss Sigma) was used extensively in the printability evaluation to determine scaffold morphology, pore morphology, and structural

features of composite printed scaffolds. Representative scaffolds from each printed group were selected for imaging. To permit imaging in the SEM, these samples were coated with gold using a sputter coater (Quorum EMS 150 sputter Coater) prior to imaging.

## Printed Skin Scaffold Evaluation:

### Ink Preparation

Inks were prepared from 50% polymer solution in ethanol for POC and POCCa. These were left to dry in still air conditions for eight hours during the preparation of porous scaffolds (i.e. salt composite inks) and for 12 hours for pure polymer inks. Then, 50% salt by weight was added to the polymer and stirred until the ink composition was homogeneous. For the PCL ink composition, a 15% concentration of PCL in chloroform was used, adding 50% salt by weight to the polymer solution and stirring until the mixture was observed to have approximately the same viscosity of the POC and POCCa compositions. Based on the rheological experiments carried out in the printability evaluation this viscosity is approximately 100 Pa\*s.

### Scaffold Fabrication: Application assessment

Scaffold fabrication was performed using the modified Ultimaker 2 3D printer. The scaffold design was created in SolidWorks® then exported as a STL file, which was then converted in CURA, Ultimaker's development software for converting stl files into Ultimaker's g-code. Skin scaffolds were designed to have 2 mm diameter pores in a 12 x 12 array centered on a 50 mm scaffold mesh (see Figure 9). To eliminate some variation between samples, some

printing parameters were held consistent. Once all the parameters in the printer were established, the ink formulations were loaded into 5 ml syringes and attached to the Norson Proformus III pressure regulator. The STL file was then run; a consist pressure of 15 psi was used for extrusion of the ink onto the print bed surface. Printed meshes were then left to air dry for 48 hours and then crosslinked for 48 hours at 80 °C. Finally, porous constructs (i.e., those printed with salt) were leached over three days with regular water changes, to leave behind only a highly porous 3D printed mesh. The resulting meshes were then freeze dried to remove any excess water present in the meshes. This process was also repeated for scaffolds created to support mechanical testing, water absorption, oxygen permeability, and water vapor permeability testing.

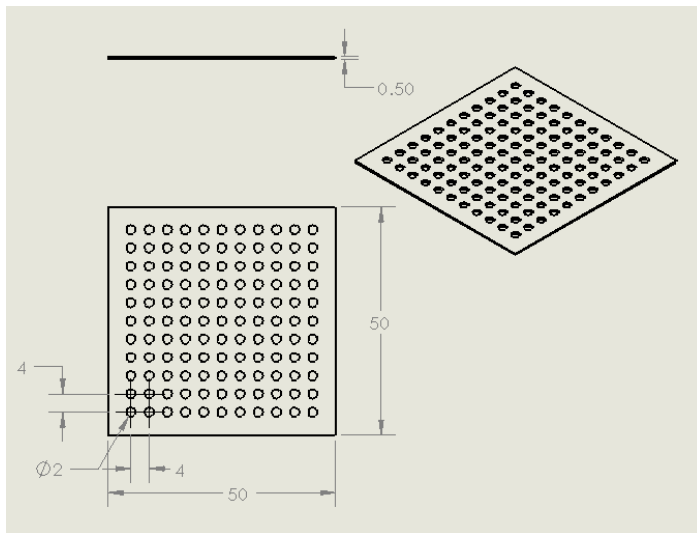
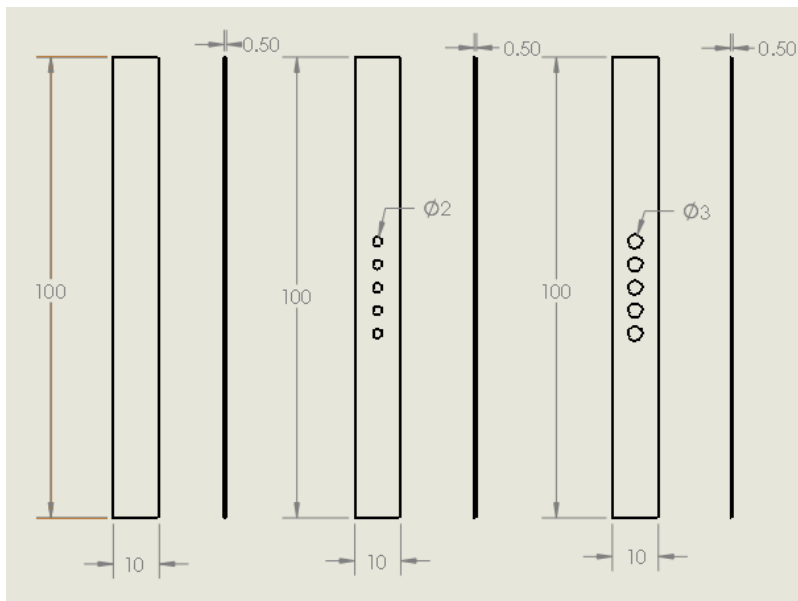


Figure 9 Highly porous printed scaffold constructs for wound dressings

## Mechanical

Mechanical testing of printed films and scaffolds was conducted using an Instron Mechanical Tester (model 5966, Norwood, MA) and in accordance with the operation procedure of ASTM D882-12 [67]. Both cast and printed samples were tested. Cast samples were cut into 10 mm x 100 mm strips, and printed samples were printed to the same dimensions. Scaffolds and films were also prepared with varying large pore dimensions, shown in Figure 10.



*Figure 10 design of printed mechanical meshes*

Varying pore sizes were created to evaluate the effects of pore geometry on the mechanical integrity of the films.

To quantify variation, sample thicknesses and widths were measured before each test. Samples were elongated to failure at a crosshead speed of 500 mm/min using a 1KN load cell. The Instron software records grip separation displacement (strain) and the load on the

material. From this information the applied engineering stress can be calculated as the product of load and initial cross-sectional area. The Instron operation software records data including specimen dimensions, load, grip separation, elongation, strain and stress. Graphs were created to show the peak stress (MPa), initial modulus (MPa), and percent of elongation at break.

#### Water Vapor Permeability

Scaffolds created for water vapor permeability did not have any manufactured holes, as through thickness holes would promote a very large water vapor transmission rate, and the goal of this test was to quantify the rate of water vapor transmission (WVT) through the scaffold.

The goal of this testing procedure is to determine the water vapor transmission of materials. WVT determines how much water is able to pass through a certain material, which is referred to as permeability. Water Vapor Transmission is defined as “the time rate of water vapor transmission through unit area of flat material of unit thickness induced by [the] unit vapor pressure difference between two specific surfaces, under specified temperature and humidity conditions.” [68].

Our testing procedure followed ASTM standard E96M-16, utilizing the water vapor permeability method, and SI units [67]. As laid out in the ASTM standard, testing was conducted in a chamber controlled to stay at 35 °C and a relative humidity of 50%. A standard test cup (EZ-Cup Vapometer Permeability Cup, Thwing-Albert Instrument Company) has an opening of 50.8 mm (3 in) and a depth of 19.05 mm, with a lipped edge with a threaded top piece having the same 50.8 mm opening permitting the film to be clamped down onto the cup surface.

A glycerol/DI water solution is placed in the sealed chamber to maintain a controlled 50% relative humidity. The glycerol/DI water solution is held in an uncovered shallow pan with a large exposed surface area. The composition of glycerol solution is calculated as follows [69]:

$$SG = [-0.189(RH) + 19.9]^{0.0806} \quad (2)$$

where SG is the specific gravity of the glycerol/water solution and RH is the relative humidity in the chamber. Following eqn 5,  $G_w$  is the glycerol by weight needed to create a solution needed to reach the relative humidity desired,

$$G_w = 383(SG) - 383 \quad (3)$$

the volumes of glycerol and water are calculated in 6 and 7 respectively.

$$G_v = \frac{G_w * W_t}{100 * 1.262} \quad (4)$$

$G_v$  is the volume of glycerol needed for the relative humidity solution.  $W_t$  is the total desired weight of the solution.

$$H_v = \frac{(100 - G_w)W_t}{100 * 1} \quad (5)$$

$H_v$  is the volume of DI water in mL. The solution is finally placed in a chamber to keep the chamber at the desired humidity.

## WVT Procedure

The chamber was given sufficient time to reach the final humidity. During this time samples were prepared. The test cup with  $\frac{1}{4}$ " (30 mL) of water, leaving a  $\frac{1}{8}$ " gap from the film to the water surface was prepared. Following the manufacturer instructions, the sample was placed into the dish and securely sealed with the threaded top piece. The dish assembly was weighed and placed in the test chamber.

The dish assembly was weighed at the predetermined time intervals. At each weighing, time, relative humidity, temperature, and pressure were recorded. Weighing was accomplished by removing the dish assembly from the test chamber and returning it to the test chamber after recording its weight.

## Data Processing

At least 8 measurements for each test specimen were recorded; weight vs elapsed time was plotted, along with a trend line. A steady state was assumed to exist when periodic weight changes matched or exceeded 20% of the multiple of 100 times the scale sensitivity. The slope of the straight line on this graph quantifies the rate of water vapor transmission (g/t) Shown in Figure 11, graphical representations of steady state water transmission .

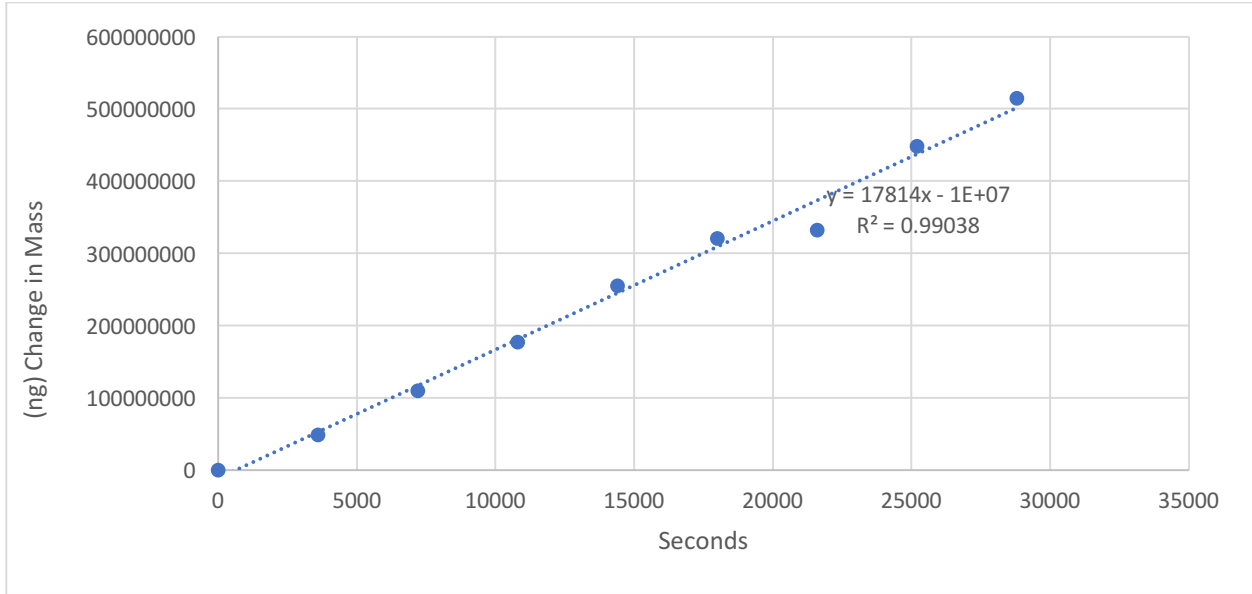


Figure 11, graphical representations of steady state water transmission

Water vapor transmission and Permeance were calculated as follows:

$$WVT = \frac{G/t}{A} \tag{6}$$

where G= weight change, gain (from the straight line, steady state plot), t = time during which G occurred. (G/t) = the slope of the straight line, A = area (cup mouth opening). Unit conversion was performed to get data into a presentable a comparable data range.

$$WVT \left( \frac{g}{m^2 \cdot day} \right) = \frac{G}{t} * \left( \frac{86400}{10^9} \right) \tag{7}$$

Finally, the materials tested, while designed to be the same thickness, in practice vary in thickness. To account for this variation an assumption was made that if the material thickness was double, the permeability would be halved. Consequently, all data sets were normalized to correspond to the thickest sample. By figuring out the ratio of thickness between the thickest sample/ thinner samples. This ratio was then divided by the permeability found during testing to normalize each result, permitting presentation of all results in a consistent manner.

## Oxygen Permeability

Oxygen permeability was carried out by collaborators in the Chemical engineering department here at The Pennsylvania University, State College. Xueyi Zhang and his students tested the oxygen permeability of our materials with there in house designed gas separation unit.

## Chapter 3: Results

### Filament Morphology

Filament morphology was observed by manual extrusion of the prepared ink, looking for consistent filament morphology, while checking to see if the ink composition runs thin or thick. The ability of the filament to maintain a diameter as close to the nozzle diameter as possible while not beading or curling is important for consistent and repeatable printing. Examples of extruded filaments are shown in Figure 12.

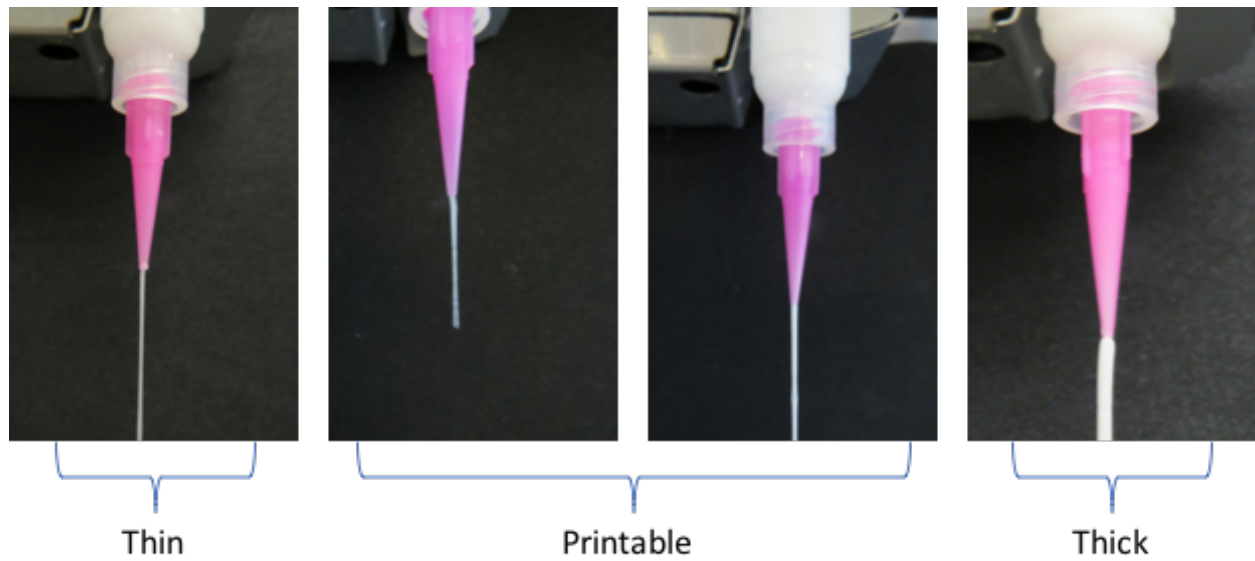


Figure 12 evaluations of extruded filament morphology, if the samples runs thick or thin morphologies of the printed part will be loss

## Rheology

Rheological testing was performed to evaluate any ink phase changes that may occur during extrusion of the bio-inks. Amplitude sweep curves were performed using the MCR 302 rheometer where the shear rate of the spindle was changed over time. The instrument outputs the Storage Modulus ( $G'$ ) and Loss Modulus ( $G''$ ). The storage modulus represents the current amount of stored energy in the solution, while the loss modulus measures the energy dissipated in heat, representing the viscous portion of the solution. Results for the amplitude sweep data are shown Figure 13. Amplitude sweep curves give insights into the state of the solution and any changes that can occur to it during the printing process.

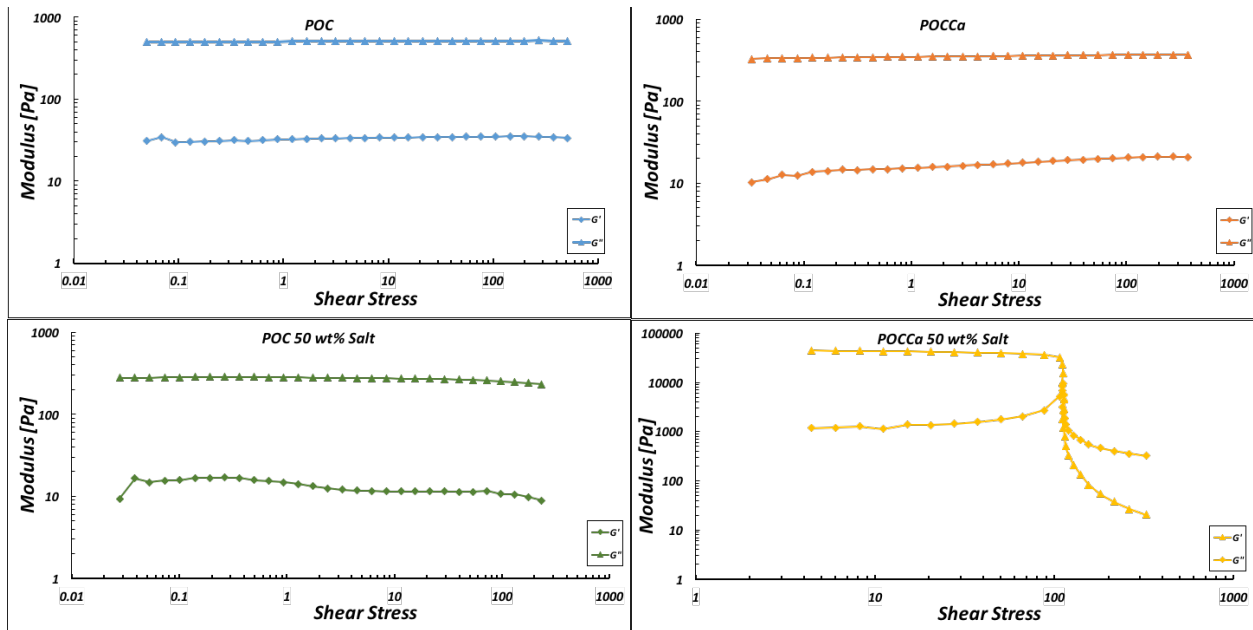


Figure 13, MCR 302 rheometer amplitude sweep, 25 mm diameter cone-plate geometry and an angle of  $1^\circ$ . A constant temperature of  $25^\circ\text{C}$ , Frequency of 1 Hz at a strain range from 0.01% to 100%

Shear stress ramp measurements were also run. Viscosity measurements were utilized to compare bio-inks and look for similarities between compositions. The shear stress ramp curves also give insight to any yield stress in the material (this would be shown by a sharp drop in viscosity). The data for the shear ramp is shown in Figure 14.

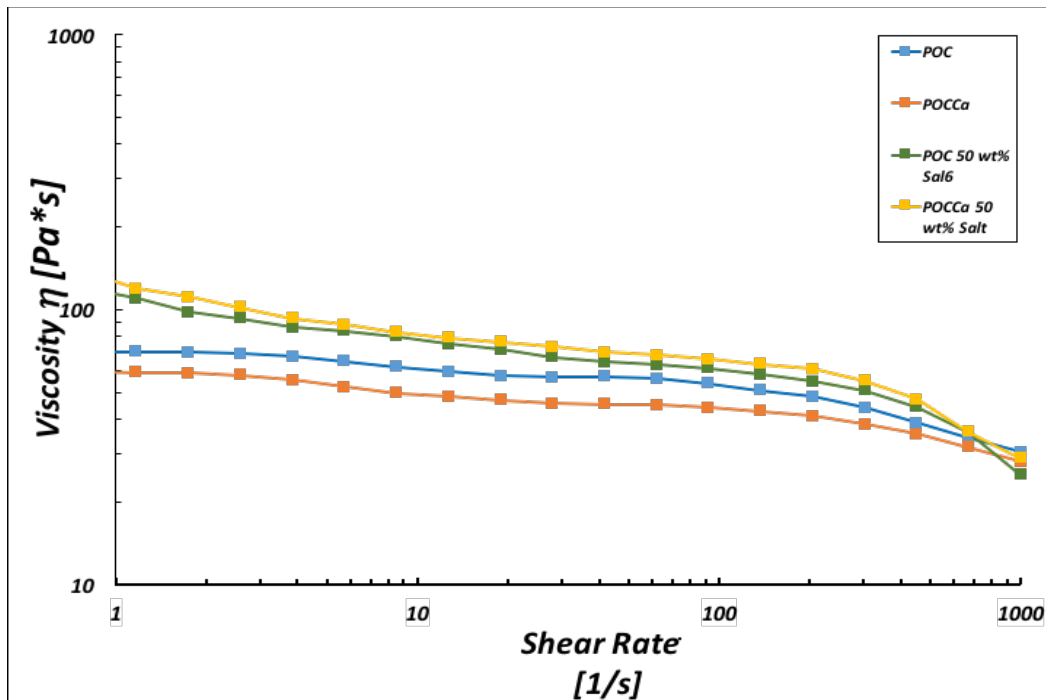


Figure 14, MCR 302 rheometer Viscosity cure, Shear rate range from 0.01/s to 1000/s

## Circularity and Area

The circularity and area of printed scaffolds was evaluated from the scanned images of printed constructs after crosslinking and drying. Scanned images from the Ethos microscope appear in Figure 15. ImageJ was used to count the number of successfully printed holes. An initial screening of results was performed, retaining only ink compositions that printed with a success rate on hole creation exceeding 85% for further evaluation. As shown in Figure 15 and Figure 16, out of 20 inks (65%) exceeded this threshold. The 14 successful inks / printed constructs were evaluated for circularity and area and analyzed using ImageJ threshold manipulation to gather the results, as shown in Figure 16 and Figure 18.

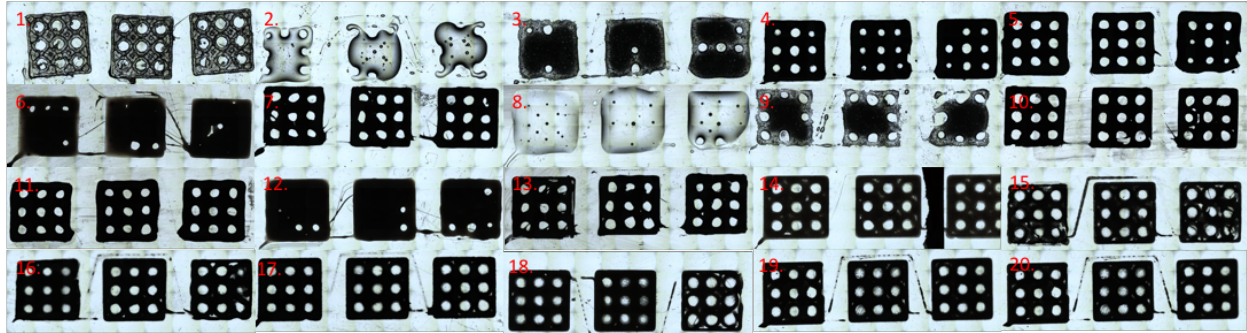


Figure 15: 1. PLA, 2. POC, 3. POC 25% Salt, 4. POC 50% Salt, 5. POC 75% Salt, 6. POC 25% HA, 7. POC 50% HA, 8. POCa, 9. POCa 25% Salt, 10. POCa 50% Salt, 11. POCa 75% Salt, 12. POCa 25% HA, 13. POCa 50% HA, 14. PCL, 15. PCL 25% Salt, 16. PCL 50% salt, 17. PCL 75% Salt, 18. PCL 25% HA, 19. PCL 50% HA, 20. PCL 75% HA

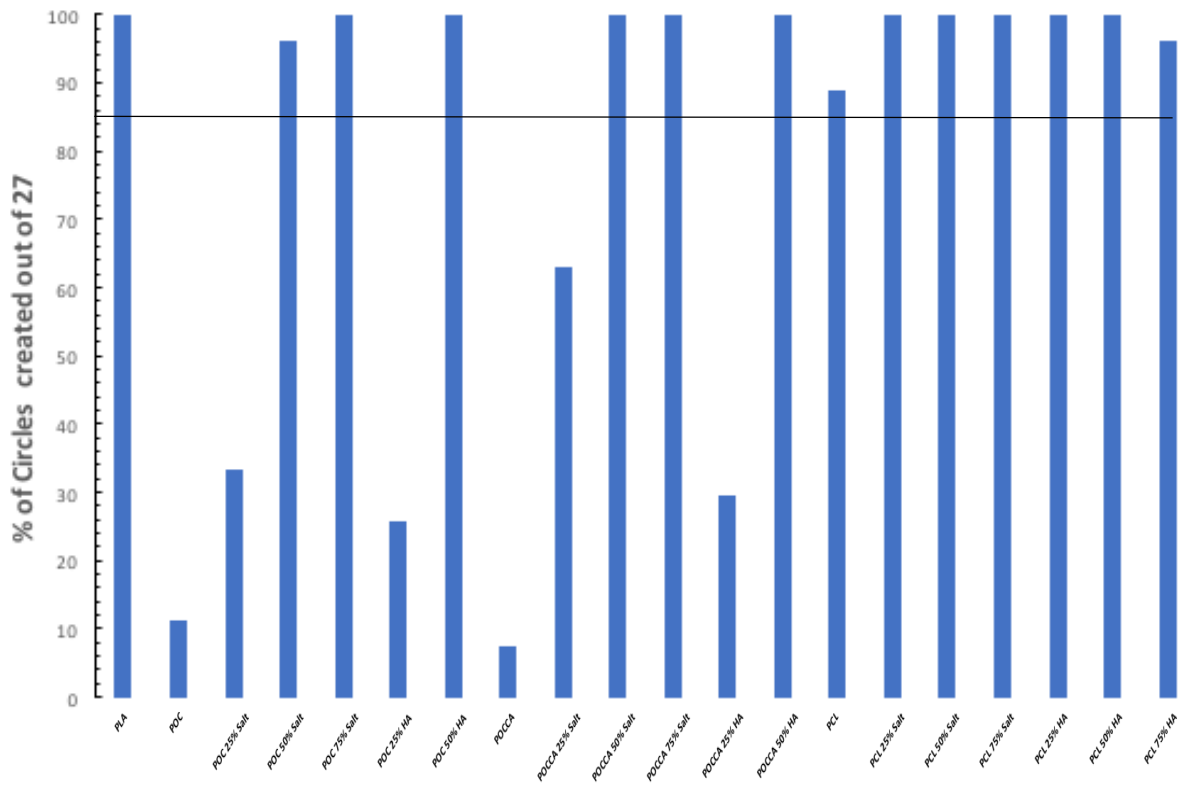


Figure 16 Percentage of successfully printed holes, the horizontal line indicates the success rate (85%) for further evaluation

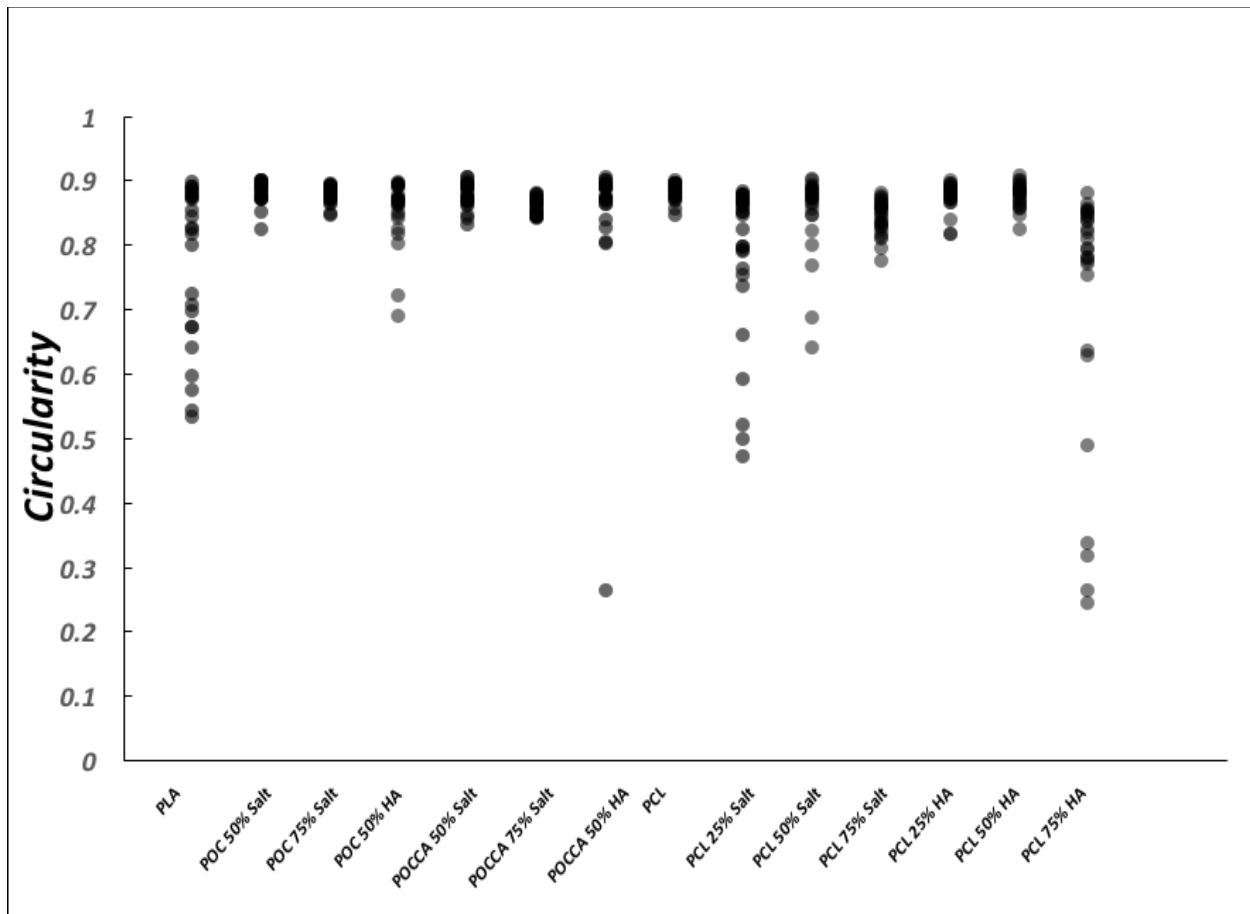


Figure 17 Distribution of Cicularity for printed holes, values closer to 1, indicate greter circularity.

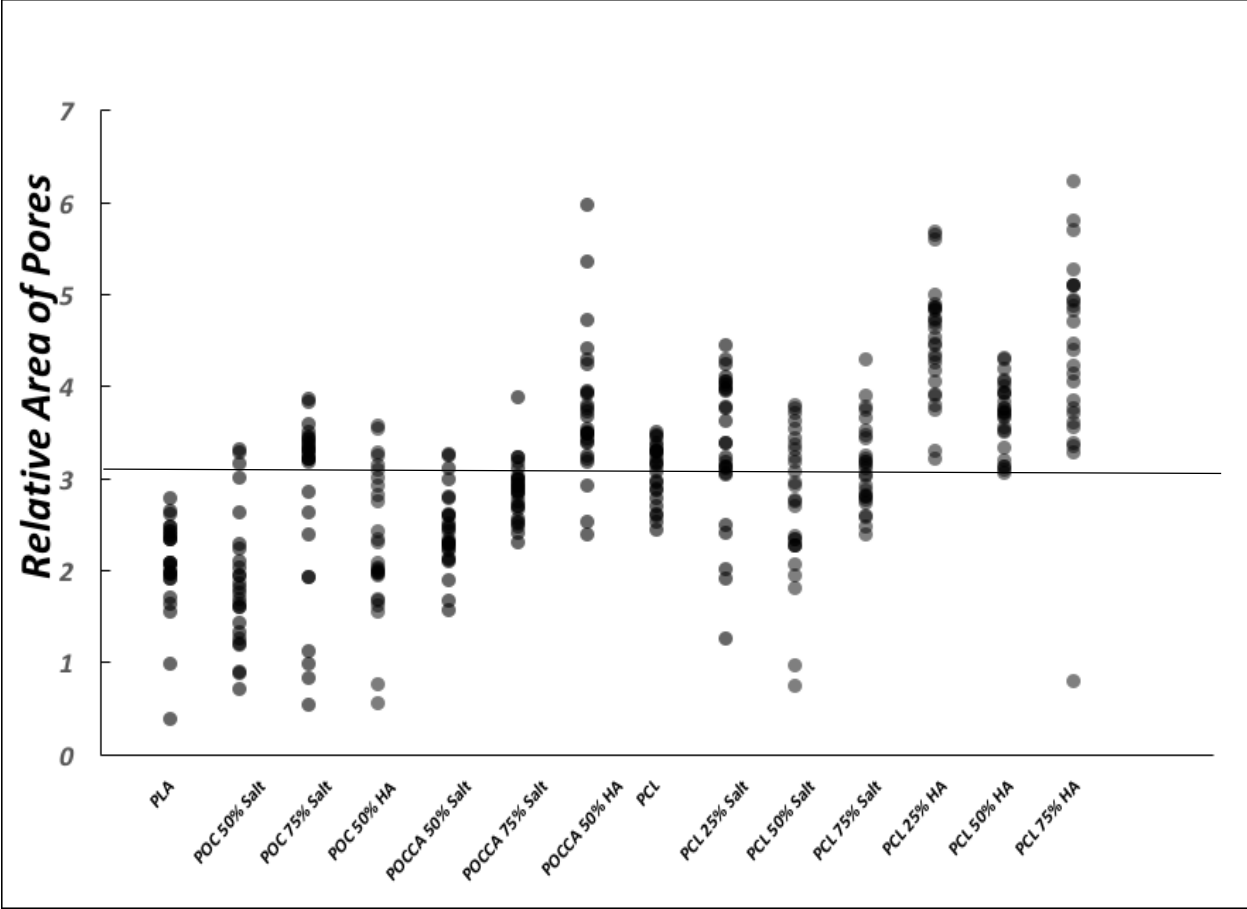


Figure 18 distribution of the areas of each pore from printed constructs, theoretical area of  $3.14 \text{ mm}^2$  is shown by the horizontal line

Table 3, evaluation of area of the printed holes and circularity of the printed holes

Sample	Area	Area % error	Curcularity	Circularity % Error
PLA	2.07 ± 0.51	34.17	0.78 ± 0.12	22.12
POC 50% Salt	1.87 ± 0.73	40.33	0.88 ± 0.02	11.69
POC 75% Salt	2.82 ± 0.96	10.04	0.88 ± 0.01	12.12
POC 50% HA	2.3 ± 0.78	26.7	0.85 ± 0.05	14.61
POCCA 50% Salt	2.43 ± 0.42	22.72	0.88 ± 0.02	12.11
POCCA 75% Salt	2.86 ± 0.32	8.96	0.86 ± 0.01	13.96
POCCA 50% HA	3.74 ± 0.76	18.96	0.85 ± 0.12	14.76
PCL	3.06 ± 0.32	2.59	0.88 ± 0.01	11.78
PCL 25% Salt	3.37 ± 0.8	7.25	0.78 ± 0.12	21.79
PCL 50% Salt	2.72 ± 0.8	13.41	0.85 ± 0.06	14.79
PCL 75% Salt	3.13 ± 0.47	0.19	0.84 ± 0.03	15.61
PCL 25% HA	4.49 ± 0.63	43.1	0.88 ± 0.02	12.48
PCL 50% HA	3.69 ± 0.36	17.45	0.88 ± 0.02	12.29
PCL 75% HA	4.68 ± 1.89	49.16	0.71 ± 0.2	29.05

Calculations were done to determine the percent error to the theoretical values of a perfect printed construct. If a perfect construct was printed it would have an ideal circularity value of 1 and an ideal area value of  $3.14 \text{ mm}^2$ . Table 3 presents the percent error of the mean area and circularity values of the 13 scaffolds that exhibited a pore success rate exceeding 85%.

## SEM morphologies

Scaffold morphology was evaluated by SEM imaging and was analyzed to compare the theoretical design parameters of the composite inks. All salt compositions were leached, revealing their pore structures. Morphologies of printed constructs are shown in Figure 19 through Figure 39. SEM imaging was used to evaluate the structure of the printed constructs, check for deformation in the print, look for un-intentional air pockets, and to examine the pore architecture and the layer geometries. During the qualitative analysis of the SEM images

important observations were made regarding pore morphology of the micro pores, circularity of the printed macro holes, and if two clear layers were formed by the ink composition.

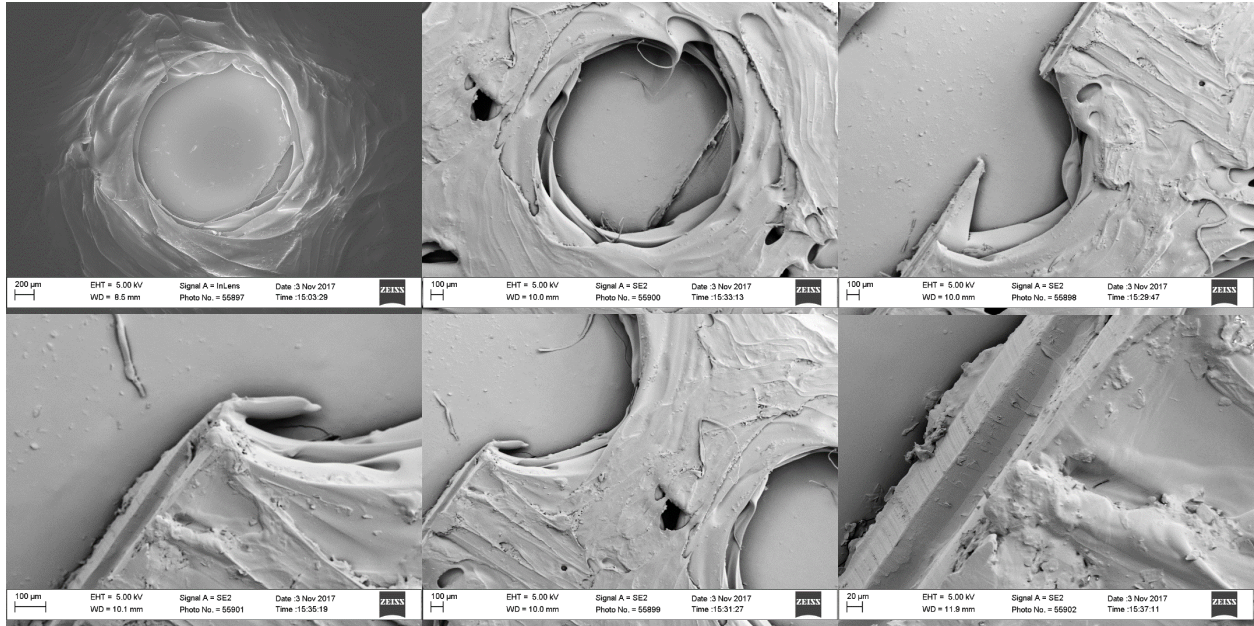


Figure 19: SEM Image of 3D printed PLA film; top view

PLA is the printing material used by the original fuse deposition portion of the ultimaker printer. This thermoplastic was extruded by filament through a heated nozzle. Printing was done under the same parameters used for all other ink formulations printed using the modified portion of the printer. Seen in Figure 19, PLA successfully printed the whole geometry, and showed two clear layers of material.

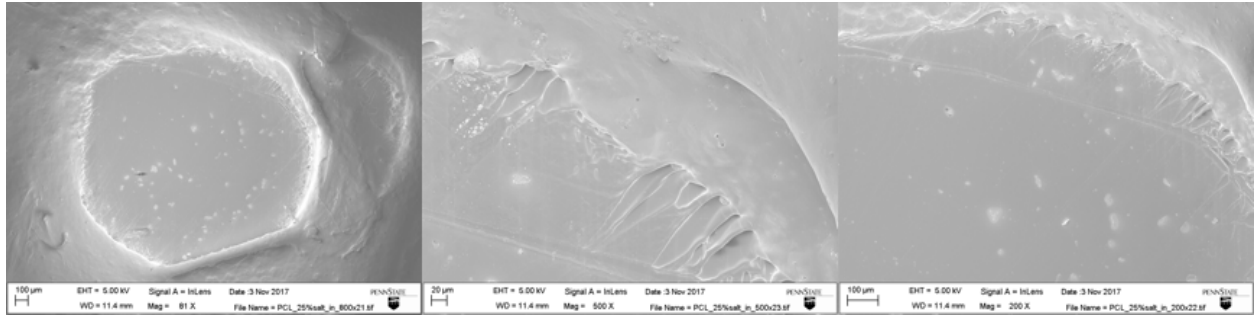


Figure 20: SEM Image of 3D printed PCL scaffold with 25% Salt incorporated and leached; top view

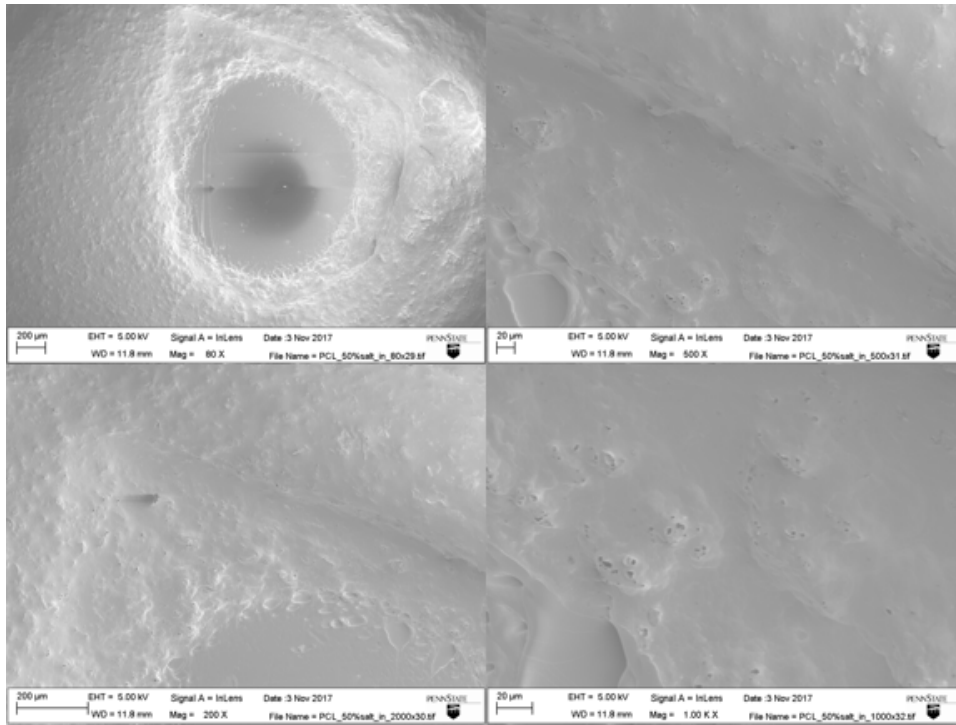


Figure 21: SEM Image of 3D printed PCL scaffolds with 50% Salt incorporated and leached; top view

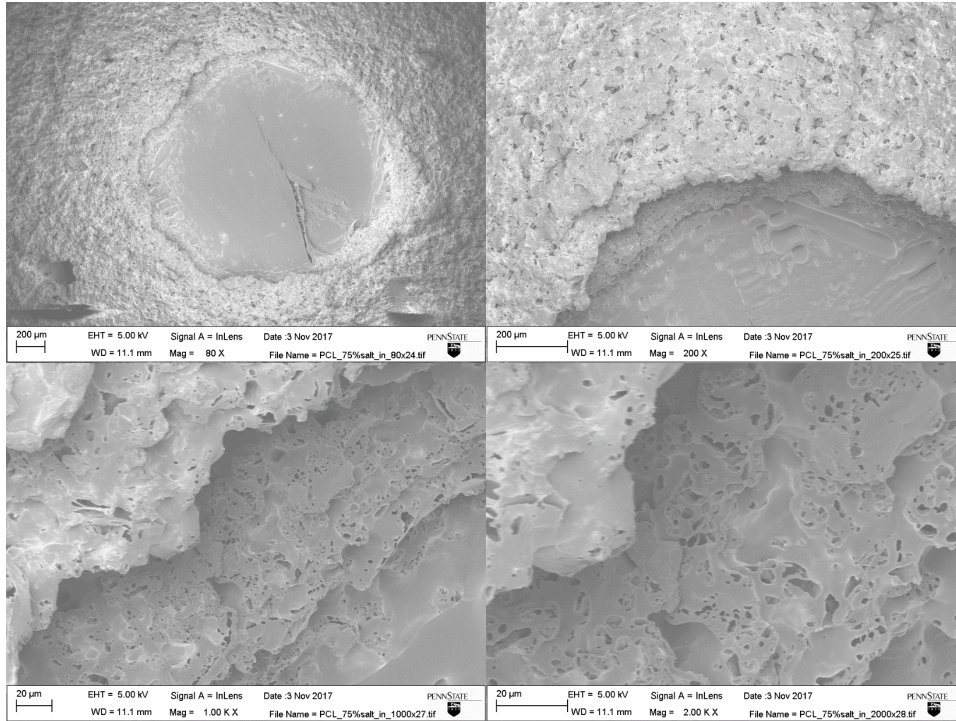


Figure 22: SEM Image of 3D printed PCL scaffolds with 75% Salt incorporated and leached; top view

PCL ink compositions showed clear distinctions between the first and second layers of printing, (Figure 21 and Figure 22). Micro pores were successfully show in Figure 22.

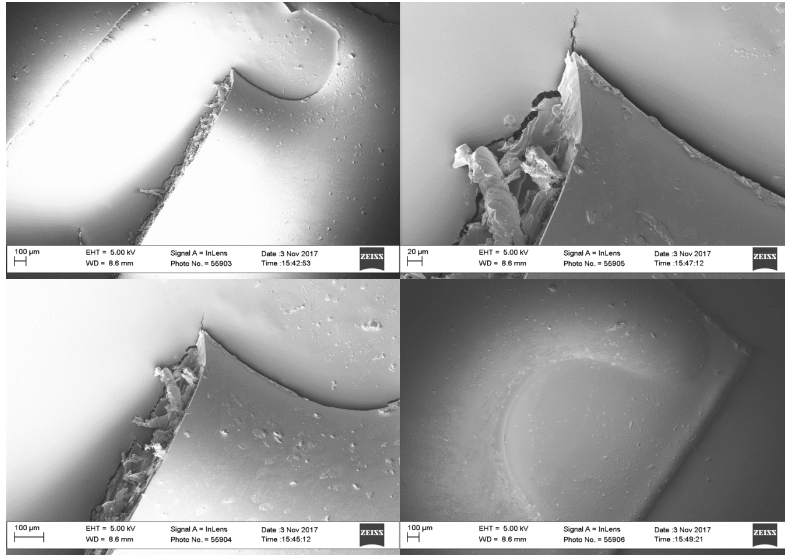


Figure 23: SEM Image of 3D printed POC film; top, cross section and side views

Printing of the pure POC ink is shown in Figure 23. Poor macro pore geometries were formed, and a contraction effect of the polymer is seen, where the thickest portion of the print is in the middle.

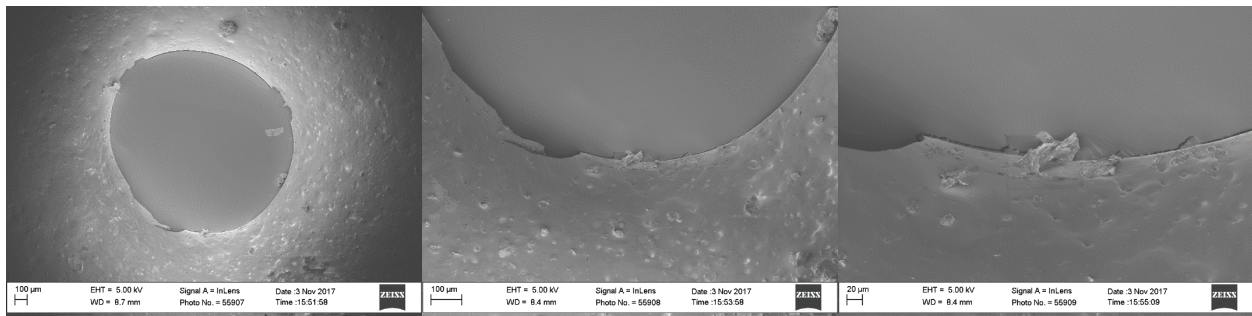


Figure 24: SEM Image of 3D printed POC scaffolds with 25% Salt incorporated and leached; top view

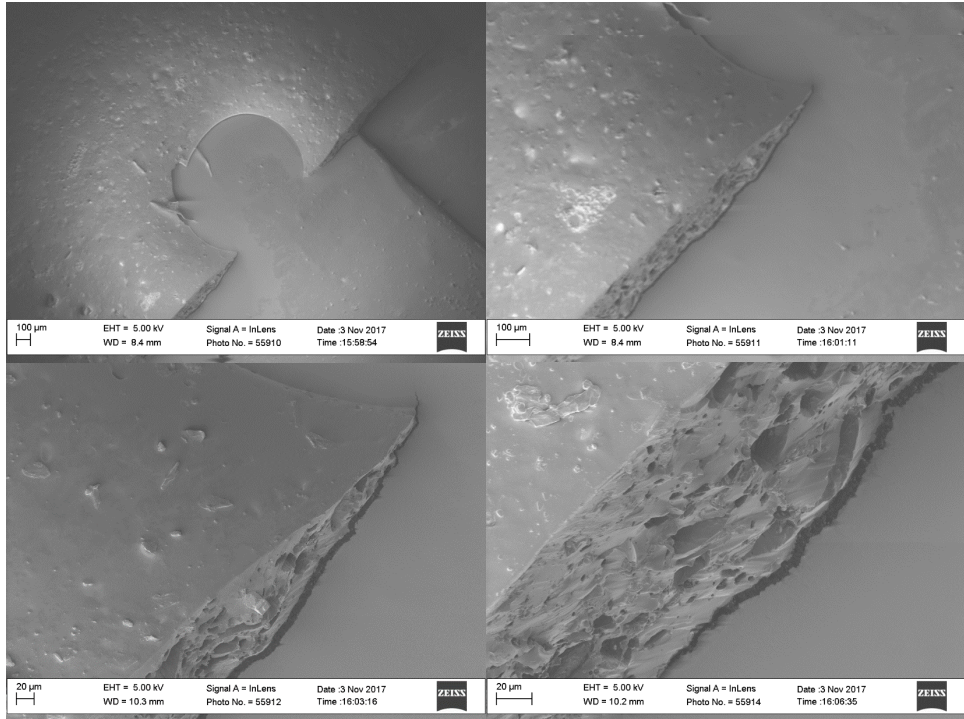


Figure 25: SEM Image of 3D printed POC scaffolds with 25% Salt incorporated and leached, cross section and side views

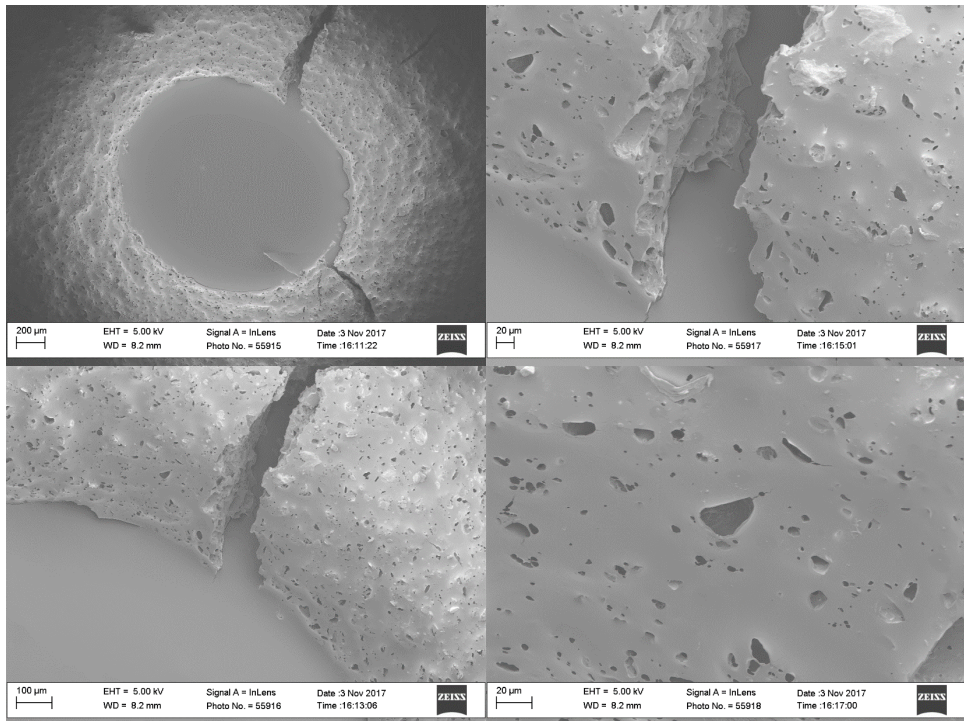


Figure 26: SEM Image of 3D printed POC scaffolds with 50% Salt incorporated and leached; top view

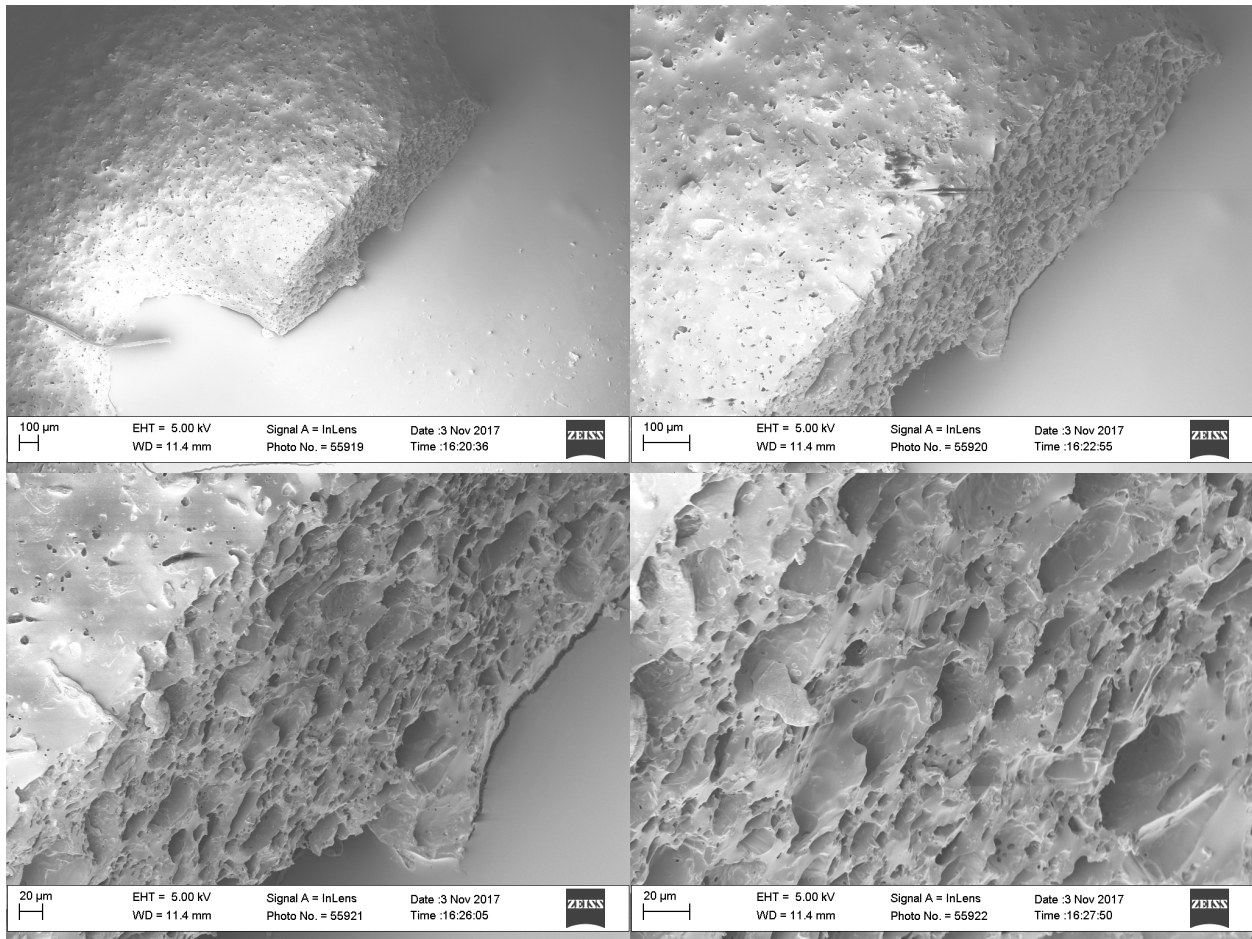


Figure 27: SEM Image of 3D printed POC scaffolds with 50% Salt incorporated and leached, cross section and side views

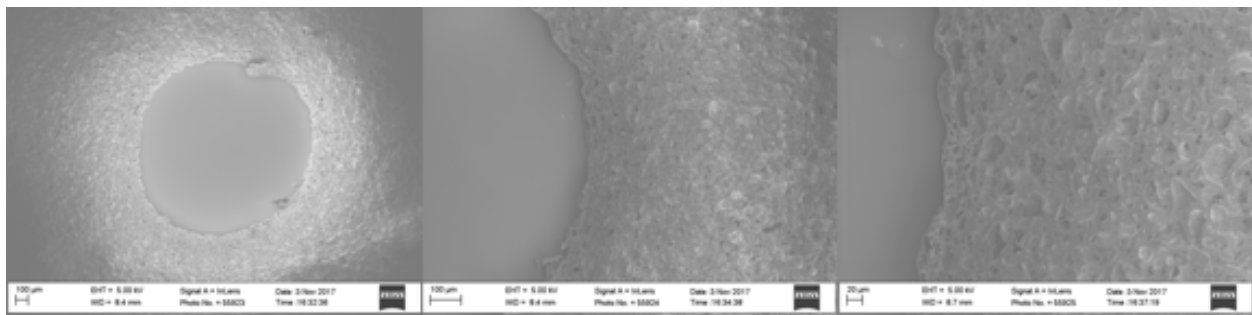


Figure 28: SEM Image of 3D printed POC scaffolds with 75% Salt incorporated and leached; top view

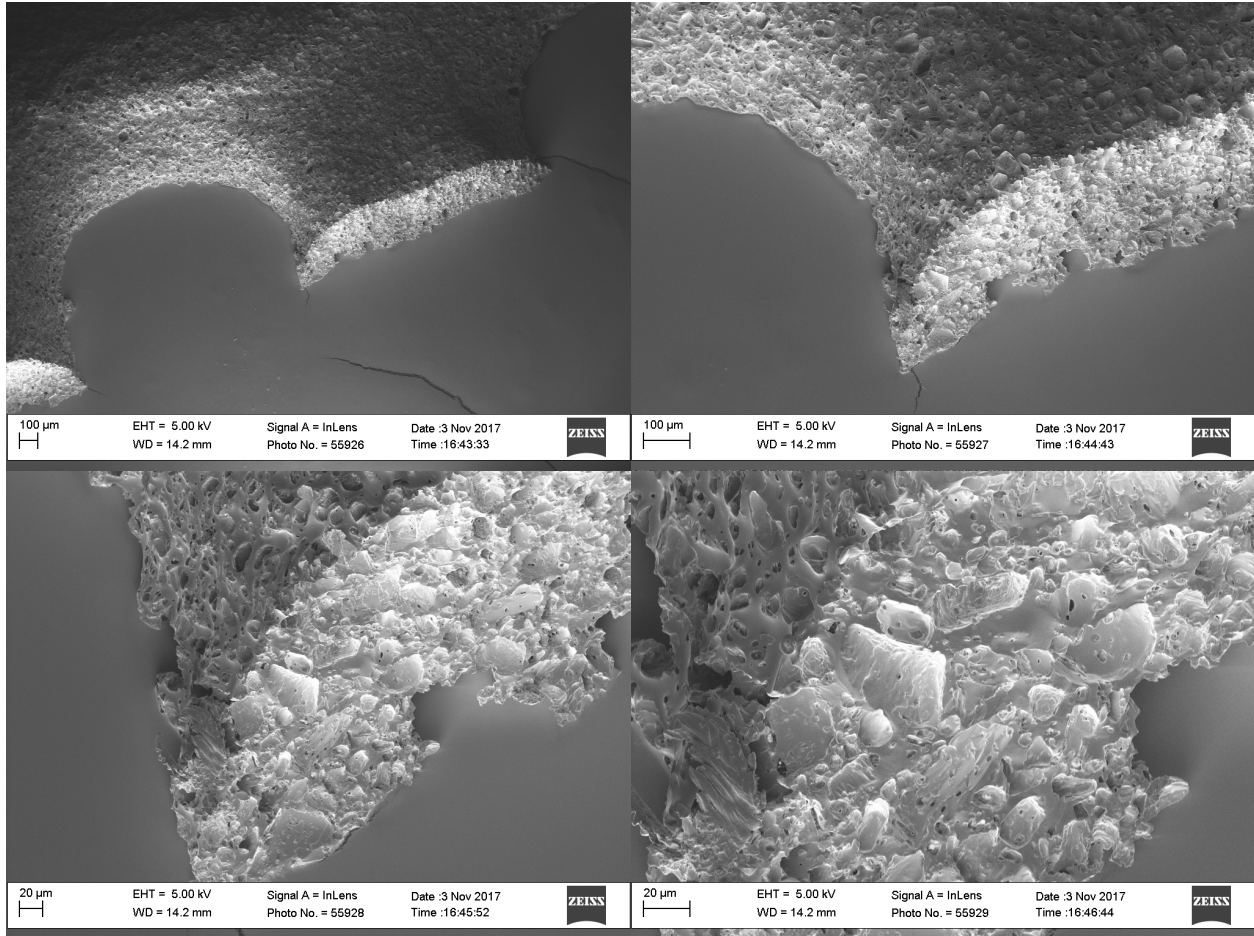


Figure 29: SEM Image of 3D printed POC scaffolds with 75% Salt incorporated and leached, cross section and side views

SEM images for all composite ink formulations with salt show the addition of salt. They show that salt leaching successfully created a microstructure within the scaffolds. When a composition of above 50% salt was used, pore structures are shown on the surface of the print and composite mixtures above 75% start to show two distinct layers.

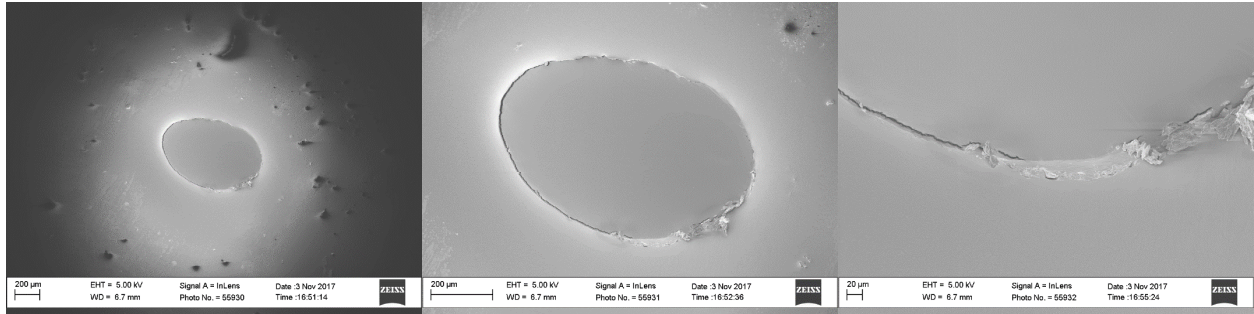


Figure 30: SEM Image of POC 25% HA top view

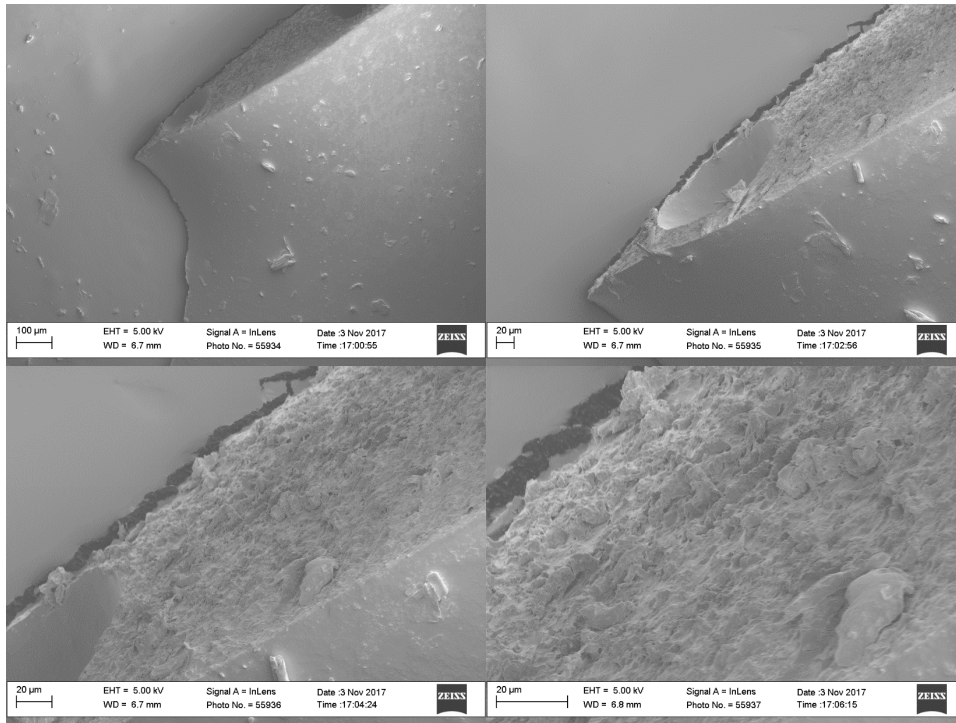


Figure 31: SEM Image of 3D printed POC scaffolds with 25% HA incorporated and leached, cross section and side views

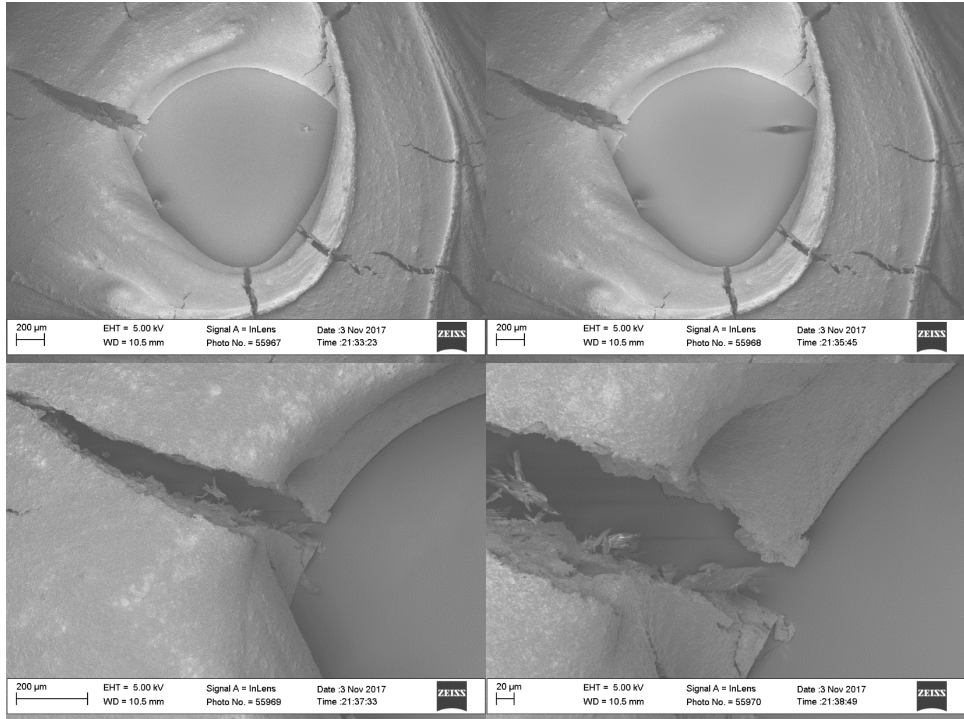


Figure 32: SEM Image of 3D printed POC scaffolds with 50% HA incorporated and leached; top view

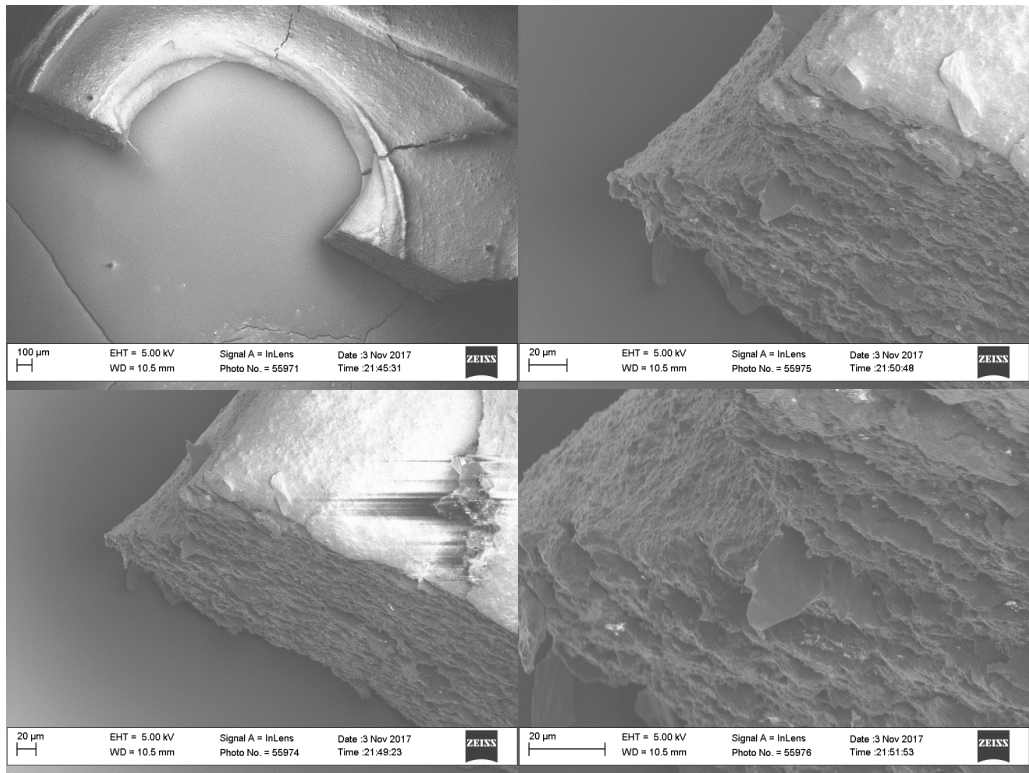
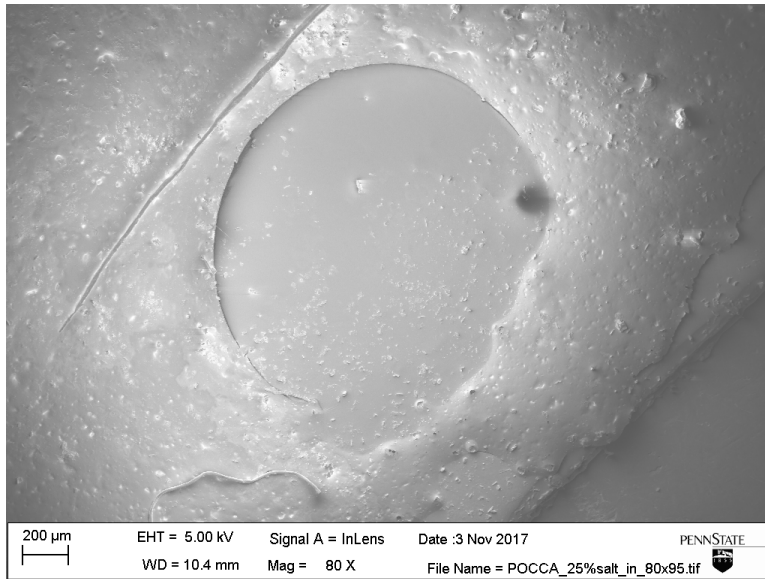


Figure 33: SEM Image of 3D printed POC scaffolds with 50% HA incorporated and leached; top, cross section and side views

With the addition of HA as the structural composite component, only 25% and 75% compositions were successfully printed. At 25% compositions, macro-pore shapes were created but tended to be not circular. At 75% composites two distinct layers were formed and pathing lines of the printer nozzle can be seen in the morphologies of the print.



*Figure 34: SEM Image of 3D printed POCCA scaffolds with 25% Salt incorporated and leached; top view*

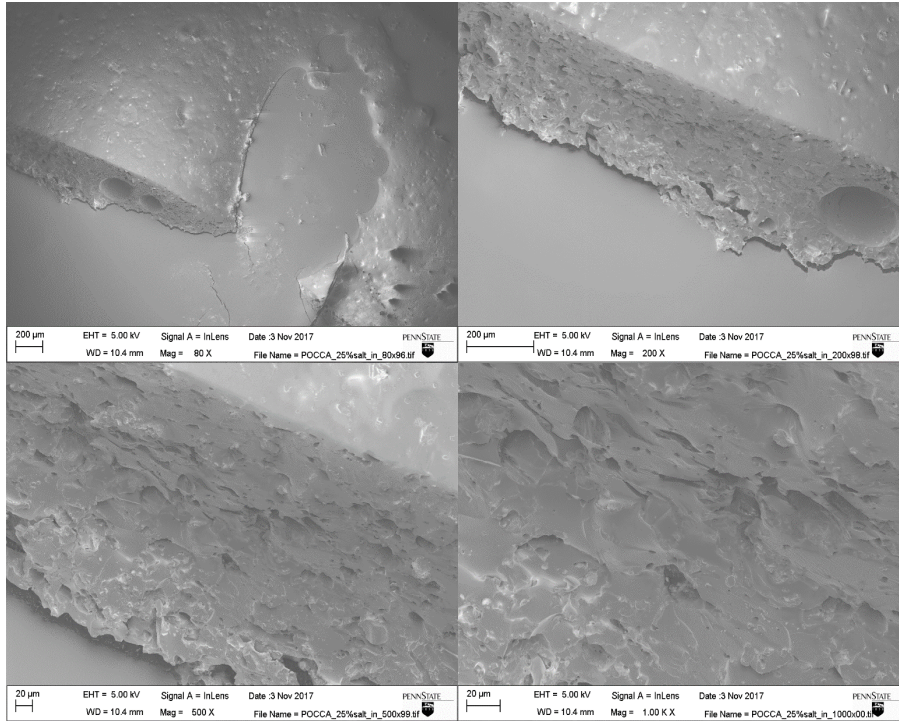


Figure 35: SEM Image of 3D printed POCcA with 25% Salt incorporated and leached, cross section and side views

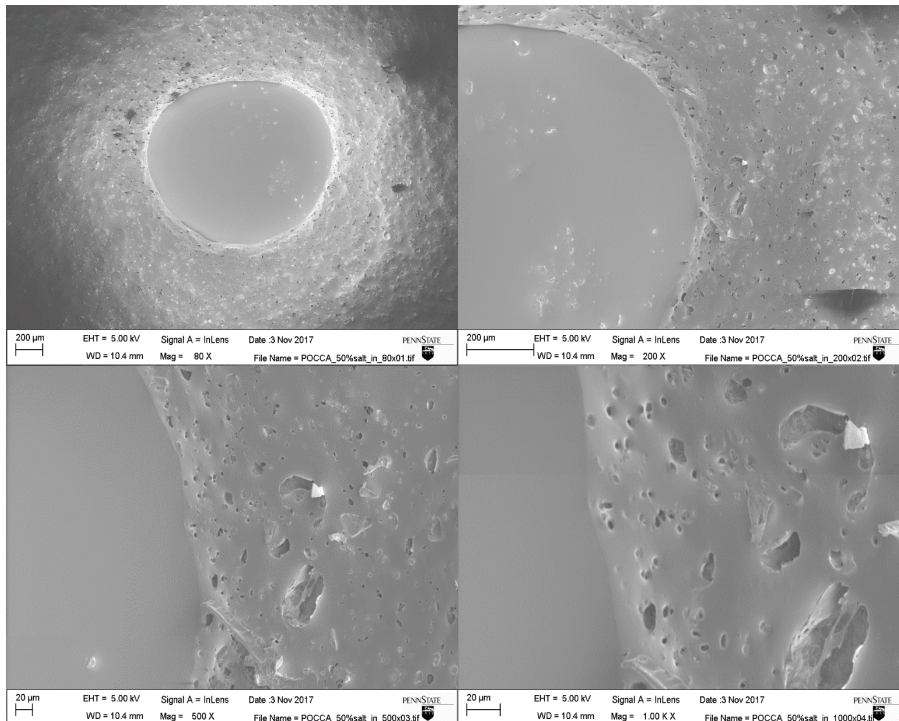


Figure 36: SEM Image of 3D printed POCcA scaffolds with 50% Salt incorporated and leached.

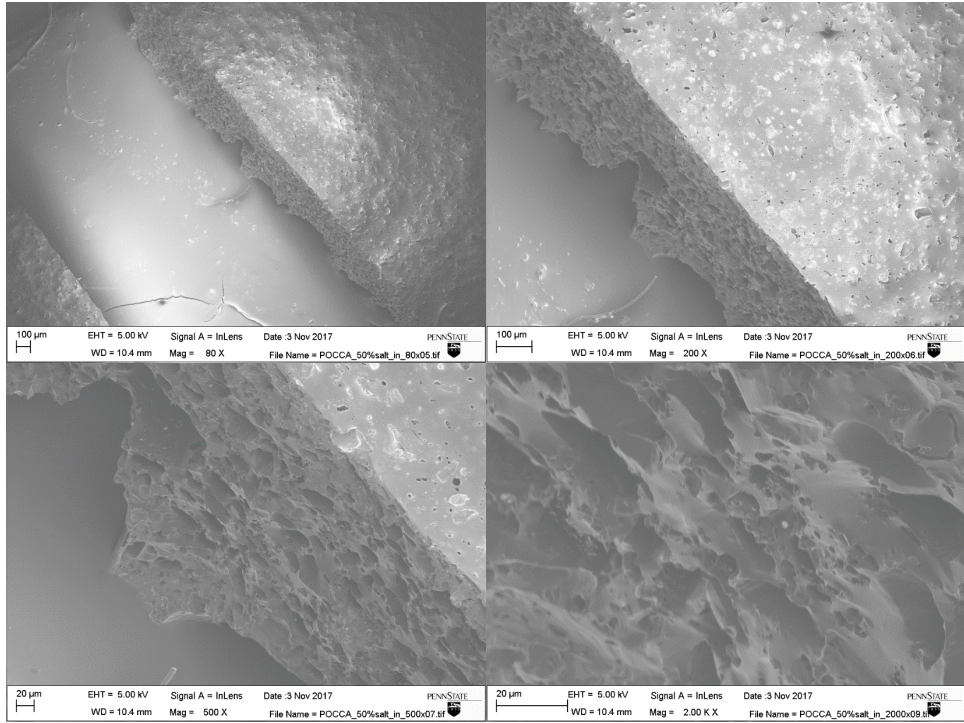


Figure 37: SEM Image of 3D printed POCca scaffolds with 50% Salt incorporated and leached, cross section and side views

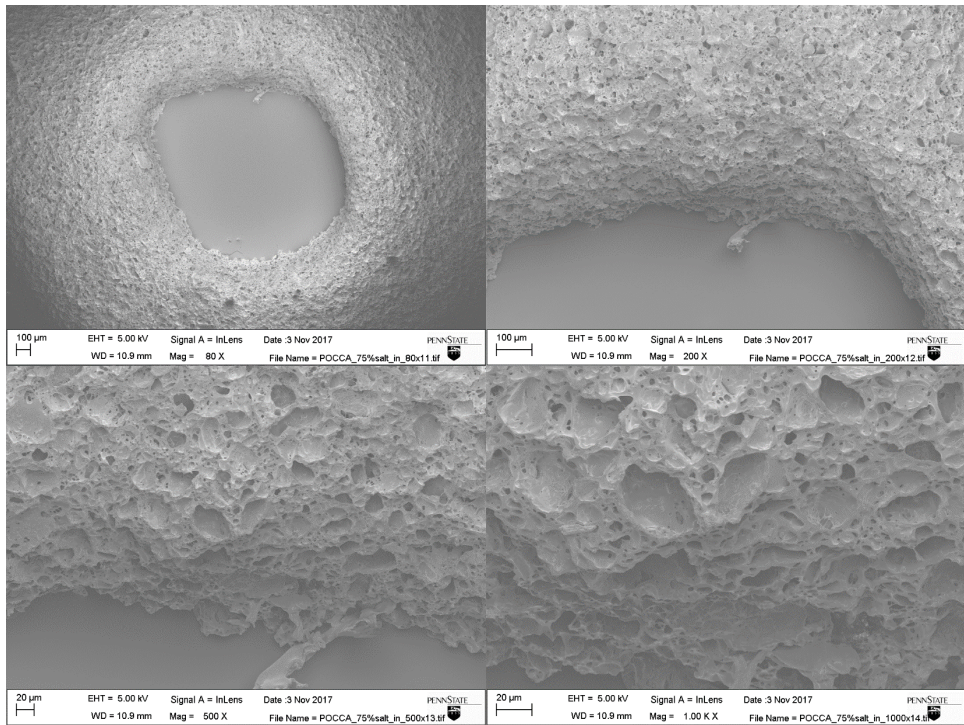


Figure 38: SEM Image of 3D printed POCca scaffolds with 75% Salt incorporated and leached.

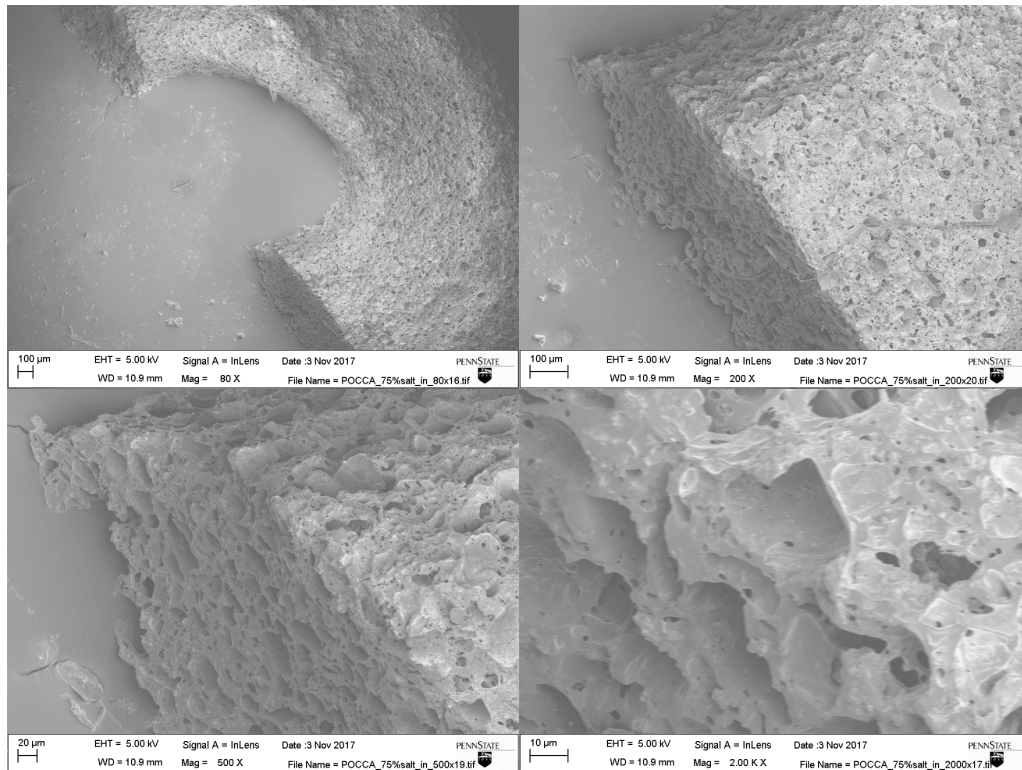


Figure 39: SEM Image of 3D printed POCa scaffolds with 75% salt incorporated and leached; top, cross section and side views

All POCa formulations showed similar characteristics to POC formulations.

## Mechanical Testing

The mechanical performance of POC and POC-Ca, along with PCL was evaluated using a tensile test with a crosshead speed of 500 mm/min for all scaffolds. Cast samples were tested as controls, then porous and non-porous printed scaffolds with varying pore sizes were tested. The resulting initial peak stress, initial modulus and strain at break are presented in Figures 40-48 and tables 4 – 6.

*PCL Mechanical Properties:*

*Table 4, PCL Mechanical Properties Overview, All Samples that do not otherwise specify are printed*

PCL	Peak Stress (MPa)	Initial Modulus (MPa)	Strain at Break (%)
Solid Film	22.19 ± 5.68	117.23 ± 18.41	1195.31 ± 135.34
2mm holes	17.59 ± 2.6	74.24 ± 19.9	712.96 ± 67.18
3mm holes	15.43 ± 0.04	110.82 ± 2.3	745.04 ± 47.73
Porus	5.38 ± 0.63	105.22 ± 9.09	71.92 ± 60.34
Porus 2mm holes	8.44 ± 0.85	110.45 ± 33.93	297.96 ± 82.34
Porus 3mm holes	6.29 ± 1.52	101.82 ± 26.58	103.24 ± 74.26
Cast	26.18 ± 2.49	155.54 ± 47.72	854.35 ± 33.57

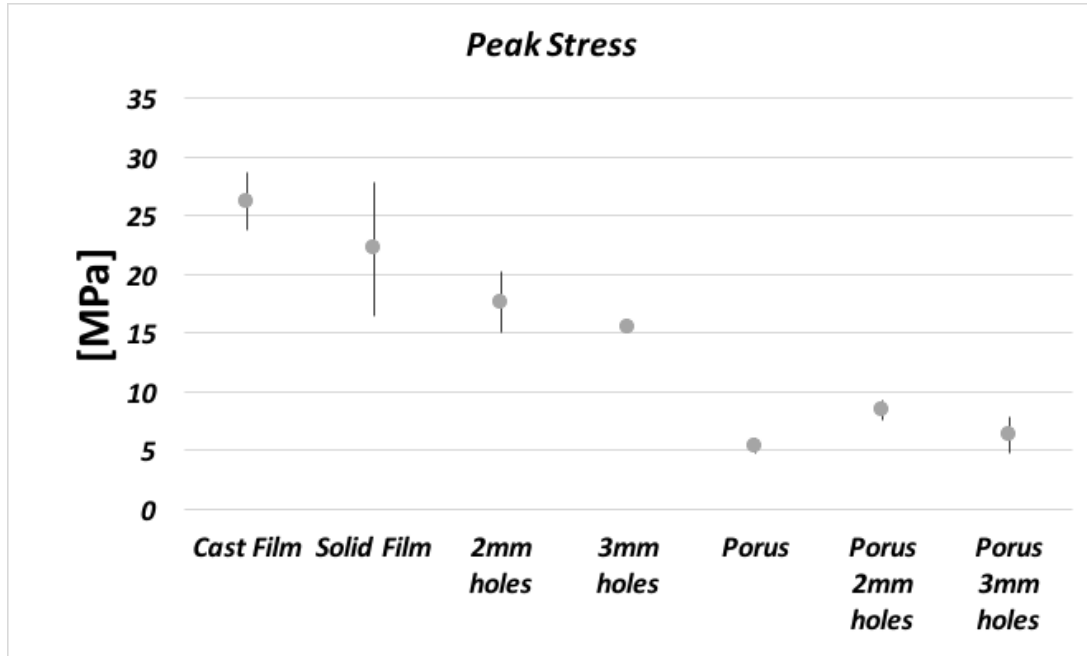


*Figure 40: Peak Stress [MPa] of PCL films, all films not otherwise labelled are printed, error bars represent 1  $\sigma$  STD.*

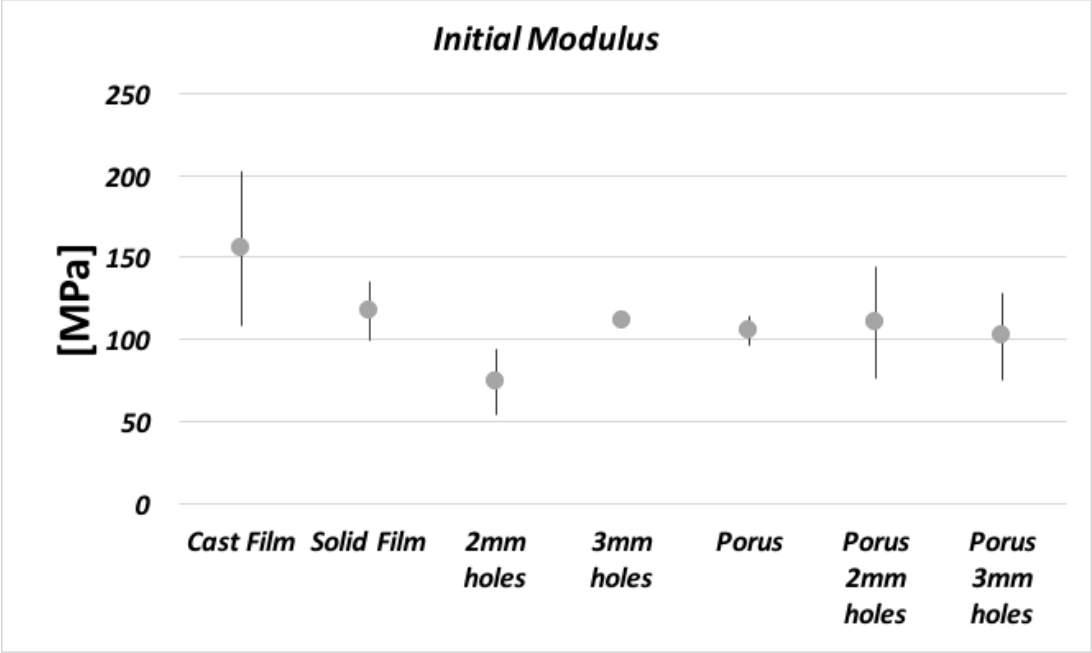


Figure 41: Initial Modulus [MPa] of PCL films, all films not otherwise labelled are printed, error bars represent 1  $\sigma$  STD.

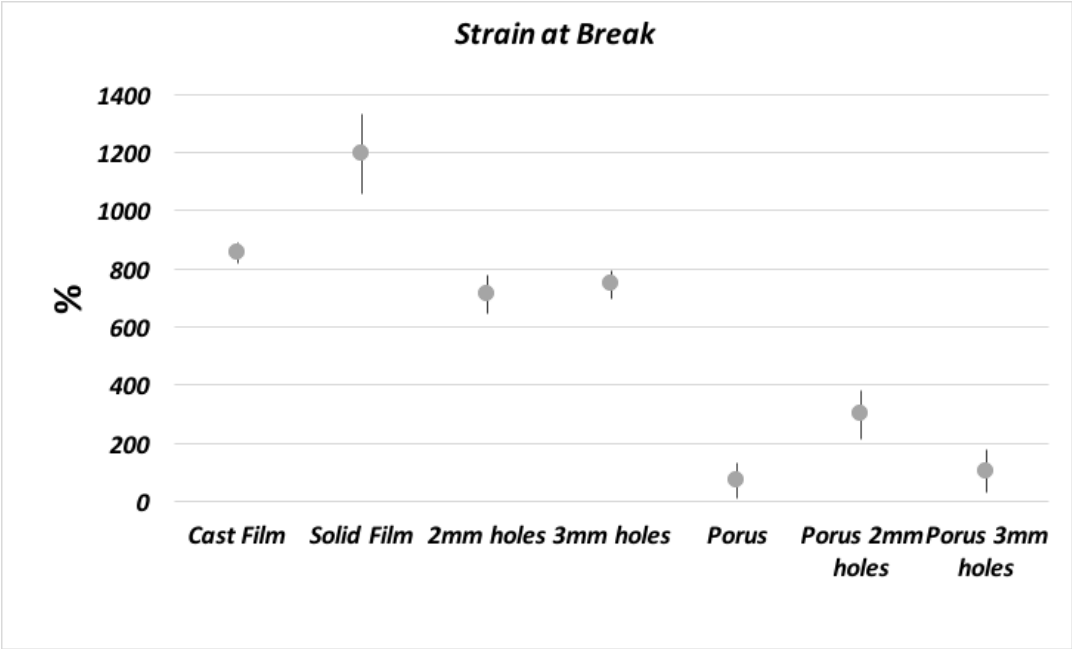


Figure 42: Strain at break [%] of PCL films, all films not otherwise labelled are printed, error bars represent 1  $\sigma$  STD.

POC Mechanics:

Table 5 POC Mechanical Properties Overview, All Samples that do not otherwise specify are printed

POC	Peak Stress (MPa)	Initial Modulus (MPa)	Strain at Break (%)
Solid Film	0.49 ± 0.06	2.84 ± 1.01	45.74 ± 17.21
2mm holes	0.63 ± 0.12	4.23 ± 1.4	30.27 ± 7.71
3mm holes	0.44 ± 0.05	3.83 ± 1.31	19.63 ± 3.82
Porus	0.72 ± 0.13	0.79 ± 0.1	161.29 ± 58.15
Porus 2mm holes	0.58 ± 0.09	0.91 ± 0.07	90.18 ± 14.56
Porus 3mm holes	0.45 ± 0.07	0.7 ± 0.08	84.29 ± 10.37
Cast	0.94 ± 0.1	1.27 ± 0.1	137.13 ± 9.35

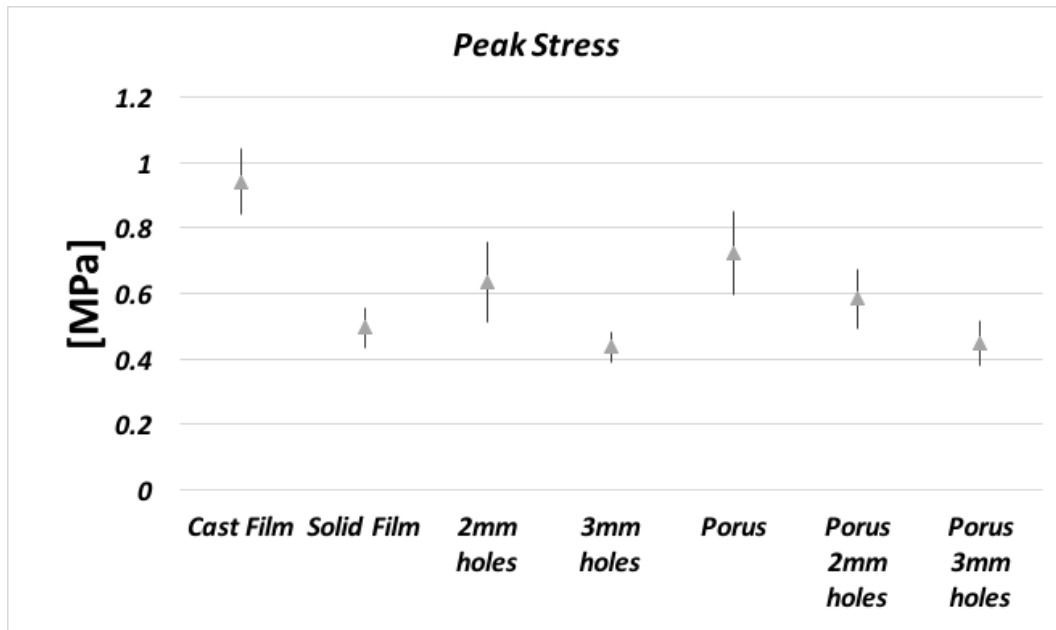


Figure 43: Peak Stress [MPa] of POC films, all films not otherwise labelled are printed, error bars represent 1  $\sigma$  STD.

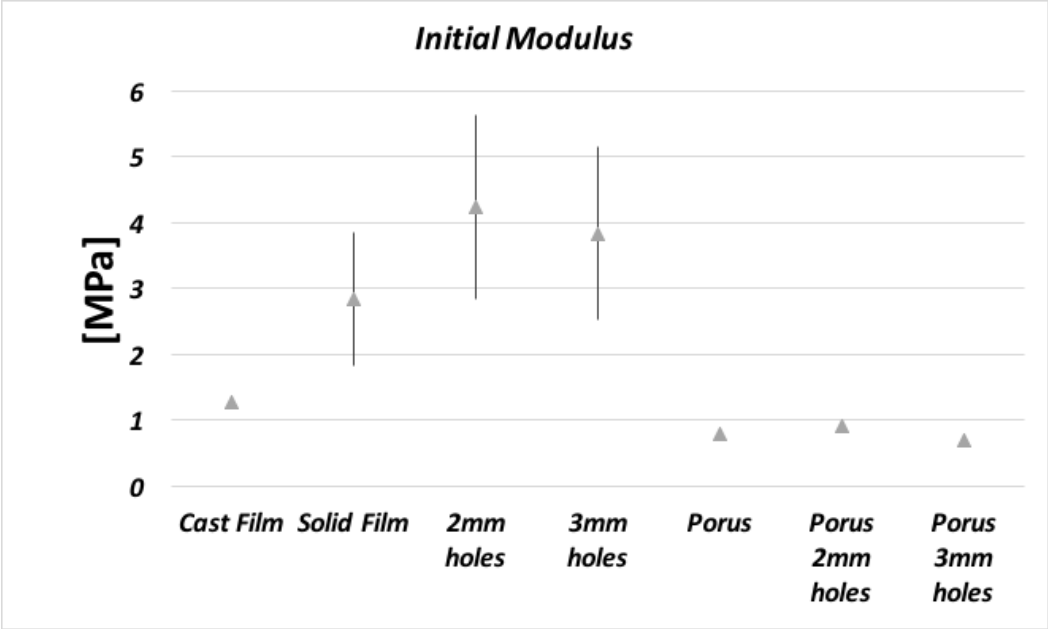


Figure 44: Initial [MPa] of POC films, all films not otherwise labelled are printed, error bars represent 1  $\sigma$  STD.

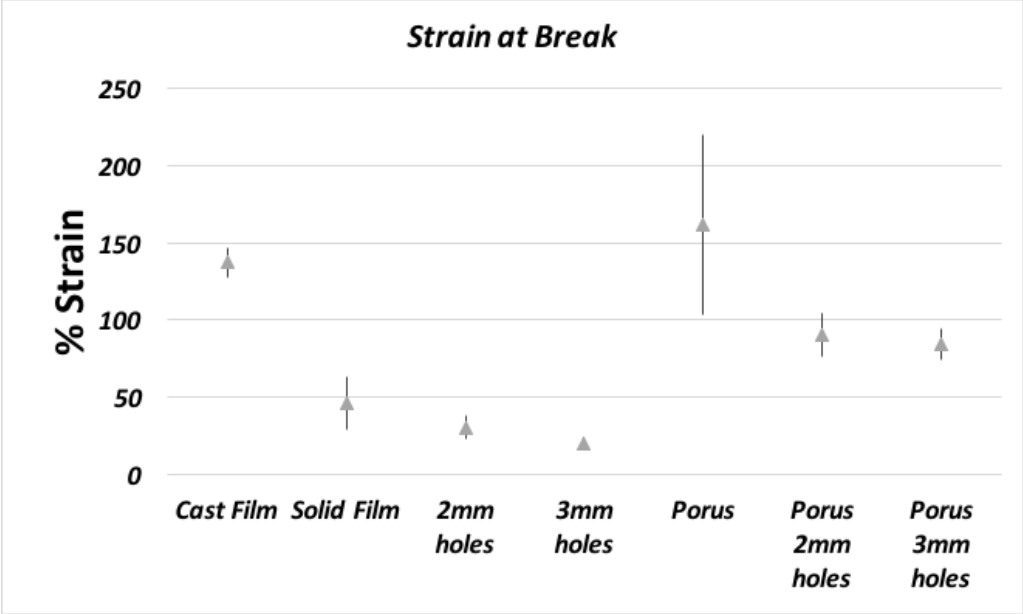


Figure 45: Strain at Break [%] of POC films, all films not otherwise labelled are printed, error bars represent 1  $\sigma$  STD.

POC-Ca Mechanics:

Table 6 POC Mechanical Properties Overview, All Samples that do not otherwise specify are printed

POCCA	Peak Stress (MPa)	Initial Modulus (MPa)	Strain at Break (%)
Solid Film	0.63 ± 0.06	5.19 ± 0.38	50.74 ± 12.37
2mm holes	0.63 ± 0.16	5.21 ± 2.08	29.9 ± 11.1
3mm holes	0.69 ± 0.11	7.88 ± 0.77	27.96 ± 1.67
Porus	0.63 ± 0.08	0.75 ± 0.06	133.63 ± 28.45
Porus 2mm holes	0.51 ± 0.17	0.66 ± 0.25	104.02 ± 2.68
Porus 3mm holes	0.42 ± 0.05	0.64 ± 0.03	92.13 ± 15.74
Cast	1.28 ± 0.12	1.59 ± 0.03	169.74 ± 24.2

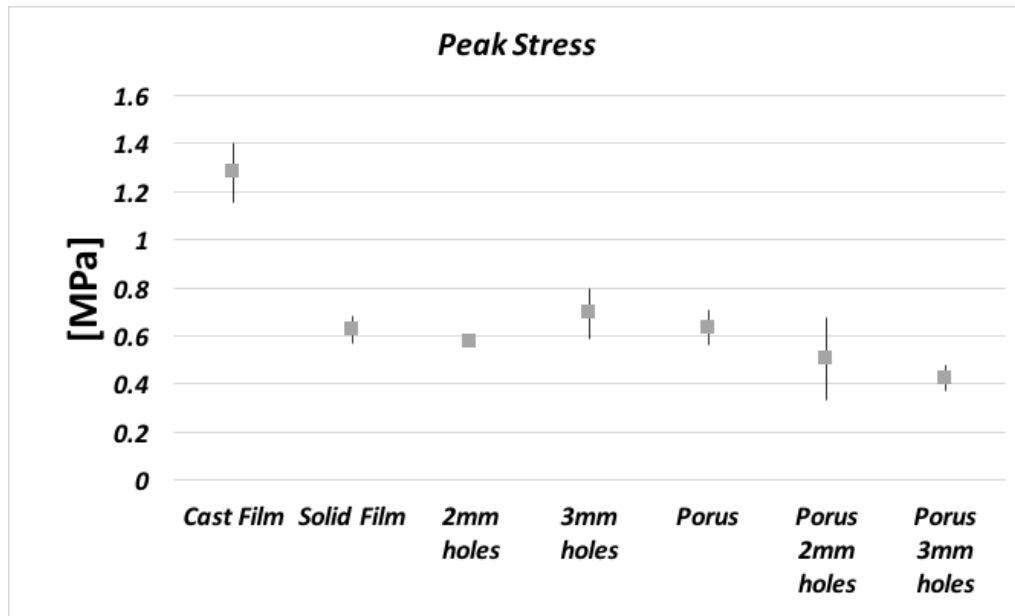


Figure 46: Peak Stress [MPa] of POC-Ca films, all films not otherwise labelled are printed, error bars represent 1  $\sigma$  STD.

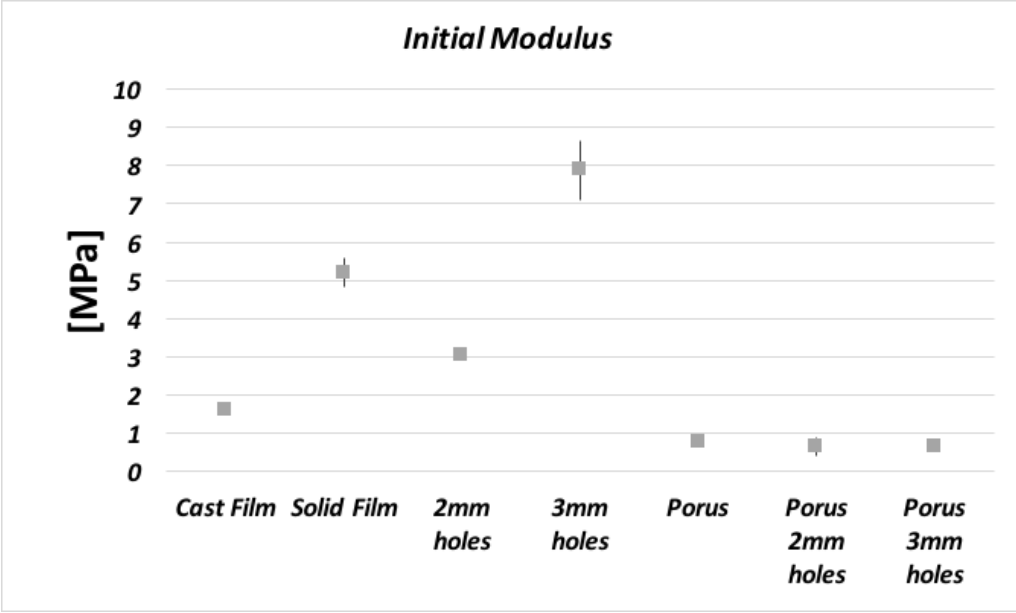


Figure 47: Initial Modulus [MPa] of POC-Ca films, all films not otherwise labelled are printed, error bars represent 1  $\sigma$  STD.

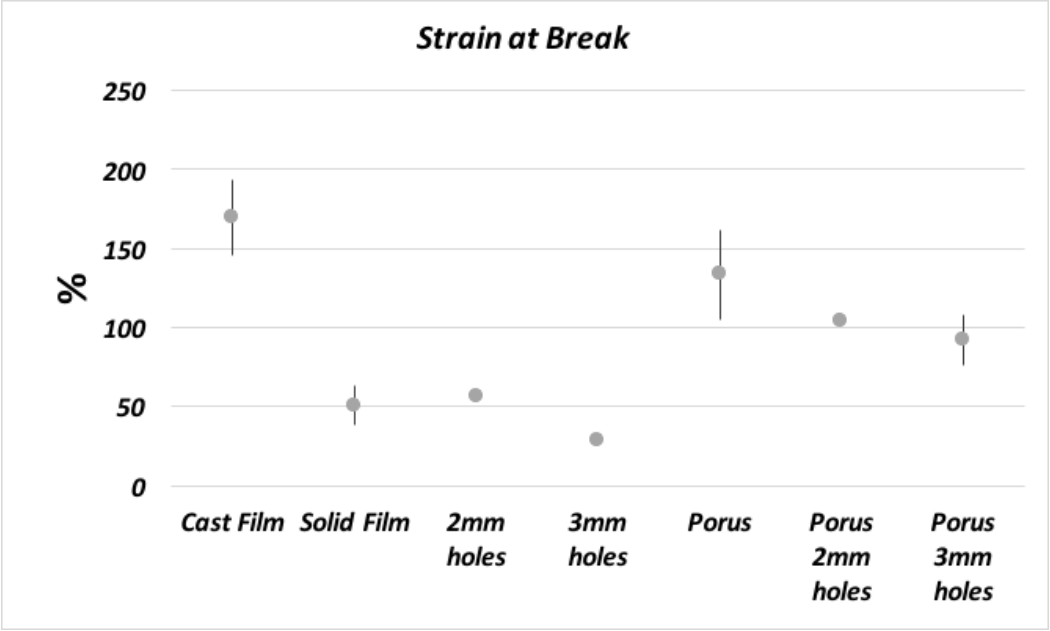


Figure 48: Strain at Break [%] of POC-Ca films, all films not otherwise labelled are printed, error bars represent 1  $\sigma$  STD.

## Water Vapor Permeability

The permeability of printed films was tested utilizing a technique described in Chapter 2, and was adapted from ASTM standard E96. The test was performed over 8 hours, recording data hourly until a steady diffusion rate was reached. This was observed by plotting the change in mass vs time as shown in figure 50. Once a steady state was reached, the water vapor transmission rates were calculated (results shown on Table 7). An example of permeance shown to be at a steady state of flux throughout the material is shown in figure 50.

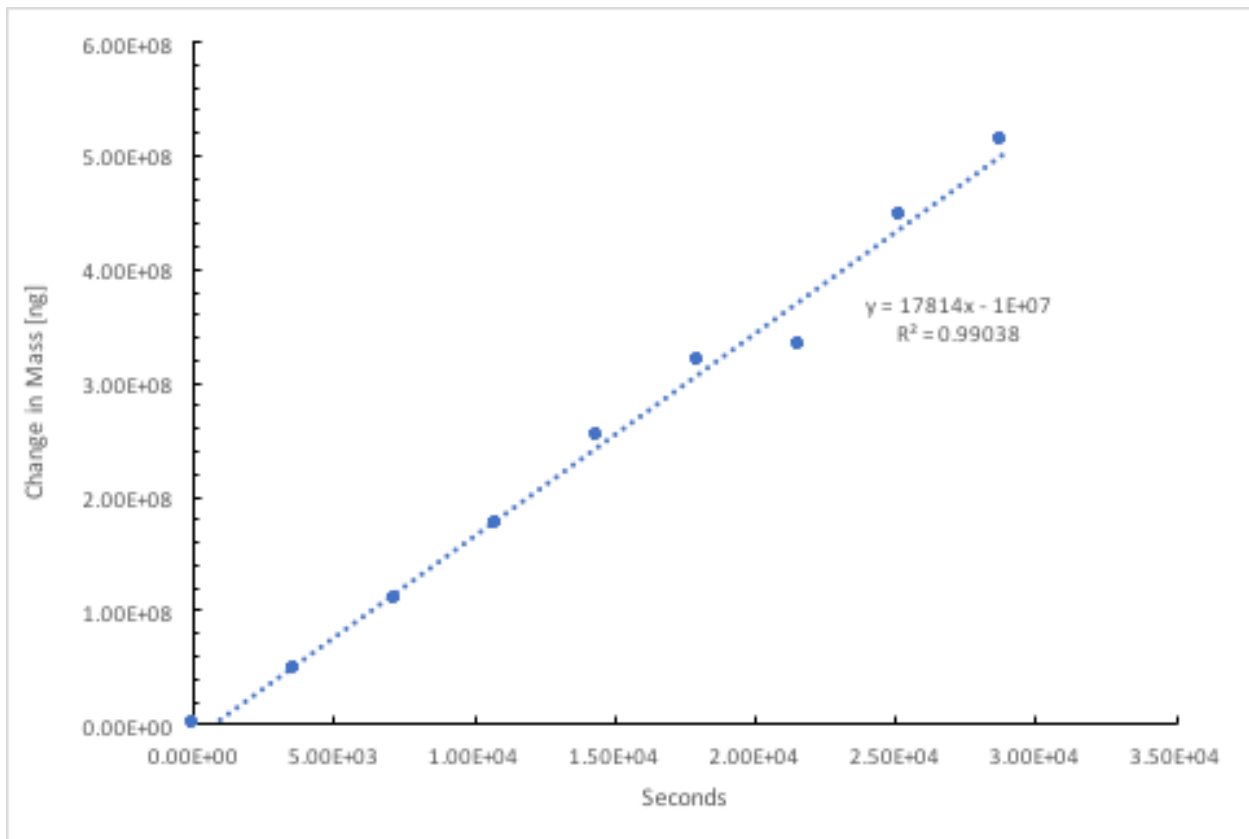


Figure 49 Permeability Graph, Showing the linearity of the permeation trend, suggesting the permeation is in steady state

Table 7: Water vapor transmission rates

Sample	Water Vapor transmission	Thickness	Water Vapor transmission, Normalized to the thickest Sample
	g/(day)(m <sup>2</sup> )	mm	g/(day)(m <sup>2</sup> )
POC	123.19	0.46	123.19
POC Porous	448.11	0.31	301.99
POCCA	68.74	0.45	67.25
POCCA Porous	453.45	0.28	276.01
PCL	76.56	0.20	33.29
PCL Porous	526.22	0.10	114.39
Skins	240-1920	Intact Skin	N/A

Oxygen Permeability

Table 8: Oxygen Permeability

Membrane	Permeance(P)	Permeability(P*I)	Permeability(P*I)
	Standard Unit	Standard Unit	Standard Unit
	mol/(m <sup>2</sup> *s*Pa)	(mol)/(m*s*Pa)	(nmol)/(m*s*GPa)
POC	1.85E-11	8.54E-15	8540.9
POCCA	1.65E-06	5.29E-10	528690000
PCL	2.41E-12	2.51E-16	250.56
POC Porous	5.13E-06	1.04E-09	1036000000
POCCA Porous	1.09E-05	6.48E-09	6483900000
PCL 50% Porous	3.48E-07	1.91E-11	19146000
Polypropylene			300
High Density Polyethylene			300
Polystyrene			600-800

## Chapter 4: Discussion

The Ultimaker 2 3D printer was successfully modified act as a micro extruder while keeping its native FDM printing components intact. The micro-extrusion printer head has a controllable pneumatic actuator capable of 0.1 psi to 100.0 psi, allowing for fine control of the extrusion force on the bio ink and ink-composite mixtures. Allowing for high viscosity fluids to be extruded and deposited in a printing process. With successful modification of the printing, ink formulation was developed to determine which combinations of composites would allow for printing of a thermoset pre-polymer. Being able to print macro pore structures in a 1mm resolutions with the use of 0.6 mm nozzle.

Even though there has been a large boom in the advances and research in the additive manufacturing field, there has been very little exploration into the printing of thermoset based materials. Printable thermosets are usually restricted to laser-assisted printing techniques that utilize laser crosslinking of the thermoset during printing. The goal of this project was to show that scaffolds could be successfully printed by using composites to provide the supporting structure during printing of the thermoset pre-polymer.

Composite ink formulations were created from our Citrate base-biomaterials, which in large are thermoset material. Two of our citrate based polymers were chosen for testing, POC which is the original citrate based polymer. POC was chosen because it's simple chemical

structure is the basis for modification into all the specialize citrate based polymers. POCCa was chosen because of some unique properties which will be discussed later. Finally, PCL, a thermoplastic, that has been used in additive manufacturing formulations, and is generally known for its excellent workability. This polymer was chosen as a control because it has been shown in many publications to be printable and bio-combatable. Each polymer solution was mix with two composite materials to be used as supporting material during printing and before curing/ cross-lining. Multiple concentrations were used to determine the bested concentration for printing was. Shown in table 2, is a overview of all the formulations tested and which test were performed on which formulation. In Table 9, is a filled in representation of Table 2, where color coding was used to suggest which results we favorable (green), needs to be reevaluated or procedural modification could make favorable results (yellow), and un-favorable results (red).



In the following sections, each test will be discussed in detail. The first five sections will go over will go over the evaluations of methods that were designs as a screening process for the printability of Inks used in microextrusion printing. The test will be presented and discussed as follows, 1. Rheological analysis, 2. Filament morphology evaluation of each ink composition, 3. Percentage of successfully printed holes from the scaffolds for those inks, 4. Area and Circularity evaluations of the macro pores printed, and 5. Qualitative morphology analysis done be SEM imaging.

In the next sections, specific formulations were tested for explorations into the use as a skin substitute. Six, formulations were chosen for further testing into this area, these tests were done in tandem with printability evaluations. Pure PCL, POC, and POCCa were tested, along with each polymer created with 50% porosity. Scaffold were printed for each test procedure using the same printing parameters use for ink evaluation. The following four tests were carried out to evaluate the properties of citrate based printed scaffolds, 6. Mechanical testing with variations in macro pores design to observe effects of macro pore geometries, 7. water vapor permeability oxygen permeability to assess the breathability of the scaffolds.

#### 1. Rheological analysis

Rheological analysis was done with two rheological analysis's, a standard viscosity curve, followed by an amplitude sweep test. The standard viscosity curves were used to compare the relative viscosity between the inks tested. POC, POCCa pure based inks comprised of 3 % ethanol left in solution for the rheological testing. While POC, POCCa 50% Salt compositions only contained 5% ethanol left in solution when tested. The viscosity curves show that a reproducible viscosity's can be maintain between pure samples and those that have composites

added for supporting structure during printing. At a shear rate of 200 (1/s) the range of viscosity present in the four ink formulations for POC, POC 50% Salt, POCCa, and POCCa 50% are 48, 54, 41, and 60 (Pa\*s) respectively. This small range suggests the drying methods used to concentrate the ink solutions for printing result in ink formulations with close to the same viscosities. This allows us to maintain a consistent pressure force between samples during printing.

The second rheological test performed is known as an amplitude sweep analysis, this test gives results of the Storage Modulus and Loss modulus. The storage and loss modulus and a given in the energy (Pa) present in each modulus at any given shear, during testing a low shear is first applied to the material and the ramped up to a high shear rate. This test is used to analyze and gelation point in the material that could be cause by changes in shear force. The only material formulation to produce any notable result was the POCCa 50% salt compositions. Around 100 Pa, a gelation point is observed, as the storage modulus very distinctly crosses one another. This could be due to the fact that the calcium ions used to dope this version of POC and forming temporary bound with eh free calcium ions present the NaCl used as the supporting material in the composite ink. All other formations the storage modulus and loss modulus never cross, suggesting the ink always stays in a liquid stay, all though the inks be at high viscosity.

## 2. Filament morphology

Filament was used to check that each ink formulation could be successfully extruded in the modified printer. From Table 9, we can see the results of the filament morphology analysis, where compositions of POC and POCCa with 75% HA, ran thick filaments, and the high

concentration of HA would cause clogging in the printer nozzle not making it feasible for printing. All other formulations were able to be extruded into filaments that were considered printable and moved into the next rounds of evaluations.

### 3. Percentages of Successfully Printed Pores

In analysis of percentage of successful pores printed, any scaffold after printing that were observed to have successfully print more than 85% of the 27 pores of the three scaffolds printed by the design Figure 7, were considered a successful print and moved onto further analysis of the morphologies of the pores. Of the 20 printed ink compositions, 14 of the ink compositions successfully passed through this screen process. Inks that were eliminated include, POC, POC 25% salt, POC 25% HA, POCCa, and POCCa 25% salt. The pores were not successfully printed due to lack of supporting structure for the citrate pre-polymer to maintain sufficient geometrical rigidity during the crosslinking process following printing. Successful printed for 50% and above composites for both POC and POCCa do have enough supporting composite to maintain rigidity during crosslinking. The remaining 14 compositions moved on to analysis of the areas of pores printed and analysis of the circularity of the holes.

### 4. Area and Circularity Evaluation of Printed Pores

The resulting areas and circularity of the remaining compositions were analyzed using ImageJ to measure the area and relative circularity of each pore printed. These results were then plotted on a scatter plot to better observe the results to the theoretical values that were calculated given the perfect scaffold was printed. If the perfect scaffold was printed each pore would be perfectly circular with a circularity of 1, and each pore would have an area of 3.14 mm<sup>2</sup>. Results for this analysis can be seen on Figure 17, Figure 18 and Table 3.

A simple evaluation method was established to analyze the data, where any circularity with less than 15% error when compared to the theoretical values was considered to be a good print and for area any area with less than 10% error when compared to the theoretical values was considered a good print. When comparing both list of good prints three material compositions passed each evaluation set laid out by this test. Two controls PCL, and PCL with 75% salt, show to be able produce areas on 2.59 and 0.19 % error compared to the theoretical 3.14 mm<sup>2</sup> value. Showing the control material PCL with 75 wt % Salt added was the best printing compositions shown in this analysis method. The salt provided enough supporting structure to material that the shaped establish the printer during deposition of the filament during printing was maintained.

From the citrate based formulations POCCa 75% Salt ink compositions produced a print area that was 8.96 % error compared to the theoretical value. As similarly shown in the control materials a 75 wt % salt to polymer, the salt provides enough supporting structure to allow the printing of citrate based thermosets in a composite solution with ethanol.

One notable mention is that POC with 50% HA, fell just outside the metrics set as a good printing formulation, have a percent error of 10.04% with comparing its area to the theoretical values suggesting the Citrate based composites with 50% HA used as its supporting material provide enough structure to produced good prints. Establishment of what printing formulations were successful were further determined by looking at the morphologies of the prints using a qualitative observation analysis, by looking at images taken using a scanning electron microscope.

## 5. SEM Analysis

Structures of the prints were closely observed using a scanning electron microscope, checking for morphological features in each print such a distinct two-layer structure in the printed scaffolds and good circularity of the printed pores. Also, micro pores left by salt leaching were observed, these were left behind in any of the composite ink formulations that used salt to as its supportive structure during printing. PCL with 75% is seen in Figure 22, shown by the SEM images a very distinct two-layer structure is form between the first and second layer of printing, also printing with 75 wt% salt, produced a highly porous structure. Creating a sufficient micro pore environment is import for tissue engineered scaffold because the interconnectivity of the pores in going to directly affect the amount of cell adhesion and surface for cell ingrowth.

Seen in Figure 38, is the POCCa ink formulations that was printed with 75% salt used as a supportive material and then removed after crosslinking via salt leaching. He a very high surface pore density was achieved, with the overall print morphology is very good. The printed scaffold shows good depth to the print suggesting each layer was printed one on top of the other, with minimal structure of the second layer completely mingling with the first. Which was seen in prints with less supporting structure such as POCCa with 25% salt used, seen in Figure 34. Also observed in ink formulations using 50% HA a very distinct two-layer structure was observed suggesting the then use of HA in concentrations around 50% can be used to print scaffold with citrate based pre-polymer. Also Salt composite formulations with concentrations around 75% can also be used as successful supporting structure of printing citrate based pre-

polymers. The use of POCCa and Salts gelation mechanics under sufficient shear stress seems to create a more solid filament during printing, effectively increasing the printing accuracies, as deposition of a more solid filament more actively brings out the features in the design scaffolds.

## 6. Mechanical

The mechanical properties of human skin were shown to have a tensile modulus between 1-40 MPa, initial modulus of 1-2 MPa, and a strain at break of between 17-70 %. These known properties of skin were used to compare to mechanical results of scaffolds that were manufactured using the modified micro-extruded designed in this thesis. Scaffold were designed using the scaffold design seen in Figure 10.

## 7. water vapor permeability and oxygen permeability.

Vapor and oxygen permeability are used to infer the breathability of printed scaffolds for use as a skin substitute. It is important to match the native permeability properties of the skin, the water vapor transmission rates of skin ranges for 240-1930 (g/(day)(m<sup>2</sup>)). Porous POC and POCCa showed water vapor transmission rates of 301 and 276 (g/(day)(m<sup>2</sup>)), this shows that POC and POCCa skin substitutes will be sufficiently breathable to allow for air exchange between the outside environment and the wound. While maintaining similar breathability properties of that of skin, these skin substitute will also form a protective barrier from external particles and microbes. Permeability of solid POC and POCCa was shown to be 123 and 67 (g/(day)(m<sup>2</sup>)) respectively. It was expected that the permeability values for POC would be similar to that of POCCa, in the results shown POC has almost double the permeability of POCCa, this is due to double formations in the POC solid film during crosslinking. The air bubble in the films cause a more favorable pathway for water vapor to escape. This causes the higher

water vapor permeability; this test will need to be repeated with newly manufacture films to eliminate the variance seen in the POC films. Oxygen permeability done by our collaborators in DREAMS lab in the chemical engineering department showed that PCL had similar oxygen permeability compared to other commercially available plastics. While POCCa and POC high oxygen permeability, and the porous versions of POC and POCCa showed very high oxygen permeability suggest that good gas exchange between the would surface will occur.

## Conclusion

After successful Modification of an off-the-shelf printer our lab now has the ability and procedure and screen bio-inks formulations. This well improve the manufacturability of and design of scaffolds for use as tissue engineered substitutes. The screening method for evaluation of printability of ink formulations can be used to evaluate any future ink formulations for there effectiveness of printing. Citrate base pre-polymers were proven to be successfully printed with the addition of a composite supporting materials in high concertation pre-polymer solutions, to maintain the scaffold features. Citrate based polymer composites structures were shown to be successfully printed with salt concentrations at 75% and HA concentrations are at 50% wt to pre-polymer. These concertation's allowed for sufficient structure to maintain printed geometries while crosslinking could be done post-printing.

Printed scaffold of 50% porosity were then printed for evaluation as a suitable skin substitute showed promising results, with elongation and initial modulus characteristics matching the native skin and the peak tensile stress data just under the 1 MPa shown to be the peak tensile stress shown in native skin. However, after cell seeding for use as a skin substitute the peak tensile stress will increase because of the seeded cells with deposited fibrogen on the

surface of the substitute increasing its mechanical peak stress. From the water vapor and transmission results and oxygen permeability it was shown that these scaffolds are very breathable allow for proper gas exchange between the scaffold and the wound's surface. From SEM imaging of scaffold at 50% porosity, the inner porosity of the scaffold is highly porous allow for the ability to absorb sufficient fluids that would be produced by the wound. While the outer layers of the scaffolds form a more solid film (Figure 27) mimicking the protective surface formed by the dermis in skin. Finally, the innate anti-microbial properties from the citric acid suggest that this material would produce advantageous result in use as a skin substitute, the unique properties of POC will provide enough mechanical support, good breathability, and reduced risk of infection.

## Chapter 5: Future Direction

### Printing of Citrate Based Polymers

With a system now in place for screening of ink formulations for the printing of biomaterials the next steps in improving the printing effectiveness of citrate based polymers is to screen the remaining unique materials created in Dr. Yang's Transformative Biomaterials and Biotechnology Lab (LTBBL). While the addition of supportive composites at high concentrations showed the pre-polymer could be successfully printed and geometries maintained while crosslinking was done in an oven after printing. Developing an effective way to crosslink our set the material during printing will allow for much larger and complex geometries to be successfully printed. Currently exploration into a self-setting citrate composite polymer is being explored. The addition of magnesium oxide (MgO), with HA in POC has shown to be able to set

the pre-polymer. More optimization of setting times is needed before printing can be done, but this property is very promising in uses for printing how citrate based polymer. Finally, further modification of the printer can be done, with the addition of a high intensity ultra-violet (UV) light citrate base polymers that can be crosslinked by UV, can be printed.

## Printed Scaffold for use as a Skin Substitute

Thin film scaffold for use as skin substitute were successfully printed in this study. Scaffold design can be improved by printing of a gradient mesh, with large interconnected pores on ones side of the skin substitute and small interconnected pore on the other, with a solid film on the surface of the scaffold. This design will allow for better cell ingrowth and penetration, all with provide a dermis like layer on the top of the scaffolds. This scaffold design can be achieved by layering polymer/salt ink compositions with increasing salt size in the micro extruder syringe. For a fully function skin scaffold, cell seeding, attachment, and proliferations studies need to be carried out, along with an animal study. Currently an animal study is ongoing with collaborators in China.

## References:

1. Groll J, Boland T, Blunk T, et al. Biofabrication: reappraising the definition of an evolving field. *Biofabrication* 2016; **8**(1):13001. doi:10.1088/1758-5090/8/1/013001.
2. Wu LQ, Payne GF. Biofabrication: Using biological materials and biocatalysts to construct nanostructured assemblies. *Trends in Biotechnology* 2004; **22**(11):593–599. doi:10.1016/j.tibtech.2004.09.008.
3. Langer R, Vacanti JP. Tissue engineering. *Science* 1993; **260**(5110):920–926. doi:10.1007/978-3-642-02824-3.
4. An J, Teoh JEM, Suntornond R, Chua CK. Design and 3D Printing of Scaffolds and Tissues. *Engineering* 2015; **1**(2):261–268. doi:10.15302/J-ENG-2015061.
5. Gottschalk U, Brorson K, Shukla AA. The need for innovation in biomanufacturing. *Nature Biotechnology* 2012; **30**(6):489–492. doi:10.1038/nbt.2263.
6. Jose RR, Rodriguez MJ, Dixon TA, Omenetto F, Kaplan DL. Evolution of Bioinks and Additive Manufacturing Technologies for 3D Bioprinting. *ACS Biomaterials Science and Engineering* 2016; **2**(10):1662–1678. doi:10.1021/acsbmaterials.6b00088.
7. Gosain A, DiPietro LA. Aging and Wound Healing. *World Journal of Surgery* 2004; **28**(3):321–326. doi:10.1007/s00268-003-7397-6.
8. Guo S, DiPietro LA. Factors Affecting Wound Healing. *Journal of Dental Research* 2010; **89**(3):219–229. doi:10.1177/0022034509359125.
9. Burns JL, Mancoll JS, Phillips LG. Impairments to wound healing. *Clinics in Plastic Surgery* 2003; **30**(1):47–56. doi:10.1016/S0094-1298(02)00074-3.

10. On H, Medicine H. *No Title*.
11. Shevchenko R V., James SL, James SE. A review of tissue-engineered skin bioconstructs available for skin reconstruction. *Journal of The Royal Society Interface* 2010; **7**(43):229–258. doi:10.1098/rsif.2009.0403.
12. Papini R. Management of burn injuries of various depths. *Bmj* 2004; **329**(7458):158–160. doi:10.1136/bmj.329.7458.158.
13. Stanton RA, Billmire DA. Skin resurfacing for the burned patient. *Clinics in plastic surgery* 2002; **29**(1):29–51. doi:10.1016/S0094-1298(03)00085-3.
14. House IE. Guidelines for. *Environment* **41**(22).
15. Schneider LA, Korber A, Grabbe S, Dissemond J. Influence of pH on wound-healing: A new perspective for wound-therapy? *Archives of Dermatological Research* 2007; **298**(9):413–420. doi:10.1007/s00403-006-0713-x.
16. Gethin G. The significance of surface pH in chronic wounds. *Wounds UK* 2007; **3**(3):52–56.
17. Nagoba BS, Suryawanshi NM, Wadher B, Selkar S. Acidic Environment and Wound Healing: A Review | WOUNDS. *Wounds* 2015; **27**(1):5–11. <http://www.woundsresearch.com/article/acidic-environment-and-wound-healing-review> Accessed.
18. Nagoba BS, Gandhi RC, Wadher BJ, Deshmukh SR, Gandhi SP. Citric acid treatment of severe electric burns complicated by multiple antibiotic resistant *Pseudomonas aeruginosa*. *Burns : journal of the International Society for Burn Injuries* 1998;

- 24(5):481–483.
19. Nagoba B, Gandhi R, Wadher B, Rao A, Selkar S. Simple and effective approach for the treatment of traumatic wounds in non-diabetic patients: A prospective open study. *International Wound Journal* 2013; **10**(5):585–589. doi:10.1111/j.1742-481X.2012.01026.x.
  20. Yun F, Firkova EI, Jun-Qi L, Xun H. Effect of non-surgical periodontal therapy on patients with type 2 diabetes mellitus. *Folia medica* 2007; **49**(1–2):32–6. <http://www.ncbi.nlm.nih.gov/pubmed/18018467> Accessed.
  21. Atiyeh BS, Costagliola M. Cultured epithelial autograft (CEA) in burn treatment: Three decades later. *Burns* 2007; **33**(4):405–413. doi:10.1016/j.burns.2006.11.002.
  22. Shakespeare PG. The role of skin substitutes in the treatment of burn injuries. *Clinics in Dermatology* 2005; **23**(4):413–418. doi:<https://doi.org/10.1016/j.clindermatol.2004.07.015>.
  23. Boer M, Duchnik E, Maleszka R, Marchlewicz M. Structural and biophysical characteristics of human skin in maintaining proper epidermal barrier function. *Postepy Dermatologii i Alergologii* 2016; **33**(1):1–5. doi:10.5114/pdia.2015.48037.
  24. Sander EA, Lynch KA, Boyce ST. Development of the Mechanical Properties of Engineered Skin Substitutes After Grafting to Full-Thickness Wounds. *Journal of Biomechanical Engineering* 2014; **136**(5):51008. doi:10.1115/1.4026290.
  25. Gallagher AJ, Ni Anniadh A, Kruyere K, Ottenio M, Xie H, Gilchrist MD. Dynamic tensile properties of human skin. *2012 IRCOBI Conference* 2012:494–502. doi:Irc-12-59.

26. Annaidh AN, Bruyère K, Destrade M, Gilchrist MD, Otténio M. Characterization of the anisotropic mechanical properties of excised human skin. *Journal of the Mechanical Behavior of Biomedical Materials* 2012; **5**(1):139–148.  
doi:<https://doi.org/10.1016/j.jmbbm.2011.08.016>.
27. Darlenski R, Fluhr JW. Influence of skin type, race, sex, and anatomic location on epidermal barrier function. *Clinics in Dermatology* 2012; **30**(3):269–273.  
doi:<https://doi.org/10.1016/j.clindermatol.2011.08.013>.
28. Chikakane K, Takahashi H. Measurement of skin pH and its significance in cutaneous diseases. *Clinics in Dermatology* 1995; **13**(4):299–306. doi:[https://doi.org/10.1016/0738-081X\(95\)00076-R](https://doi.org/10.1016/0738-081X(95)00076-R).
29. Verdier-S??vrain S, Bont?? F. Skin hydration: A review on its molecular mechanisms. *Journal of Cosmetic Dermatology* 2007; **6**(2):75–82. doi:10.1111/j.1473-2165.2007.00300.x.
30. Bettinger CJ. Biodegradable Elastomers for Tissue Engineering and Cell-Biomaterial Interactions. *Macromolecular Bioscience* 2011; **11**(4):467–482.  
doi:10.1002/mabi.201000397.
31. Laurencin CT, Khan Y. Regenerative engineering. *Science Translational Medicine* 2012; **4**(160):1–3. doi:10.1126/scitranslmed.3004467.
32. Tran RT, Yang J, Ameer GA. Citrate-Based Biomaterials and Their Applications in Regenerative Engineering. *Annual Review of Materials Research* 2015; **45**(1):277–310.  
doi:10.1146/annurev-matsci-070214-020815.

33. Matsumura S, Hlil AR, Lepiller C, et al. Ionomers for proton exchange membrane fuel cells with sulfonic acid groups on the end-groups: Novel branched poly(ether-ketone)s. *American Chemical Society, Polymer Preprints, Division of Polymer Chemistry* 2008; **49**(1):511–512. doi:10.1002/pola.
34. Su L-C, Xie Z, Zhang Y, Nguyen KT, Yang J. Study on the Antimicrobial Properties of Citrate-Based Biodegradable Polymers. *Frontiers in Bioengineering and Biotechnology* 2014; **2**:23. doi:10.3389/fbioe.2014.00023.
35. Luo Y, Engelmayr G, Auguste DT, et al. 3D scaffolds. *Principles of Tissue Engineering* 2013:475–494. doi:10.1016/B978-0-12-398358-9.00024-0.
36. Bártolo PJ, Almeida HA, Rezende RA, Laoui T, Bidanda B. Advanced processes to fabricate scaffolds for tissue engineering. *Virtual Prototyping and Bio Manufacturing in Medical Applications* 2008:149–170. doi:10.1007/978-0-387-68831-2\_8.
37. Mooney DJ, Baldwin DF, Suh NP, Vacanti JP, Langer R. Novel approach to fabricate porous sponges of poly(D,L-lactic-co-glycolic acid) without the use of organic solvents. *Biomaterials* 1996; **17**(14):1417–1422. doi:10.1016/0142-9612(96)87284-X.
38. Bártolo PJ, Chua CK, Almeida HA, Chou SM, Lim ASC. Biomanufacturing for tissue engineering: Present and future trends. *Virtual and Physical Prototyping* 2009; **4**(4):203–216. doi:10.1080/17452750903476288.
39. Bidanda B, Bártolo PJ. *Virtual Propotyping & Bio Manufacturing in Medical Applications.*; 2008.
40. Lo H, Ponticello MS, Leong KW. Fabrication of Controlled Release Biodegradable

- Foams by Phase Separation. *Tissue Engineering* 1995; **1**(1):15–28.  
doi:10.1089/ten.1995.1.15.
41. Cui W, Zhou Y, Chang J. Electrospun nanofibrous materials for tissue engineering and drug delivery. *Science and Technology of Advanced Materials* 2010; **11**(1):14108.  
doi:10.1088/1468-6996/11/1/014108.
  42. Lannutti J, Reneker D, Ma T, Tomasko D, Farson D. Electrospinning for tissue engineering scaffolds. *Materials Science and Engineering C* 2007; **27**(3):504–509.  
doi:10.1016/j.msec.2006.05.019.
  43. Arslan-yildiz A, Assal R El, Chen P, Guven S, Inci F, Demirci U. Towards artificial tissue models : past , present , and future of 3D bioprinting Towards arti fi cial tissue models : past , present , and future of 3D bioprinting. 2016; **14103**.
  44. Murphy S V, Atala A. 3D bioprinting of tissues and organs. *Nature Biotechnology* 2014; **32**(8):773–785. doi:10.1038/nbt.2958.
  45. Xu T, Olson J, Zhao W, Atala A, Zhu J-M, Yoo JJ. Characterization of Cell Constructs Generated With Inkjet Printing Technology Using In Vivo Magnetic Resonance Imaging. *Journal of Manufacturing Science and Engineering* 2008; **130**(2):21013.  
doi:10.1115/1.2902857.
  46. Xu T, Kincaid H, Atala A, Yoo JJ. High-Throughput Production of Single-Cell Microparticles Using an Inkjet Printing Technology. *Journal of Manufacturing Science and Engineering* 2008; **130**(21017):1–5. doi:10.1115/1.2903064.
  47. Goldman T, Gonzalez JS. DNA-printing: Utilization of a standard inkjet printer for the

- transfer of nucleic acids to solid supports. *Journal of Biochemical and Biophysical Methods* 2000; **42**(3):105–110. doi:10.1016/S0165-022X(99)00049-4.
48. No Title.
  49. Xu T, Jin J, Gregory C, Hickman JJ, Boland T. Inkjet printing of viable mammalian cells. *Biomaterials* 2005; **26**.
  50. Tekin E, Smith PJ, Schubert US. Inkjet printing as a deposition and patterning tool for polymers and inorganic particles. *Soft Matter* 2008; **4**(4):703. doi:10.1039/b711984d.
  51. Saunders RE, Gough JE, Derby B. Delivery of human fibroblast cells by piezoelectric drop-on-demand inkjet printing. *Biomaterials* 2008; **29**(2):193–203.  
doi:10.1016/j.biomaterials.2007.09.032.
  52. Kim JD, Choi JS, Kim BS, Chan Choi Y, Cho YW. Piezoelectric inkjet printing of polymers: Stem cell patterning on polymer substrates. *Polymer* 2010; **51**(10):2147–2154.  
doi:10.1016/j.polymer.2010.03.038.
  53. Tasoglu S, Demirci U. Bioprinting for stem cell research. *Trends Biotechnol* 2013; **31**(1):10–19. doi:10.1016/j.tibtech.2012.10.005.
  54. Khalil S, Sun W. Biopolymer deposition for freeform fabrication of hydrogel tissue constructs. *Materials Science and Engineering C* 2007; **27**(3):469–478.  
doi:10.1016/j.msec.2006.05.023.
  55. Murphy S V., Skardal A, Atala A. Evaluation of hydrogels for bio-printing applications. *Journal of Biomedical Materials Research - Part A* 2013; **101 A**(1):272–284.  
doi:10.1002/jbm.a.34326.

56. Hennink WE, van Nostrum CF. Novel crosslinking methods to design hydrogels. *Advanced Drug Delivery Reviews* 2012; **64**(SUPPL.):223–236.  
doi:10.1016/j.addr.2012.09.009.
57. Tan K, Chua C, Leong K, Cheah C, Cheang P, Abu Bakar M. Scaffold development using selective laser sintering of polyetheretherketone--hydroxyapatite biocomposite blends. *Biomaterials* 2003; **24**.
58. Lee G, Barlow J. Selective laser sintering of bioceramic materials for implants. *Proceedings of the solid freeform fabrication* 1996:376–380.
59. Colina M, Serra P, Fernández-Pradas JM, Sevilla L, Morenza JL. DNA deposition through laser induced forward transfer. *Biosensors and Bioelectronics* 2005; **20**(8 SPEC. ISS.):1638–1642. doi:10.1016/j.bios.2004.08.047.
60. Ringeisen BR, Kim H, Barron JA, et al. Laser Printing of Pluripotent Embryonal Carcinoma Cells. *Tissue Engineering* 2004; **10**(3–4):483–491.  
doi:10.1089/107632704323061843.
61. Laser-assisted cell printing: principle, physical parameters versus cell fate and perspectives in tissue engineering. *Nanomedicine* 2010; **5**(3):507–515.  
doi:10.2217/nmm.10.14.
62. Guillotin B, Souquet A, Catros S, et al. Laser assisted bioprinting of engineered tissue with high cell density and microscale organization. *Biomaterials* 2010; **31**(28):7250–7256.  
doi:10.1016/j.biomaterials.2010.05.055.
63. Specification & Description. 2012; (December).

64. Seol YJ, Kang HW, Lee SJ, Atala A, Yoo JJ. Bioprinting technology and its applications. *European Journal of Cardio-thoracic Surgery* 2014; **46**(3):342–348.  
doi:10.1093/ejcts/ezu148.
65. Chang CC, Boland ED, Williams SK, Hoying JB. Direct-write bioprinting three-dimensional biohybrid systems for future regenerative therapies. *Journal of Biomedical Materials Research - Part B Applied Biomaterials* 2011; **98 B**(1):160–170.  
doi:10.1002/jbm.b.31831.
66. Smith CM, Stone AL, Parkhill RL, et al. Three-Dimensional BioAssembly Tool for Generating Viable Tissue-Engineered Constructs. *Tissue Engineering* 2004; **10**(9–10):1566–1576. doi:10.1089/ten.2004.10.1566.
67. ASTM International. ASTM D882: Standard Test Method for Tensile Properties of Thin Plastic Sheeting. *ASTM Standards* 2012:12. doi:10.1520/D0882-12.2.
68. Factors C, Europeias DASC, Comissão Europeia, ASTM. Standard Test Methods for Water Vapor Transmission of Materials 1. *Astm* 2002; **14**(July 2000):1–10.  
doi:10.1520/E0096.
69. Tran RT, Yang J, Ameer GA. Citrate-Based Biomaterials and Their Applications in Regenerative Engineering. *Annual Review of Materials Research* 2015; **45**(1):277–310.  
doi:10.1146/annurev-matsci-070214-020815.